

ISWS Contract Report 2006-04

High-Throughput Computing for the Analysis of Tracer Tests in Fractured Aquifers


by

Douglas D. Walker
Illinois State Water Survey

Pablo A. Cello and Albert J. Valocchi
Department of Civil and Environmental Engineering
University of Illinois at Urbana-Champaign

Bruce Loftis
Rosen Center for Advanced Computing
Purdue University

April 2006



Illinois State Water Survey
Center for Groundwater Science
Champaign, Illinois

A Division of the Illinois Department of Natural Resources

**High-Throughput Computing for the Analysis of Tracer Tests
in Fractured Aquifers**

By

Douglas D. Walker, Illinois State Water Survey;

Pablo A. Cello and Albert J. Valocchi,
Department of Civil and Environmental Engineering,
University of Illinois at Urbana-Champaign; and

Bruce Loftis, Rosen Center for Advanced Computing,
Purdue University

Illinois State Water Survey,
Champaign, IL

Contents

	<u>Page</u>
Abstract.....	1
Introduction.....	2
Objectives and Tasks	5
Acknowledgments.....	6
Approach.....	7
Results.....	13
Multivariate Gaussian (mvG)	15
Fractional Brownian Motion (fBm).....	30
Percolation Network	34
Log Gaussian (Uncorrelated).....	49
Summary.....	54
Discussion.....	57
Conclusions.....	63
References.....	64
Appendix A. Code Description and Performance Requirements	71
Appendix B. Code Verification Problem mip_V2.....	75
Appendix C. Code Verification Problem h11_S1.....	79
Appendix D. Monte Carlo Stability Analyses	83

List of Tables

	<u>Page</u>
Table 1. Transport Parameters Used in Simulating the Converging-Flow Tracer Test, after Meigs and Beauheim (2001).....	10
Table 2. Summary of Models and Parameters Analyzed in This Study	14
Table 3. Summary of CFTT Results by Model.....	25

List of Figures

	<u>Page</u>
Figure 1. An aquifer test in a fractured dolomite aquifer in Kankakee County, Illinois, USA.	3
Figure 2: The Monte Carlo sequence of programs used in this study.	8
Figure 3. Model schematic and grids.	9
Figure 4a. Drawdown (closed symbols), derivative (open symbols with line), and flow dimension (open symbols without line) for two realizations of case kG3b3: mvG with $\sigma^2_{\ln T} = 0.25$ and $I = 7$ m.	16
Figure 4b. Average (circle) and 95 percent normal CI for the population (solid lines) and for the mean (dashed lines) for 100 realizations of the flow dimension, case kG3b3: mvG with $\sigma^2_{\ln T} = 0.25$ and $I = 7$ m.	16
Figure 4c. Relative concentration versus time for a CFTT in two realizations of case kG3b3: mvG with $\sigma^2_{\ln T} = 0.25$ and $I = 7$ m.	17
Figure 4d. Relative concentration versus time for 100 realizations of a CFTT, median (solid line) and 95 percent nonparametric CI for the population (dashed lines), case kG3b3: mvG with $\sigma^2_{\ln T} = 0.25$ and $I = 7$ m.	17
Figure 5a. Drawdown (closed symbols), derivative (open symbols with line), and flow dimension (open symbols without line) for two realizations of case kG2b3: mvG with $\sigma^2_{\ln T} = 0.0625$ and $I = 7$ m.	18
Figure 5b. Average (circle) and 95 percent normal CI for the population (solid lines) and for the mean (dashed lines) for 100 realizations of the flow dimension, case kG2b3: mvG with $\sigma^2_{\ln T} = 0.0625$ and $I = 7$ m.	19
Figure 5c. Relative concentration versus time for a CFTT in two realizations of case kG2b3: mvG with $\sigma^2_{\ln T} = 0.0625$ and $I = 7$ m.	19
Figure 5d. Relative concentration versus time for 100 realizations of a CFTT, median (solid line) and 95 percent nonparametric CI for the population (dashed lines), case kG2b3: mvG with $\sigma^2_{\ln T} = 0.0625$ and $I = 7$ m.	19
Figure 6a. Drawdown (closed symbols), derivative (open symbol with line), and flow dimension (open symbols without line) for two realizations of case kG4b3: mvG with $\sigma^2_{\ln T} = 1.0$ and $I = 7$ m.	20
Figure 6b. Average (circle) and 95 percent normal CI for the population (solid lines) and for the mean (dashed lines) for 100 realizations of the flow dimension, case kG4b3: mvG with $\sigma^2_{\ln T} = 1.0$ and $I = 7$ m.	20
Figure 6c. Relative concentration versus time for a CFTT in two realizations of case kG4b3: mvG with $\sigma^2_{\ln T} = 1.0$ and $I = 7$ m.	21
Figure 6d. Relative concentration versus time for 100 realizations of a CFTT, median (solid line) and 95 percent nonparametric CI for the population (dashed lines), case kG4b3: mvG with $\sigma^2_{\ln T} = 1.0$ and $I = 7$ m.	21
Figure 7a. Drawdown (closed symbols), derivative (open symbols with line), and flow dimension (open symbols without line) for two realizations of case kG6b3: mvG with $\sigma^2_{\ln T} = 0.25$ and $I = 3.5$ m.	23
Figure 7b. Average (circle) and 95 percent normal CI for the population (solid lines) and for the mean (dashed lines) for 100 realizations of the flow dimension, case kG6b3: mvG with $\sigma^2_{\ln T} = 0.25$ and $I = 3.5$ m.	23

Figure 7c. Relative concentration versus time for a CFTT in two realizations of case kG6b3: mvG with $\sigma^2_{\ln T} = 0.25$ and $I = 3.5$ m.	24
Figure 7d. Relative concentration versus time for 100 realizations of a CFTT, median (solid line) and 95 percent nonparametric CI for the population (dashed lines), case kG6b3: mvG with $\sigma^2_{\ln T} = 0.25$ and $I = 3.5$ m.	24
Figure 8a. Drawdown (closed symbols), derivative (open symbols with line), and flow dimension (open symbols without line) for two realizations of case kG5b3: mvG with $\sigma^2_{\ln T} = 4.0$ and $I = 7$ m.	26
Figure 8b. Average (circle) and 95 percent normal CI for the population (solid lines) and for the mean (dashed lines) for 100 realizations of the flow dimension, case kG5b3: mvG with $\sigma^2_{\ln T} = 4.0$ and $I = 7$ m.	26
Figure 8c. Relative concentration versus time for a CFTT in two realizations of case kG5b3: mvG with $\sigma^2_{\ln T} = 4.0$ and $I = 7$ m.	27
Figure 8d. Relative concentration versus time for 100 realizations of a CFTT, median (solid line) and 95 percent nonparametric CI for the population (dashed lines), case kG5b3: mvG with $\sigma^2_{\ln T} = 4.0$ and $I = 7$ m.	27
Figure 9a. Drawdown (closed symbols), derivative (open symbols with line), and flow dimension (open symbols without line) for two realizations of case kG8b3: mvG with $\sigma^2_{\ln T} = 8.0$ and $I = 7$ m.	28
Figure 9b. Average (circle) and 95 percent normal CI for the population (solid lines) and for the mean (dashed lines) for 100 realizations of the flow dimension, case kG8b3: mvG with $\sigma^2_{\ln T} = 9.0$ and $I = 7$ m.	28
Figure 9c. Relative concentration versus time for a CFTT in two realizations of case kG8b3: mvG with $\sigma^2_{\ln T} = 9.0$ and $I = 7$ m.	29
Figure 9d. Relative concentration versus time for 100 realizations of a CFTT, median (solid line) and 95 percent nonparametric CI for the population (dashed lines), case kG8b3: mvG with $\sigma^2_{\ln T} = 9.0$ and $I = 7$ m.	29
Figure 10. Experimental semivariogram for one realization of $\ln T$ as a fBm process, $H = 0.25$	31
Figure 11a. Drawdown (closed symbols), derivative (open symbol with line), and flow dimension (open symbols without line) for two realizations of case kB1b3: fBm with $H = 0.25$	32
Figure 11b. Average (circle) and 95 percent normal CI for the population (solid lines) and mean (dashed lines) for 100 realizations of the flow dimension, case kB1b3: fBm with $H = 0.25$	32
Figure 11c. Relative concentration versus time for a CFTT in two realizations of case kB1b3: fBm with $H = 0.25$	33
Figure 11d. Relative concentration versus time for 100 realizations of a CFTT, median (solid lines) and 95 percent nonparametric CI for the population (dashed lines), case kB1b3: fBm with $H = 0.25$	33
Figure 12a. Average (circle) and 95 percent normal CI for the population (solid lines) and mean (dashed lines) for 1000 realizations of the flow dimension, case kPfb3: percolation with $p = 0.61$, $T_{1-p} = T_p / 10^4$, no trimming.	36

Figure 12b. Drawdown (closed symbols), derivative (open symbols with line), and flow dimension (open symbols without line) for two realizations outside $0.5 < n^* < 2.5$ from case kPfb3: percolation with $p = 0.61$, $T_{1-p} = T_p / 10^4$	36
Figure 13a. Drawdown (closed symbols), derivative (open symbols with line), and flow dimension (open symbols without line) for two realizations $0.5 < n^* < 2.5$, case kPfb3: percolation with $p = 0.61$, $T_{1-p} = T_p / 10^4$	38
Figure 13b. Average (circle) and 95 percent normal CI for the population (solid lines) and mean (dashed lines) flow dimension for 200 realizations $0.5 < n^* < 2.5$, case kPfb3: percolation with $p = 0.61$, $T_{1-p} = T_p / 10^4$	38
Figure 13c. Relative concentration versus time for a CFTT in two realizations with $0.5 < n^* < 2.5$, case kPfb3: percolation with $p = 0.61$, $T_{1-p} = T_p / 10^4$	39
Figure 13d. Relative concentration versus time of a converging flow tracer test for 200 realizations with $0.5 < n^* < 2.5$, median (solid line) and 95 percent nonparametric CI for the population (dashed lines), case kPfb3: percolation with $p = 0.61$, $T_{1-p} = T_p / 10^4$	39
Figure 14a. Drawdown (closed symbols), derivative (open symbols with line), and flow dimension (open symbols without line) for two realizations with $0.5 < n^* < 2.5$, case kPeb3: percolation with $p = 0.61$, $T_{1-p} = T_p / 10^6$	41
Figure 14b. Average (circle) and 95 percent normal CI for the population (solid lines) and mean (dashed lines) flow dimension for 58 realizations with $0.5 < n^* < 2.5$, case kPeb3: percolation with $p = 0.61$, $T_{1-p} = T_p / 10^6$	41
Figure 14c. Relative concentration versus time for a CFTT in two realizations with $0.5 < n^* < 2.5$, case kPeb3: percolation with $p = 0.61$, $T_{1-p} = T_p / 10^6$	42
Figure 14d. Relative concentration versus time of a converging flow tracer test for 58 realizations with $0.5 < n^* < 2.5$, median (solid line) and 95 percent nonparametric CI for the population (dashed lines), case kPeb3: percolation with $p = 0.61$, $T_{1-p} = T_p / 10^6$	42
Figure 15a. Drawdown (closed symbols), derivative (open symbols with line), and flow dimension (open symbols without line) for two realizations with $0.5 < n^* < 2.5$, case kPcb3: percolation with $p = 0.61$, no-flow cells	44
Figure 15b. Average (circle) and 95 percent normal CI for the population (solid lines) and mean (dashed lines) flow dimension for 200 realizations $0.5 < n^* < 2.5$, case kPcb3: percolation with $p = 0.61$, no-flow cells	44
Figure 15c. Relative concentration versus time for a CFTT in two realizations $0.5 < n^* < 2.5$, case kPcb3: percolation with $p = 0.61$ and no-flow cells	45
Figure 15d. Relative concentration versus time of a converging flow tracer test for 200 realizations $0.5 < n^* < 2.5$, median (solid line) and 95 percent nonparametric CI for the population (dashed lines), case kPcb3: percolation with $p = 0.61$ and no-flow cells	45
Figure 16a. Relative concentration versus time for a CFTT in two realizations with $0.5 < n^* < 2.5$ from case kPdb3: percolation with $p = 0.61$, no matrix diffusion	46
Figure 16b. Relative concentration versus time for 200 realizations of a converging flow tracer test with $0.5 < n^* < 2.5$, median (solid line) and 95 percent nonparametric CI for the population (dashed lines), case kPdb3: percolation with $p = 0.61$, no matrix diffusion	46
Figure 17a. Drawdown (closed symbols), derivative (open symbols with line), and flow dimension (open symbols without line) for two realizations with $0.5 < n^* < 2.5$, case kPbb3: percolation with $p = 0.60$, $T_{1-p} = T_p / 10^4$	47

Figure 17b. Average (circle) and 95 percent normal CI for the population (solid lines) and mean (dashed lines) flow dimension for 200 realizations $0.5 < n^* < 2.5$, case kPbb3: percolation with $p = 0.60$, $T_{1-p} = T_p / 10^4$	47
Figure 17c. Relative concentration versus time for a CFTT in two realizations $0.5 < n^* < 2.5$, case kPbb3: percolation with $p = 0.60$, $T_{1-p} = T_p / 10^4$	48
Figure 17d. Relative concentration versus time of a converging flow tracer test for 200 realizations $0.5 < n^* < 2.5$, median (solid line) and 95 percent nonparametric CI for the population (dashed lines), case kPbb3: percolation with $p = 0.60$, $K_{1-p} = K_p / 10^4$	48
Figure 18a. Drawdown (closed symbols), derivative (open symbols with line), and flow dimension (open symbols without line) for two realizations of case kN1b3: log Gaussian with $\sigma^2_{\ln T} = 1.0$	50
Figure 18b. Average (circle) and 95 percent normal CI for the population (solid lines) and for the mean (dashed lines) for 100 realizations of the flow dimension, case kN1b3: log Gaussian with $\sigma^2_{\ln T} = 1.0$	50
Figure 18c. Relative concentration versus time for a CFTT in two realizations of case kN1b3: log Gaussian with $\sigma^2_{\ln T} = 1.0$	51
Figure 18d. Relative concentration versus time for 100 realizations of a CFTT, median (solid line) and 95 percent nonparametric CI for the population (dashed lines), case kN1b3: log Gaussian with $\sigma^2_{\ln T} = 1.0$	51
Figure 19a. Drawdown (closed symbols), derivative (open symbols with line), and flow dimension (open symbols without line) for two realizations of case kN16b3: log Gaussian with $\sigma^2_{\ln T} = 16.0$	52
Figure 19b. Average (circle) and 95 percent normal CI for the population (solid lines) and for the mean (dashed lines) for 100 realizations of the flow dimension, case kN16b3: log Gaussian with $\sigma^2_{\ln T} = 16.0$	52
Figure 19c. Relative concentration versus time for a CFTT in two realizations of case kN16b3: log Gaussian with $\sigma^2_{\ln T} = 16.0$	53
Figure 19d. Relative concentration versus time for 100 realizations of a CFTT, median (solid line) and 95 percent nonparametric CI for the population (dashed lines), case kN16b3: log Gaussian with $\sigma^2_{\ln T} = 16.0$	53
Figure 20. Apparent flow dimensions for a constant-rate aquifer test in a two-dimensional domain.....	58
Figure 21. Relative concentration versus time for a CFTT influenced by matrix diffusion.....	60

High-Throughput Computing for the Analysis of Tracer Tests in Fractured Aquifers

By

Douglas D. Walker, Illinois State Water Survey;

Pablo A. Cello and Albert J. Valocchi,
Department of Civil and Environmental Engineering,
University of Illinois at Urbana-Champaign; and

Bruce Loftis, Rosen Center for Advanced Computing,
Purdue University

Abstract

Traditional approaches to characterization and modeling of fractured dolomite aquifers face many conceptual and technical challenges. One alternative strategy begins with the Generalized Radial Flow interpretation of hydraulic tests, which infers an additional parameter, the flow dimension, to describe the geometry of groundwater flow. This study examines the behavior and variability of the apparent flow dimension, n^* , and advective transport for four stochastic models of heterogeneous transmissivity, $T(x)$. This is accomplished through Monte Carlo analysis of numerical models simulating aquifer tests and converging flow tracer tests (CFTTs) in two-dimensional systems. For $\ln T(x)$ distributed as a multivariate Gaussian (mvG) variable of variance less than one, the apparent flow dimension of an aquifer test converges to $n^* = 2$ if the scale of the test is large relative to the scale of correlation. The variability of the apparent flow dimension depends on the variance and integral scale of the transmissivity, suggesting that it may be possible to identify the variance and integral scale from a set of aquifer tests. For variances greater than one, the results suggest that the average of the apparent flow dimension is less than two initially, then converges to $n^* = 2$, similar in some respects to a percolation network. The simulation of an uncorrelated log-Gaussian model suggests that the flow dimension of an aquifer test converges to $n^* = 2$ even for large variances. For $\ln T(x)$ distributed as fractional Brownian motion (fBm), the apparent flow dimension averages to $n^* = 2$ and its variability increases with time. An approximation of a percolation network model showed an average apparent flow dimension stabilizing between $n^* = 1.4$ to 1.6, followed by an increasing trend. These characteristics apparently are functions of the transmissivity contrast between the percolating and nonpercolating fractions. In the low-variance mvG, uncorrelated log-Gaussian, and fBm models, CFTTs influenced by matrix diffusion showed late-time breakthrough curves (BTCs) with log-log slopes of $-3/2$, the characteristic behavior of matrix diffusion. In the percolation network model, a simulated CFTT influenced by matrix diffusion had late-time BTC with log-log slopes of $-5/4$, attributed to slow advection through low transmissivity regions. This indicates that some heterogeneity models can systematically affect the late-time behavior of a BTC for a CFTT. These results suggest that the flow dimension may be a useful diagnostic for selecting models of heterogeneity, and that flow dimensions $n \neq 2$ may be associated with unique tracer behavior. Additional research is advocated to infer the general behavior of the flow dimension at various field sites, to assess a broader range of parameters, to examine other stochastic models, and to conduct a more detailed examination of transport behavior versus the flow dimension.

Introduction

The characterization and analysis of fluid flow and contaminant transport in fractured rocks is a common challenge faced by scientists and engineers worldwide. These rock formations form economically important aquifers and oil reservoirs throughout the world, ranging from the dolomite aquifers of Northeastern Illinois (NIPC, 2001); to carbonate oil reservoirs in South America, the North Sea, and the Mideast (Acuna and Yortsos, 1995; Raghavan, 2004; Sahimi and Mukhopadhyay, 1996); and to dolomite aquifers in the Southwestern United States that form pathways critical to the performance of nuclear waste disposal sites (Meigs and Beauheim, 2001). Despite their importance, the characterization and modeling of fluid flow and contaminant transport in fractured rocks continue to be a challenge because they tend to be highly heterogeneous. This heterogeneity concentrates flow into erratic channels that are not addressed by traditional analysis techniques. Responsible management requires reliable field characterization methods and modeling analyses to assess the impact of management options, yet currently available techniques are poorly suited to the analysis of flow and transport in fractured rocks (NRC, 1996).

One such technique for field characterization is aquifer testing, where water level changes (drawdowns) are observed in the aquifer surrounding a pumped well. These drawdowns over time are interpreted by fitting a simple model of flow to a well, yielding estimates of hydraulic properties that are used in subsequent assessments of water resources. However, fractured rock aquifers often have complex flow geometries that are ignored by traditional interpretation approaches that assume radial (two-dimensional) flow. Figure 1 is a log-log diagnostic plot of the drawdown, s , and drawdown derivative $s' = (ds/d \ln t)$ versus time. The plot compares a traditional model for interpreting an aquifer test with data from an aquifer test in a fractured dolomite aquifer in Kankakee County, in northeastern Illinois. The producing zone of this aquifer is a few meters thick, parallel to the plane of bedding, and laterally extensive. In this circumstance, the traditional approach to interpreting an aquifer test would fit the Theis model of radial flow in an infinite, two-dimensional domain (Theis, 1935). However, the slope of the Theis model fits the data poorly, as evidenced by the mismatch of the derivatives of the data and the model. Alternative combinations of hydraulic properties result in equally poor fits to the data, translating into unreliable parameter estimates and increased uncertainties in managing this water resource.

The characterization of fractured rocks requires an approach that addresses the complex, often non-radial flow geometry experienced by aquifer tests in these systems. One starting point is the Generalized Radial Flow (GRF) model for interpreting aquifer tests in fractured rocks (Barker, 1988), which includes an additional parameter, n , called the flow dimension. In the GRF approach, the cross-sectional area of flow for an aquifer test is given by $A(r) = \alpha_n r^{n-1}$, so that the surface area of a unit sphere in n dimensions is

$$\alpha_n = b^{3-n} \frac{2\pi^{n/2}}{\Gamma(\frac{n}{2})} \quad (1)$$

where $A(r)$ is the cross-sectional area of flow [L^2], r is the radial distance from the borehole [L], b is the extent of the flow zone [L], n is the flow dimension [$]$, and $\Gamma()$ is the gamma function [$]$. The flow dimension n describes the geometry of the system by defining the rate that the cross-sectional area of flow changes with respect to distance from the test well, i.e., the flow dimension is the power by which the flow area changes with respect to radial distance, plus one. For example, in a homogeneous, radial system, the cross-sectional area of flow at any radius is proportional to r^1 , i.e., $A(r) = 2\pi r b$, so that the flow dimension is $n = 2$. Mishra (1991) examined the late-time slope of the log-log plot of the derivative for infinite-acting aquifers:

$$v = \lim_{t \rightarrow \infty} \frac{d}{d(\log t)} \left[\log \left(\frac{ds}{d \ln t} \right) \right] \quad (2)$$

and found that it is related to the flow dimension by $n = 2 - 2 \cdot v$. Thus, for an aquifer test in a homogeneous, infinite, two-dimensional domain, the late-time slope of its derivative will be $v = 0$, so that the flow dimension is $n = 2 - 2 \cdot 0 = 2$. Where strong heterogeneities restrict flow to a portion of the aquifer, the flow dimension can be less than the spatial (Euclidean) dimension of the aquifer. Figure 1 shows such an aquifer test in a fractured dolomite formation, where the pressure derivative has an upward slope of approximately $v \approx 0.15$, so that $n \approx 1.7$, even though the aquifer arguably is two dimensional.

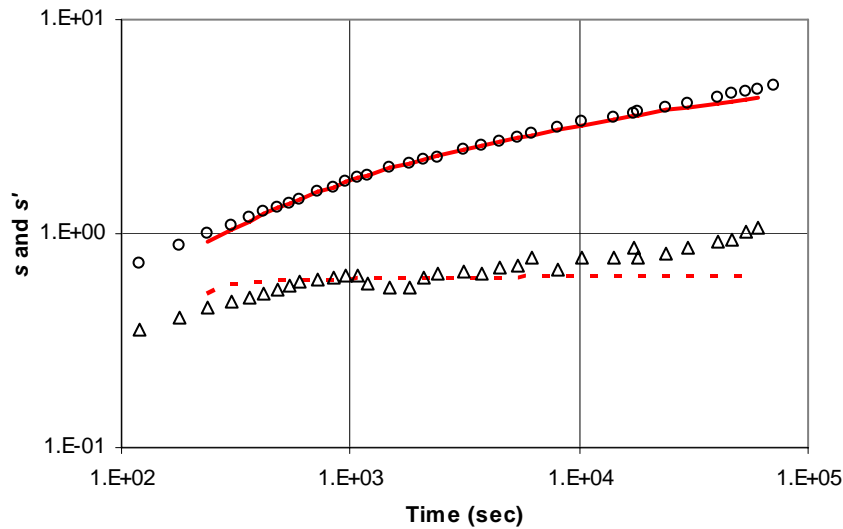


Figure 1. An aquifer test in a fractured dolomite aquifer in Kankakee County, Illinois, USA. Circles denote the observed decline in water levels (drawdown, s) vs. time; triangles denote the derivative, s' . The Theis model of radial flow in a two-dimensional domain is the solid line and its derivative is the dashed line. ISWS archival data for observation well number 4, April 19-20, 1988, aquifer test of Hopkins Park Well #2 (Cravens et al., 1990).

Unlike the parameters inferred from traditional interpretations of aquifer tests, the relationship between the flow dimension and aquifer heterogeneity has received little attention. For example, many fractured dolomites arguably have a Euclidean dimension of two, yet their flow dimensions are often less than two (Figure 1). Barker (1988) noted that hydraulic tests in fractured media often show noninteger flow dimensions and conjectured that this was caused by a non-space-filling fracture network acting as a fractal object. Polek (1990) verified Barker's conjecture using numerical simulations of flow in a percolation network. Acuna and Yortsos (1995) confirmed that the GRF model could be viewed as radial diffusion on a fractal lattice, and that a perfectly connected lattice had a flow dimension equal to the fractal dimension. Doe (1991) noted that the interpreted flow dimension of a hydraulic test might be the consequence of either heterogeneity, variations in flow geometry, or some combination of both. Several studies suggest that flow and transport models should reproduce the flow dimensions inferred from aquifer tests, but they provide little advice on what behavior should be reproduced or how to achieve this (Borgne et al., 2004; Riemann et al., 2002). Walker and Roberts (2003) used analytical and semianalytical approaches to determine the flow dimensions corresponding to several idealized hydrogeologic conditions in two-dimensional systems. They found that the flow dimension decreases initially but returns to $n = 2$ for a linear no-flow boundary, stabilizes to $n = 4$ for a linear constant-head boundary, and is $n \geq 2$ and increases without bound for the leaky-aquifer problem of Hantush (Hantush and Jacob, 1955). They also showed that a stationary (statistically homogeneous) field of transmissivity with a modest variance tended to show $n = 2$, but the flow dimension of a nonstationary heterogeneity depended on the form of nonstationarity. Determining the flow dimension of widely used stochastic models of heterogeneity requires Monte Carlo simulation using numerical models of aquifer tests (Walker and Roberts, 2003).

Still scarcer are studies relating the flow dimension to transport behavior. Although not specifically examining the flow dimension, Moreno and Tsang (1994) used numerical models to examine flow and transport in three-dimensional lognormal ($\ln T$ distributed as a multivariate Gaussian (mvG) variable). They found that increasing the variance of these fields tended to increase the linearity of flow channels, and that this contributed to skewed breakthrough curves (BTCs). Doughty and Karasaki (2002) numerically modeled transport under uniform, two-dimensional flow through a fractal geometry. They found that the flow dimensions were less than both the Euclidian fractal dimensions, and that transport was non-Fickian and consistent with flow channeling across a range of scales. There has been extensive research addressing diffusion on fractal lattices, suggesting that transport in such systems has unique behaviors that partially are related to the geometry of flow (Benson et al., 2004; Berkowitz et al., 2002; O'Shaughnessy and Procaccia, 1985). Such results suggest the possibility of using tracer data with the flow dimension to constrain models of heterogeneity and thus reduce uncertainties in aquifer characterization.

The Illinois State Water Survey (ISWS) and the University of Illinois at Urbana-Champaign (UIUC) have developed a Monte Carlo process to estimate flow dimensions corresponding to stochastic models of aquifer heterogeneity. The approach is similar to that of Meier et al. (1998): create a synthetic aquifer with a particular stochastic model of spatially variable transmissivity, numerically simulate an aquifer test in the field, and then repeat the simulation to infer the behavior of the aquifer test for that stochastic model. In this study, the flow dimension is approximated numerically for each realization of the simulated aquifer test.

Preliminary analyses have tentatively identified the characteristic flow dimensions of two stochastic models of heterogeneity and suggest that the variability of the flow dimension is a function of the variability and spatial scale of the heterogeneity. However, the simulations to date have been limited to small sets of realizations for a few stochastic models, and have not examined transport.

Objectives and Tasks

This report summarizes research conducted by the ISWS in collaboration with UIUC, the National Center for Supercomputing Applications (NCSA), and Purdue University to extend the capabilities of the Monte Carlo simulator and perform simulations of aquifer tests and tracer tests in heterogeneous aquifers. The objectives of this study are to establish the expected behavior and variability of the flow dimension for widely used stochastic models of aquifer heterogeneity, and to perform a preliminary assessment of the relationship between the flow dimension and the breakthrough curves (BTCs) of converging-flow tracer tests (CFTTs). This project includes the following specific tasks:

Task 1: Extend the capabilities of the preliminary Monte Carlo simulator by incorporating the transport program THEMM, and thus permit the analysis of a CFTT influenced by matrix diffusion.

Task 2: Conduct Monte Carlo simulations to determine flow dimensions, transmissivities, and BTCs in realizations of heterogeneous transmissivity. Evaluate two stochastic models of aquifer heterogeneity (fractional Brownian motion (fBm) and uncorrelated log Gaussian) to complement the two stochastic models (multivariate lognormal (mvG) and percolation network) being analyzed in parallel as part of a complementary NCSA-funded research project.

Task 3: Construct animations for the evolution of a tracer test in heterogeneous media, using examples of single realizations from each stochastic model of heterogeneity.

Task 4: Report findings, including the present report and the preparation of manuscripts for publication in peer-reviewed journals.

The combination of these research efforts will identify models of aquifer heterogeneity that produce the observed flow dimension and evaluate the consequences of these models for transport. The products of Task 3, animation of tracer tests, are available separately on CD on request from the authors. This study uses parameter ranges from the inferred characteristics of the Culebra Dolomite at the Waste Isolation Pilot Plant (WIPP) site near Carlsbad, New Mexico. This enables the study to take advantage of the abundant, high quality hydraulic and tracer test data collected at the WIPP site, as well as augmenting the ongoing site characterization at the WIPP site. However, no attempt is made to calibrate or choose optimal model parameters to match the WIPP data, and the research results are broadly applicable to aquifer tests conducted in the fractured dolomite aquifers elsewhere, including those of northeastern Illinois.

Acknowledgments

This material is based upon work supported by Sandia National Laboratories under SNL PO# 24699, the Illinois Water Resources Center under Award Number 01HQGR0112; the National Center for Supercomputing Applications under the Faculty Fellows Program; and the Illinois State Water Survey. Any opinions, findings, and conclusions or recommendations expressed in this publication are those of the authors and do not necessarily reflect the views of the sponsors.

The authors acknowledge the assistance of Christine Doughty and Chin-Fu Tsang (Lawrence Berkeley Laboratories) for access to and assistance with THEMM; Steffan Mehl (U.S. Geological Survey) for access to and assistance with MODFLOW-2000 and the draft version of the GMG solver; and Susan Altman, Rick Beauheim, Glenn Hammond, Sean McKenna, and Randy Roberts (Sandia National Laboratories) for thoughtful discussion and debate regarding this research.

The review comments of Al Wehrmann, and Mark Anliker (ISWS), Sean McKenna and Rick Beauheim (Sandia National Laboratories), and Srikanta Mishra (INTERA) led to substantial improvements in this report.

Approach

This study is a Monte Carlo analysis conducted on a massively parallel, distributed computing network, using a numerical approach similar to that of Butler (1991) and Meier et al. (1998). Starting from a Monte Carlo procedure previously developed by the research team, this project adds a model of advective transport influenced by matrix diffusion to analyze the relationship between tracer tests and the flow dimension.

Figure 2 shows the sequence of programs used in this project to: 1) create a field of transmissivity using algorithms corresponding to specific stochastic models of spatial heterogeneity; 2) simulate a constant-rate aquifer test in the heterogeneous field using a finite-difference model of transient groundwater flow; 3) determine the flow dimension from the simulated drawdowns of the aquifer test using finite difference approximations for the pressure derivative and its slope (Equation 2), and use least squares regression to apply a traditional two-dimensional interpretive model to infer the apparent transmissivity of the aquifer; 4) simulate steady, uniform flow across the domain under a known gradient to estimate the effective transmissivity; and 5) simulate a CFTT influenced by matrix diffusion, recording the arrival times of particles to obtain a BTC at the pumped well. This sequence is repeated for many realizations of the transmissivity field, and the results from the set of realizations are used to infer the distribution of the flow dimension, the BTCs, and the effective transmissivities of each stochastic model of heterogeneity. The programs used in this simulation are well-documented groundwater flow and transport codes taken from the public domain, augmented by several programs written and tested as part of this study (see the appendices for program development and testing).

Because each realization of the sequence is computationally independent, the problem is well suited to distributed computing environments. In collaboration with NCSA, the Monte Carlo simulator was tested and the simulations were performed using computing resources from the TeraGrid project (<http://www.teragrid.org/>, funded by the National Science Foundation). The TeraGrid is a multi-year effort to build and deploy the world's largest and fastest distributed infrastructure for open scientific research. The TeraGrid has more than 20 teraflops of computing power distributed at nine sites, with capabilities for managing and storing nearly 1 petabyte of data and toolkits for grid computing. These heterogeneous components are connected with a 40 gigabit per second network backbone, which is the fastest research network currently available.

Using grid tools written by one of the authors permits running thousands of realizations on many different machines for the problems described herein. The general strategy is to build, submit, and manage jobs from a local grid-enabled desktop workstation without logging into the remote machines. A master host decides which remote resources to use, how many processors to use, and how many realizations should be assigned to each remote machine. Each realization requires 6-10 hours on a Linux cluster with new IA32 processors and somewhat longer on most other architectures. Approximately 100 or more of these 6-10 hour realizations can be completed each day using 20-40 processors on the largest TeraGrid clusters. Fewer processors are used on 3-6 other grid-enabled resources.

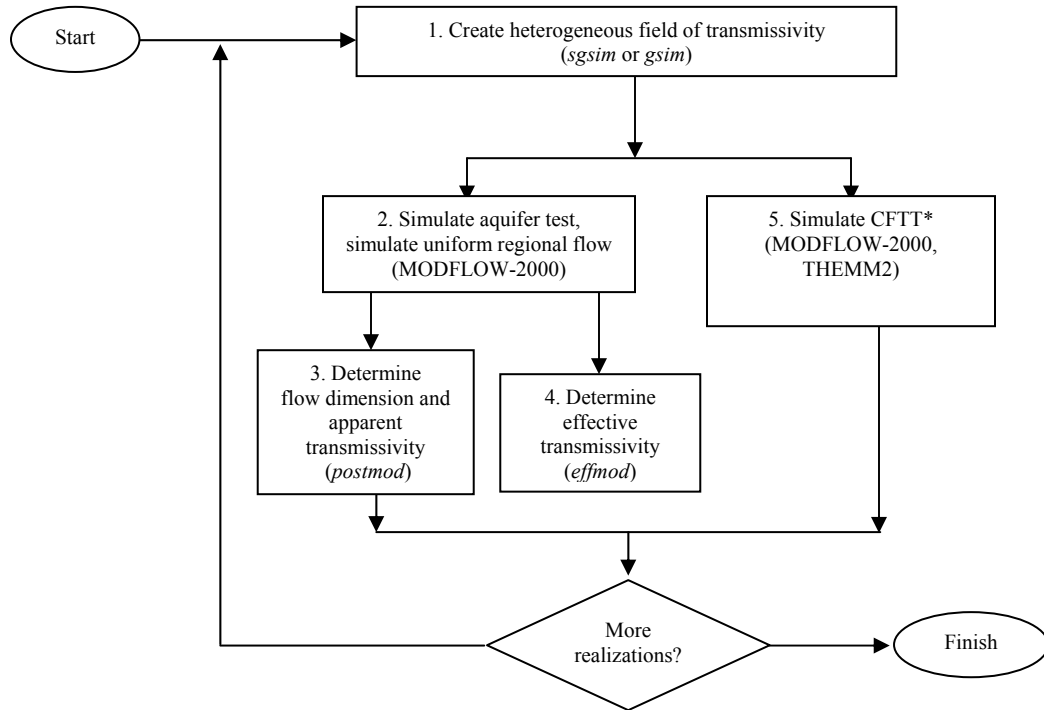


Figure 2. The Monte Carlo sequence of programs used in this study. The asterisk (*) denotes features added during this project, items in parentheses are computer codes.

As shown in Figure 3, the finite difference grid used in this study consists of 3001 x 3001 nodes with uniform one-meter spacing. Table 1 presents the aquifer parameters, chosen to be similar to those of the lower 4.4 m of the Culebra Dolomite, and the pumping rates similar to those used in tests at the H-11 hydropad (well cluster) (Beauheim and Ruskauff, 1998). The simulated aquifer has a uniform thickness of 4.4 m and a uniform storage coefficient of 4.7×10^{-5} (4.7×10^{-6} is used at the pumping node to compensate for the otherwise overwhelming wellbore storage of the one-meter grid). For the aquifer test simulation (step 2) and the estimation of the flow dimension (step 3), a constant-rate well withdrawing at a rate of 0.228 L/sec is assigned to the central node of the grid. The aquifer test simulation consists of a single transient stress period of 345600 seconds, 44 time steps, and a multiplier of 1.3; this was sufficient to reproduce the analytical solution of Theis (1935) for a homogeneous aquifer (see Appendices A and B). Flow dimensions are reported for the pumping well, whose effective radius is approximately 0.1982 m (Peaceman, 1978). The apparent transmissivity of the aquifer test is found using the Cooper-Jacob interpretation method (Cooper and Jacob, 1946), applying linear regression to the linear portion of the drawdown data (between 1.2×10^4 and 5.5×10^4 sec) for an observation well 20.6 m distance from the pumped well. The effective transmissivity (step 4) is estimated by simulating uniform flow across the entire domain using constant-head boundaries on opposing sides to impose a gradient with no-flow boundaries parallel to the gradient. Steady-state flow is

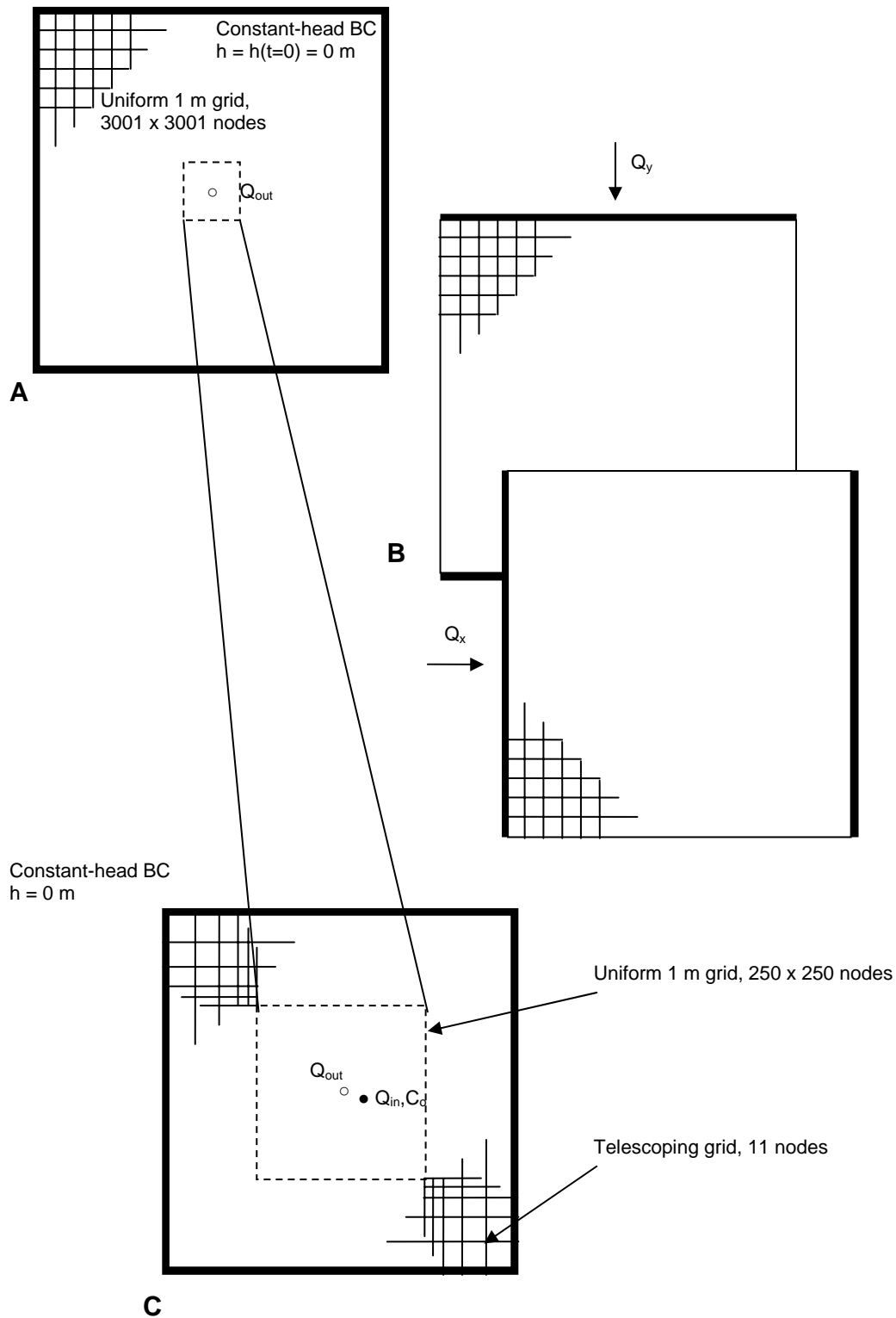


Figure 3. Model schematic and grids. In each realization of transmissivity, grid A simulates transient flow (aquifer test and estimating flow dimension); grid B simulates uniform, steady flow (estimating effective transmissivity); and grid C simulates transport (CFTT). Grids A and B have the same extent, but the center of grid C is from the center of grid A. Figure not to scale.

Table 1. Transport Parameters Used in Simulating the CFTT, after Meigs and Beauheim (2001).

<i>Parameter</i>	<i>Value</i>	<i>Comments</i>
Distance between injection and recovery wells	20.6 m	Similar to H-11b3 to H-11b1 pathway (20.9 m)
Pumping well rate (tracer recovery)	0.233 L/sec	Constant, for duration of simulation
Tracer injection rate	0.0957 L/sec	For 1974 sec, for injected volume of 189 L
Chaser injection rate	0.0976 L/sec	For 3810 sec, for chaser volume of 372 L
Tracer concentration, C_0 (2,3,4,5-TFBA)	10.85 g/L	Total injected mass of 2.049 kg
Aqueous Diffusion Coefficient (2,3,4,5-TFBA)	7.9×10^{-10} m ² /sec	
Formation thickness	4.4 m	
Apparent effective T (interpreted for H-11 b3 (Beauheim and Ruskauff, 1998))	4.70×10^{-5} m ² /sec	After Sánchez-Vila et al. (1999) this study assumes this is T_g , the geometric mean T of the field
Matrix tortuosity	0.1 []	
Matrix porosity	0.16 []	
Fracture (flow) porosity	4×10^{-4} []	

simulated over the domain to determine the one-dimensional flow rate, and the one-dimensional transmissivity estimated using Darcy's law. The exercise is conducted in x and y directions, and the effective transmissivity inferred from the geometric average of the one-dimensional transmissivities.

Figure 3 also shows the grid used for simulating the CFTT (step 5) in a subregion of the heterogeneous field centered on the pumped well. Similar to Altman et al. (2002), the transport grid is a 250 x 250 nodes with one-meter spacing, surrounded by a telescoping mesh of 11 nodes wide and uniform constant-head boundaries. The telescoping region has a homogeneous transmissivity equal to the geometric mean of the heterogeneous field. The transmissivities of the wellbores are multiplied by a factor of 10 for the steady-state flow fields of the CFTT simulation to improve numerical stability and for compatibility with THEM. The simulations mimic the CFTT conducted at the WIPP site at the H-11 hydropad (well cluster), on February 15, 1996. That CFTT used H-11b1 as a pumping well and injected 2,3,4,5- tetrafluorobenzoic acid (TFBA)

into H-11b3 (approximately 20.6 m to the east-southeast). Because the transport time of the test was relatively short, the infinite block approximation was used to represent matrix diffusion. The injected tracer mass was represented by 2,049,000 particles.

Numerical models are susceptible to approximation errors and to artifacts of the finite domain. The flow balance error of MODFLOW-2000 was monitored carefully throughout the study, and in all cases was less than ± 0.05 percent of outflow or inflow. The time discretization for the simulation of the aquifer test was evaluated and refined to match a comparable solution for the homogeneous case (see Appendix B). The impact of the finiteness of the domain was monitored using constant-head boundaries on the exterior of the model; as the cone of depression expands, the model calculates the flow induced from these constant-head nodes. In this study, the total flow from the exterior constant-head boundaries versus the well flow is generally less than the flow balance error of the model, with the exception of the last three or four time steps displayed. The flow dimension values for these last time steps are plotted in the figures to show the effects of the boundary on the flow dimension (an abrupt increase), but these last few values of the flow dimension should be disregarded otherwise. Grid effects can be nontrivial in percolation networks and can overwhelm the results. As suggested by Stauffer and Aharony (1994), the analysis presented herein was checked for grid effects by repeating the flow dimension analyses using a 2001 x 2001 grid of uniform 5-m spacing (h-grid cases). The differences between the average flow dimensions for the 5-m and 1-m grids were typically ± 0.02 , and are otherwise unremarkable. The results for the 5-m grid are not discussed further in this report.

In addition to numerical accuracy, the relative scales of the grid, the stochastic model, and the simulated flow and transport processes have important ramifications for this study. Adequate representation of the stochastic models of heterogeneity requires that the grid be sufficiently dense and extensive with respect to the integral scale, I , the length scale of spatial correlation (Ababou et al., 1988). The (linear) integral scale of the variable u is defined by:

$$I = \int (1 - \gamma_u(h) / \sigma_u^2) dh \quad (3)$$

where the spatial correlation is given by $\gamma_u(h)$, the semivariogram of u , h is the separation distance, and σ_u^2 is the variance of u (Dagan, 1989). For an mvG field of modest variance ($\sigma_{\ln T}^2 < 1.0$), a grid spacing of $\Delta x = 10I$ and an extent of $L = 10I$ will yield estimates of the effective transmissivity with approximately 1 percent error (Meier et al., 1998). The grid spacing in this analysis is $\Delta x = I/7$, which should be sufficiently dense for mvG models of low variance but may be insufficient for larger variances ($\sigma_{\ln T}^2 > 1.0$). The domain used in this analysis is extensive to permit simulating aquifer tests without boundary effects, and is very large relative to the integral scale of the mvG model ($L \approx 429I$). In practical terms, this extensive domain implies that each realization of the transmissivity field is a very large sample of the mvG model, thus the estimates of the geometric mean and semivariogram from each realization will approximate the input parameters (i.e., each realization will be strongly ergodic with respect to the field parameters). Similarly, the aquifer test has a large area of investigation (nearly the entire domain) so that each realization will also be strongly ergodic with respect to the apparent effective T estimated via the Cooper-Jacob method. In contrast, Mishra et al. (1991) have pointed out that tracer tests typically are conducted over much smaller length scales than hydraulic tests,

so that aquifer and tracer tests experience much different kinds of variability. For this study, the representative length scale of the tracer test is 20.6 m, the travel distance from the injection well to the recovery well. Because the integral scale of the mvG model is $I = 7$ m, realizations of the tracer test may not be ergodic and many realizations of the tracer test will be necessary for stable Monte Carlo estimates of the breakthrough curves. The fBm and percolation models also have characteristic length scales that will affect the accuracy and stability of the results; these are discussed in their respective sections of this report.

The Monte Carlo approach is robust, but requires minimizing the computational expense of Monte Carlo realizations (trials) without compromising the stability of the Monte Carlo estimates. This study used 100 realizations for the simulation case of the mvG, fBm, and uncorrelated lognormal models, and 200 realizations for each case of the percolation model. Appendix D shows that the realization arithmetic means, medians, and variances of the apparent flow dimension for mvG with $\sigma_{\ln T}^2 < 1.0$ and the percolation model change only slightly with additional realizations. The differences between the realization arithmetic means and the medians suggest that the flow dimension may have a slightly skewed distribution (to be investigated in future studies). As the duration of the aquifer test increases, the averaging effect of the test increases and the Monte Carlo estimates are stable with even fewer realizations. The median BTCs presented in the main body of the report differ little from the median BTC of 1000 realizations.

Results

Many stochastic models might be considered as possible representations of a heterogeneous field of transmissivity, but the current project considers only four models. As summarized in Table 2, these are the lognormal case, i.e., representing $\ln T(x)$ as a spatially correlated (multivariate) Gaussian (mvG) field; fractional Brownian motion (fBm), which is the mvG model using a power model for the semivariogram with an exponent of 0.5; an approximation of a site percolation network with a percolation probability near the critical threshold; and log Gaussian model, i.e., values of $\ln T(x)$ randomly taken from the normal (Gaussian) distribution with no spatial correlation between finite difference blocks. The research proposal for this project had originally suggested examining the sequential indicator (sIs) model of aquifer heterogeneity, as used by McKenna (2000) in analyses of the WIPP tracer tests. The GSLIB sIs algorithm, *sisim*, is a memory-intensive algorithm whose demand for these large finite-difference grids exceeds that of most individual machines available on the TeraGrid. While it may be possible to modify *sisim* to use less memory or to switch to a more generous computational environment, this could not be accomplished within the project schedule. The log Gaussian model has been substituted in place of the sIs model.

As noted by Neuman (1995), an unconditional fBm field has no defined mean and thus requires at least one conditioning value. For hydrogeologic investigations, this conditioning value logically is located at the pumped well where core testing would provide a transmissivity estimate. For the sake of consistency, all stochastic models examined in this study use a conditioning datum at the pumped well of $T = T_g = 4.70 \times 10^{-5} \text{ m}^2/\text{sec}$. The consequences of this assumption are discussed in the section summarizing the results for the fBm model.

For some systems, the slope of the derivative in the log-log diagnostic plot varies over time, such that the flow dimension varies as the aquifer test evolves. One approach is to plot the apparent flow dimension, $n^* = 2 - 2 \cdot v^*$, versus time, where:

$$v^*(t) = \frac{d}{d(\log t)} \left[\log \left(\frac{ds}{d \ln t} \right) \right] \quad (4)$$

An alternative perspective on the apparent flow dimension would be to plot n^* versus the radius of influence, $r_e^* = \beta(T^* t / S)^{1/2}$ (Strack, 1989). However, cited values for the constant β range widely (Horne, 1995; Oliver, 1990), and the apparent transmissivity, T^* , is ambiguous since the T^* varies with time in the heterogeneous case (Neuman and di Federico, 2003). For the purposes of this study, the apparent flow dimension will be plotted versus time, though we note that this is a topic for future investigation. The results for the flow dimension are presented using log-log diagnostic plots for two randomly selected realizations, and as plots summarizing the realizations with the average (sample arithmetic mean) and 95 percent normal confidence intervals (CI).

Table 2. Summary of Models and Parameters Analyzed in This Study. I is the input linear integral scale, T_g is the input geometric mean of transmissivity, and $\sigma_{\ln T}^2$ is the input variance of $\ln T$. The asterisk (*) denotes the average (arithmetic mean) over all realizations, so that T_g^* is the average of the realization geometric means, T_e^* is the average of the realization effective transmissivity, and T_{CJ}^* is the average of the apparent transmissivity using the Cooper-Jacob interpretation. Altman et al. (2002) inferred values of $4.0 < \sigma_{\ln T}^2 < 16.0$ and $1.875 < I < 15$ m for the Culebra Dolomite at the WIPP site in Carlsbad, New Mexico, USA.

Stochastic Model (algorithm)	Case	$\sigma_{\ln T}^2$	I (m)	T_g^*/T_g	T_e^*/T_g^*	T_{CJ}^*/T_g^*	Comments
mvG (sgsim)	kG2b3	0.0625	7	1.00	0.999	0.998	100 realizations
	kG3b3	0.25	7	1.00	0.995	0.993	100 realizations
	kG4b3	1.0	7	1.00	0.981	0.982	100 realizations (1000 for stability analysis)
	kG6b3	0.25	3.5	1.00	0.991	0.991	100 realizations
	kG5b3	4.0	7	1.00	0.936	0.926	100 realizations
	kG8b3	9.0	7	1.00	0.883	0.852	100 realizations
fBm (sgsim)	kB1b3	NA	NA	1.03	0.997	1.10	$\gamma(h) = 0.027 h^{0.5}$ $\sigma_{\ln T}^2 \approx 1.4$ field wide 100 realizations
Percolation (gsim) Percolating fraction = K_g	kPfb3	20.2	$p = 0.61$	2.75×10^{-2}	0.880	1.06	nonpercolating = $T_g/10^4$ 200 realizations [‡] (654 [‡] of 1000 for stability analysis)
	kPeb3	45.4	$p = 0.61$	4.57×10^{-3}	3.83	5.12	nonpercolating = $T_g/10^6$ 58 [‡] of 100 realizations
	kPcb3	NA	$p = 0.61$	1.00	NA	0.849	Via no-flow cells; T_g^* from flowing cells = T_g 200 realizations [‡]
	kPdb3	20.2	$p = 0.61$	2.75×10^{-2}	0.879	1.09	nonpercolating = $T_g/10^4$ No matrix diffusion 200 realizations [‡]
	kPbb3	20.4	$p = 0.60$	2.51×10^{-2}	0.595	0.839	nonpercolating = $T_g/10^4$ 200 realizations [‡]
Uncorrelated (sgsim)	kN1b3	1.0	< 1 m	1.00	0.875	0.875	
	kN16b3	16.0	< 1 m	1.00	0.445	0.445	

[‡] infinite-acting realizations (trimmed to $0.5 < n^* < 2.5$)

The results of the CFTT are presented as the median (sample median) and 95 percent nonparametric CI for the realizations of the BTC plotted as log relative concentration, C/C_0 [], versus log time in seconds. Nonparametric statistics are used because the BTC distributions are skewed. It should be noted that simply taking the median of the realizations may be misleading; it may be more appropriate to normalize each realization of the BTC to the mean velocity of the realization before pooling the BTC, but this is left to future studies. Similar to other studies (Becker and Shapiro, 2000; Tsang, 1995), this study infers the late-time slope of the BTC by inspection. A procedure to evaluate the statistical significance of the slope estimates for the BTC is being developed, but is unavailable at the time of writing of this report. Except for case kPdb3, all transport simulations in this study include the influence of matrix diffusion. Tsang (1995) concluded that, in the case of matrix diffusion, a log-log BTC is expected to have late-time slopes of $-3/2$, although highly heterogeneous aquifers can obscure this distinctive behavior.

Multivariate Gaussian (mvG)

This stochastic model represents $\ln T(x)$ as a spatially correlated (multivariate) Gaussian variable, denoted mvG. This model commonly is assumed for the spatial variability of transmissivity, and thus warrants a brief evaluation of the effects of its parameters (integral scale and variance). In this study, realizations of the mvG model are created using *sgsim*, a sequential algorithm taken from GSLIB (Deutsch and Journel, 1998), and an exponential model for the semivariogram. The input geometric mean of the transmissivity is $T_g = 4.70 \times 10^{-5}$ m²/sec (Beauheim and Ruskauff, 1998). For a two-dimensional mvG field, Dagan (1989) (citing (Matheron, 1967)) gives the effective transmissivity as $T_e = T_g$, the geometric mean of the field, which this study uses to check the adequacy of the representation of heterogeneity for this model. A series of scoping calculations showed that, for $\sigma_{\ln T}^2 = 1.0$, approximately 7 finite difference nodes per linear integral scale are necessary to reproduce Matheron's solution satisfactorily (i.e., $T_e/T_g \approx 1$). Table 2 indicates that the average geometric mean of the realizations is a good match to the estimated effective transmissivity for modest variances (i.e., $T_e^*/T_g^* = 0.999$ to 0.981 for $\sigma_{\ln T}^2 < 1.0$), and degrades with increasing variance and decreasing integral scale. Likewise, the average apparent transmissivity of the Cooper-Jacob solution is a good estimator of the average geometric mean of the realizations for modest variances (i.e., $T_{CJ}^*/T_g^* = 0.998$ to 0.982 for $\sigma_{\ln T}^2 < 1.0$).

The central case for the mvG model is kG3b3, with $\sigma_{\ln T}^2 = 0.25$ and $I = 7$ m. The apparent flow dimension of aquifer tests in this stochastic model gradually stabilizes to a value of $n^* = 2$ (Figure 4a). The variability between realizations decreases with time (Figure 4b), suggesting that any aquifer test in an mvG field will tend to show $n = 2$ if the test is of sufficient duration that the scale of the test (radius of investigation) is greater than the spatial scale of the heterogeneity (the integral scale). Comparing cases kG2b3, kG3b3, and kG4b3 (Figures 5, 4 and 6, respectively, in order of increasing variance), the variability of the apparent flow dimension generally increases with the variance of $\ln T$.

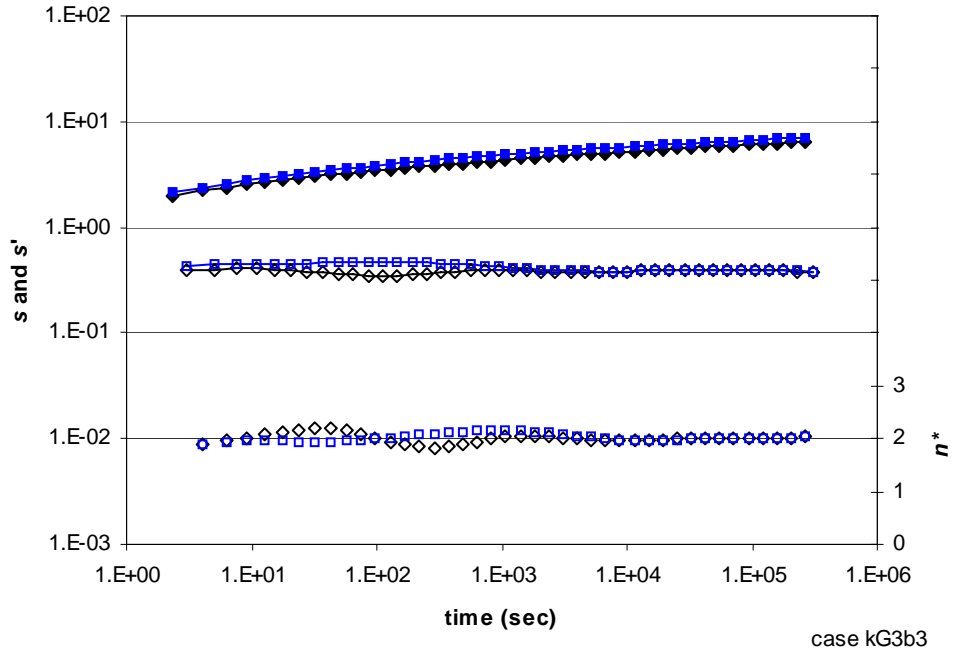


Figure 4a. Drawdown (closed symbols), derivative (open symbols with line), and flow dimension (open symbols without line) for two realizations of case kG3b3: mvG with $\sigma^2_{\ln T} = 0.25$ and $I = 7$ m; symbol shapes denote realizations.

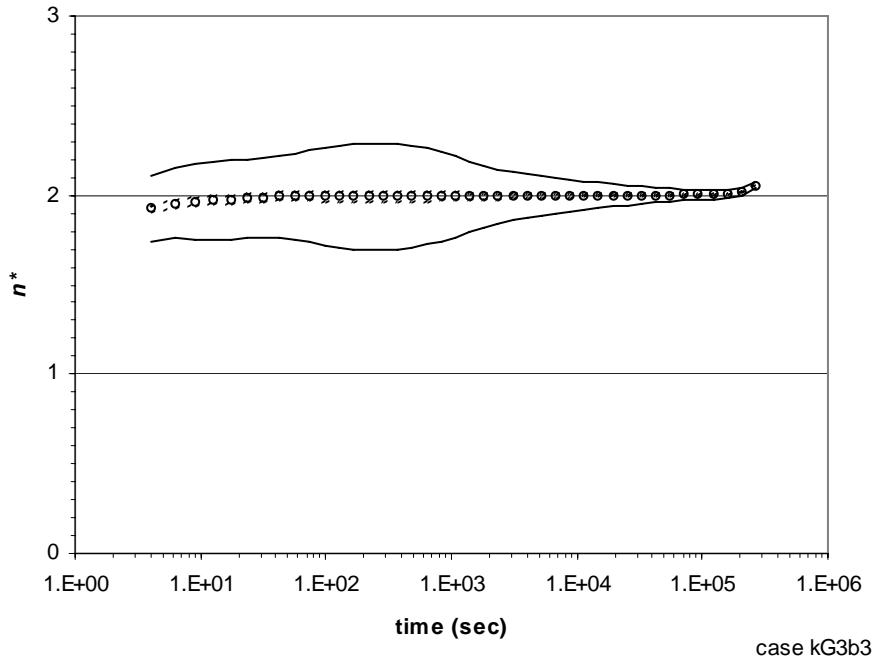


Figure 4b. Average (circle) and 95 percent normal CI for the population (solid lines) and for the mean (dashed lines) for 100 realizations of the flow dimension, case kG3b3: mvG with $\sigma^2_{\ln T} = 0.25$ and $I = 7$ m.

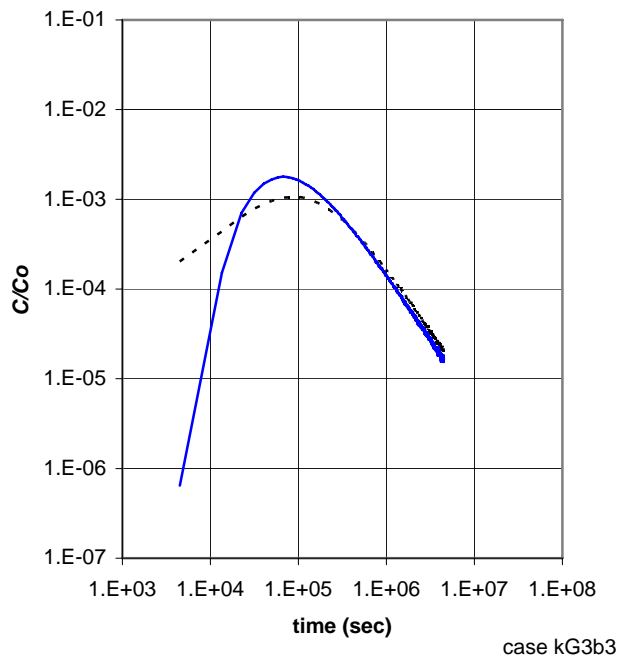


Figure 4c. Relative concentration versus time for a CFTT in two realizations of case kG3b3: mvG with $\sigma_{\ln T}^2 = 0.25$ and $I = 7$ m.

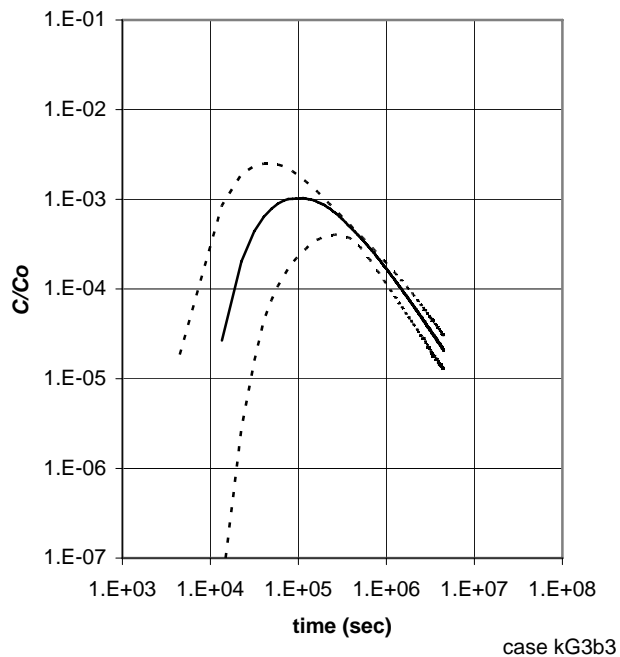


Figure 4d. Relative concentration versus time for 100 realizations of a CFTT, median (solid line) and 95 percent nonparametric CI for the population (dashed lines), case kG3b3: mvG with $\sigma_{\ln T}^2 = 0.25$ and $I = 7$ m.

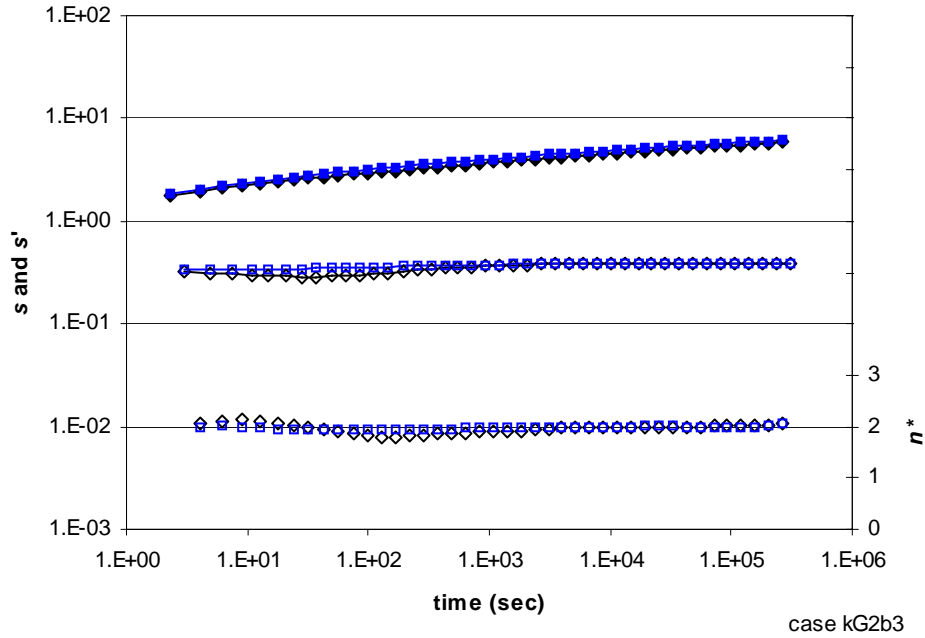


Figure 5a. Drawdown (closed symbols), derivative (open symbols with line), and flow dimension (open symbols without line) for two realizations of case kG2b3: mvG with $\sigma^2_{\ln T} = 0.0625$ and $I = 7$ m; symbol shapes denote realizations.

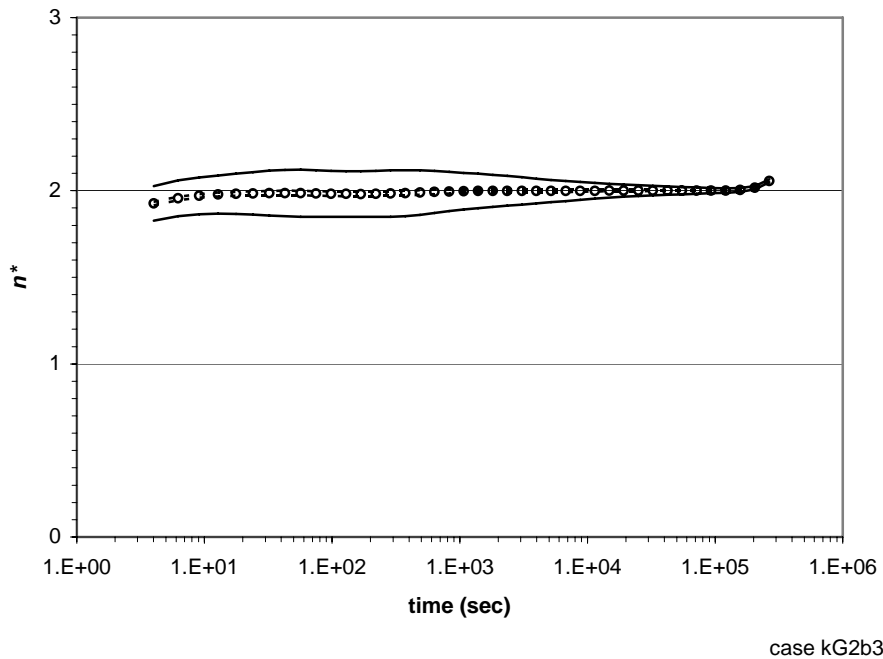


Figure 5b. Average (circle) and 95 percent normal CI for the population (solid lines) and for the mean (dashed lines) for 100 realizations of the flow dimension, case kG2b3: mvG with $\sigma^2_{\ln T} = 0.0625$ and $I = 7$ m.

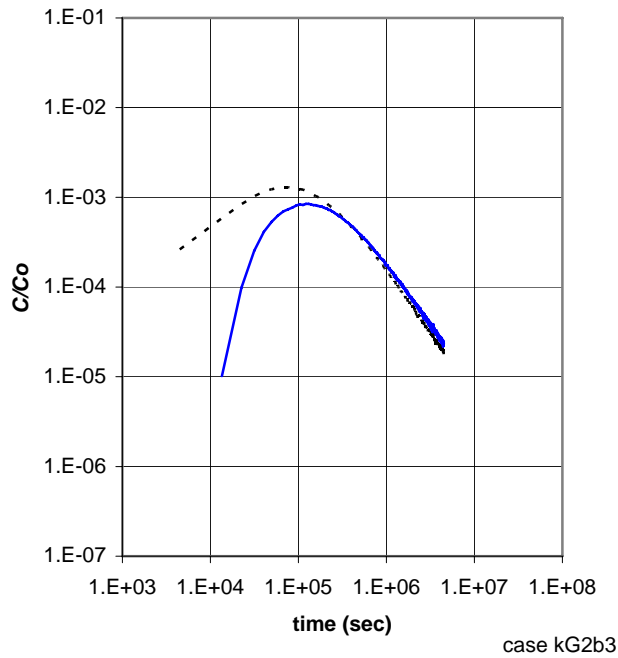


Figure 5c. Relative concentration versus time for a CFTT in two realizations of case kG2b3: mvG with $\sigma_{\ln T}^2 = 0.0625$ and $I = 7$ m.

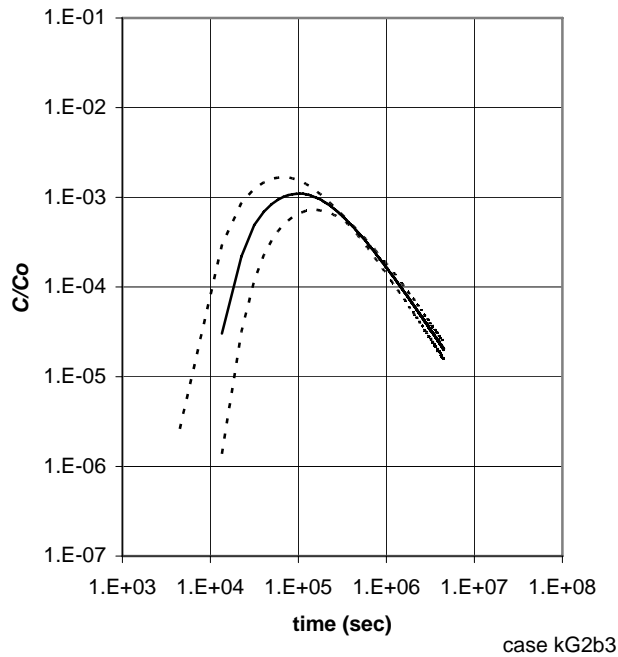


Figure 5d. Relative concentration versus time for 100 realizations of a CFTT, median (solid line) and 95 percent nonparametric CI for the population (dashed lines), case kG2b3: mvG with $\sigma_{\ln T}^2 = 0.0625$ and $I = 7$ m.

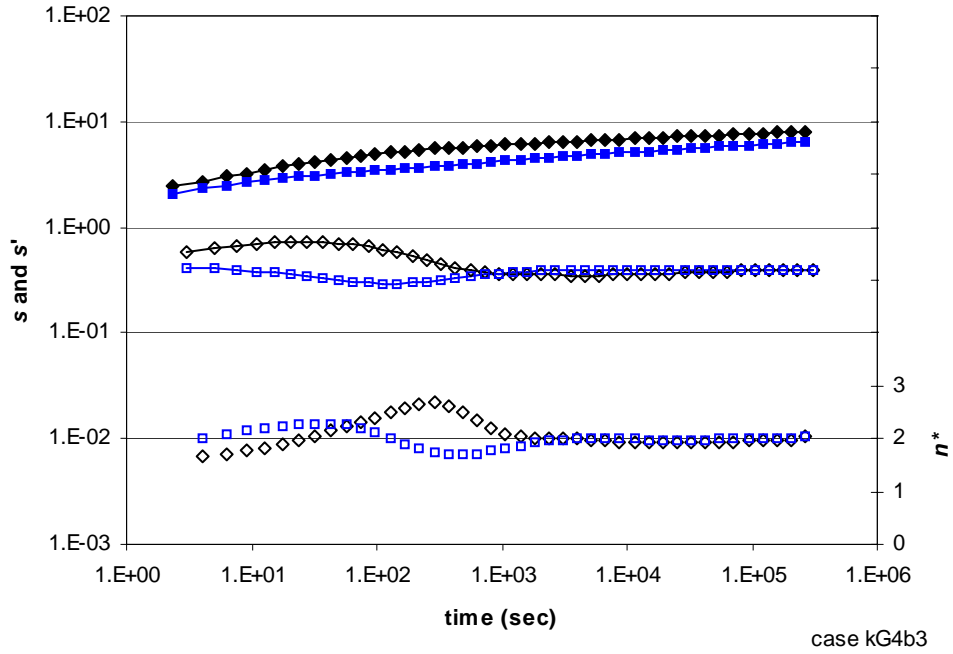


Figure 6a. Drawdown (closed symbols), derivative (open symbol with line), and flow dimension (open symbols without line) for two realizations of case kG4b3: mvG with $\sigma_{\ln T}^2 = 1.0$ and $I = 7$ m; symbol shapes denote realizations.

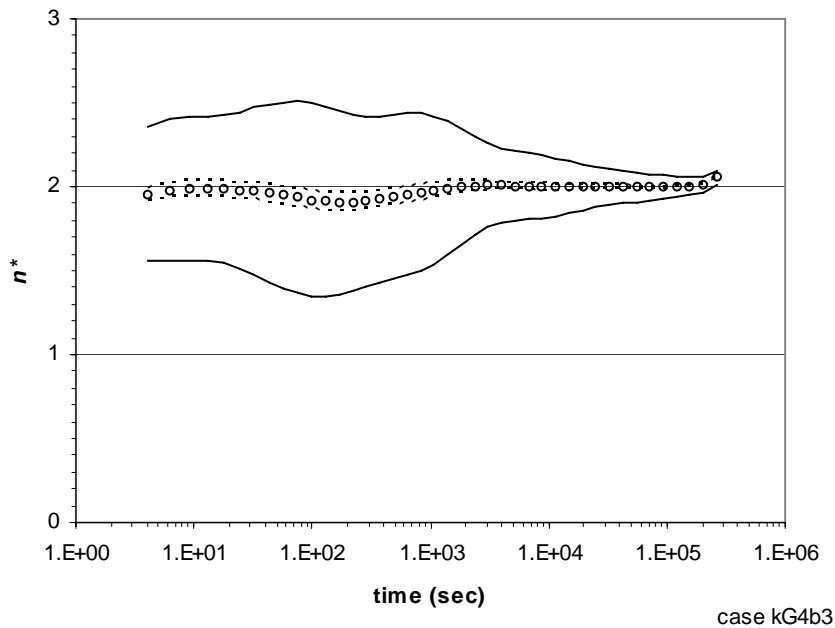


Figure 6b. Average (circle) and 95 percent normal CI for the population (solid lines) and for the mean (dashed lines) for 100 realizations of the flow dimension, case kG4b3: mvG with $\sigma_{\ln T}^2 = 1.0$ and $I = 7$ m.

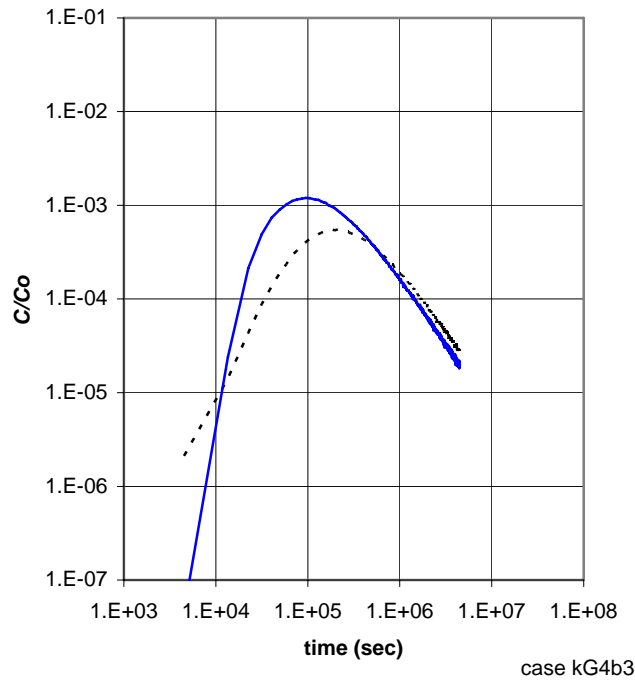


Figure 6c. Relative concentration versus time for a CFTT in two realizations of case kG4b3: mvG with $\sigma_{\ln T}^2 = 1.0$ and $I = 7$ m.

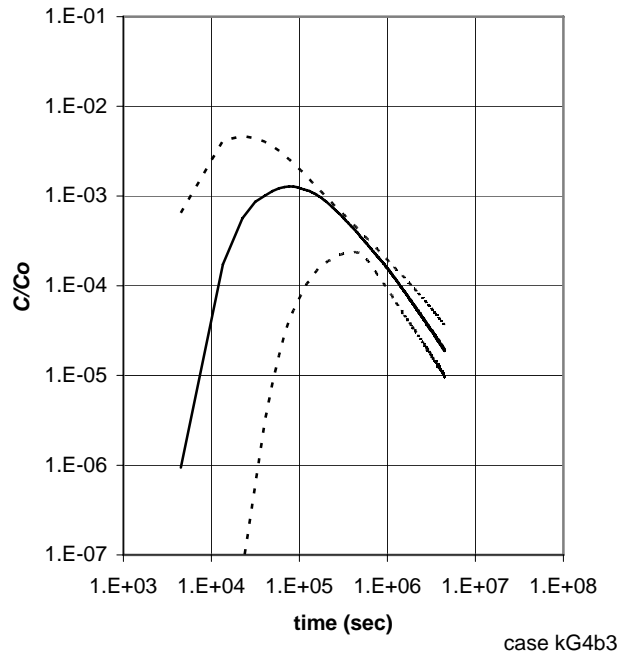


Figure 6d. Relative concentration versus time for 100 realizations of a CFTT, median (solid line) and 95 percent nonparametric CI for the population (dashed lines), case kG4b3: mvG with $\sigma_{\ln T}^2 = 1.0$ and $I = 7$ m.

Case kG6b3 (Figure 7) examines the effects of changing the integral scale of the mvG model while keeping $\sigma_{\ln T}^2$ unchanged. Reducing the integral scale from $I = 7$ m (Figures 4b) to $I = 3.5$ m (Figure 7b) results in a more rapid decrease in the variability of the flow dimension. Comparing Figures 5b, 4b, and 6b, the maximum variability of the apparent flow dimension occurs at approximately the same time, regardless of $\sigma_{\ln T}^2$. Comparing Figures 4b and 7b, it can be seen that this maximum variability shifts earlier in time with a decrease in the integral scale.

Figure 4c presents two realizations of the BTC for the CFTT of the central case of the mvG model (case kG3b3, with $\sigma_{\ln T}^2 = 0.25$ and $I = 7$ m). Both realizations eventually approach the characteristic $-3/2$ slope of matrix diffusion (Tsang, 1995), although their early arrival times differ substantially. Figure 4d presents the median and the upper and lower percentiles of the 95 percent nonparametric CI for the BTC of 100 realizations. The median BTC also approaches the characteristic $-3/2$ slope of matrix diffusion, and the confidence interval (CI) is widest for the early arrival times. Figures 5d, 4d, and 6d show that increasing the variance tends to increase the width of the confidence intervals for the BTC, but Figure 7d shows that decreasing the integral scale has little effect on the appearance of the median BTC. Table 3 summarizes the peak median relative concentration, C/C_{0p} , and t_p , the time to C/C_{0p} , for each case. These suggest that, as the variance of $\ln T$ increases, t_p decreases — that is, a higher variance yields earlier arrival times (cases kG2b3, kG3b3, and kG4b3). The decrease in t_p with the integral scale (case kG3b3 versus kG6b3) is attributed to the combination of scale and variance: the CFTT scale (20.6 m) is only three times greater than the integral scale for the base case, and decreasing the integral scale to $I = 3.5$ m increases the variability sampled by the CFTT. The increasing level of heterogeneity adds regions of high transmissivity that become fast pathways that channel flow between the injection well to the pumping well, decreasing t_p from 1.31 days to 1.09 days.

Two cases are simulated for the mvG model for relatively high variances, examining $\sigma_{\ln T}^2 = 4.0$ (case kG5b3) and $\sigma_{\ln T}^2 = 9.0$ (case kG8b3). The apparent flow dimensions of aquifer tests in these cases (Figures 8a and 9a) have a higher variability than the mvG cases of lower variance, but the variability between realizations still decreases over time and the apparent flow dimension converges to a value of $n^* = 2$ (Figures 8b and 9b). Unlike the mvG cases of lower variances, the average of the apparent flow dimension is significantly less than $n^* = 2$ at early time, and the degree of departure increases with the variance. Table 2 indicates that Matheron's relationship is only weakly satisfied for $\sigma_{\ln T}^2 = 4.0$ where $T_e^*/T_g^* = 0.936$, and is poorly satisfied for $\sigma_{\ln T}^2 = 9.0$ where $T_e^*/T_g^* = 0.883$. The average apparent transmissivities of the Cooper-Jacob solution are poor estimators of the estimated effective transmissivities (i.e., $T_{CJ}^*/T_e^* = 0.926$ and 0.852 for $\sigma_{\ln T}^2 = 4.0$ and $\sigma_{\ln T}^2 = 9.0$, respectively).

These high-variance cases continue the trend in the level of disagreement with Matheron's relationship $T_e = T_g$ that was established by cases kG2b3, kG3b3, and kG4b3 (Table 2). As noted in the "Approach" section, this is comparable to the results of other investigators and with scoping calculations that suggest 7 to 10 nodes per integral scale and an extensive domain are necessary to estimate the effective transmissivity 1 percent error for modest variances ($\sigma_{\ln T}^2 < 1.0$) (Meier et al., 1998). While modifying the grid or redesigning the problem to solve for a quadrant of the domain (under the assumption of radial symmetry) might reduce this error, these are extensive efforts and are outside the scope of this study. In the interim, we

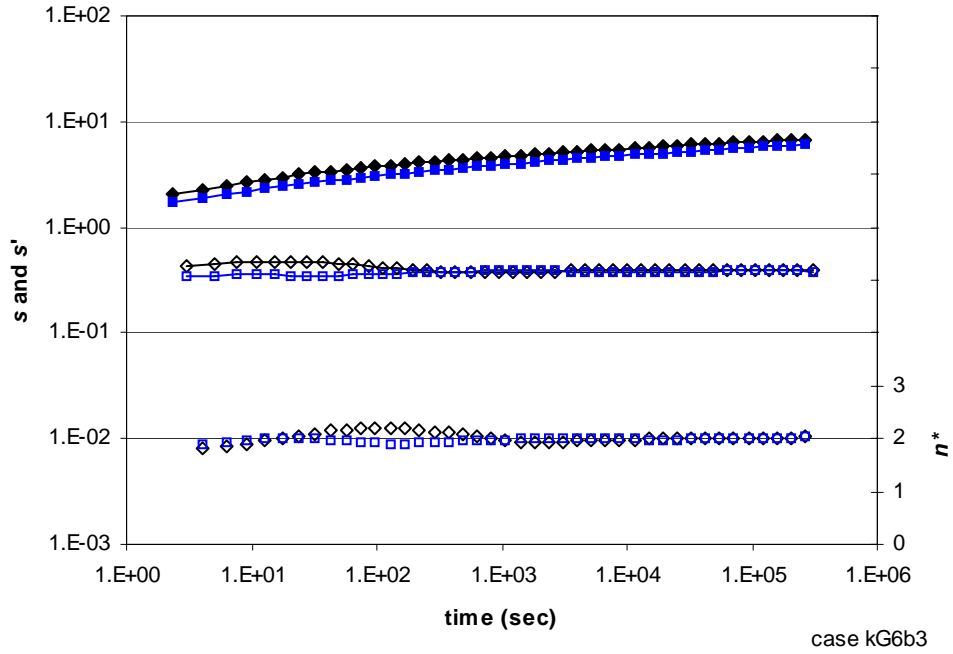


Figure 7a. Drawdown (closed symbols), derivative (open symbols with line), and flow dimension (open symbols without line) for two realizations of case kG6b3: mvG with $\sigma^2_{\ln T} = 0.25$ and $I = 3.5$ m; symbol shapes denote realizations.

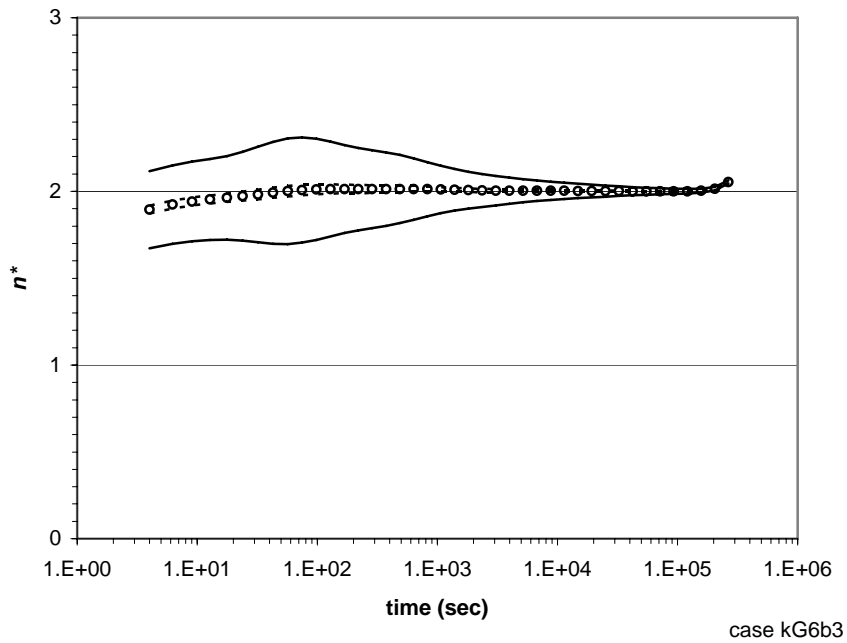


Figure 7b. Average (circle) and 95 percent normal CI for the population (solid lines) and for the mean (dashed lines) for 100 realizations of the flow dimension, case kG6b3: mvG with $\sigma^2_{\ln T} = 0.25$ and $I = 3.5$ m.

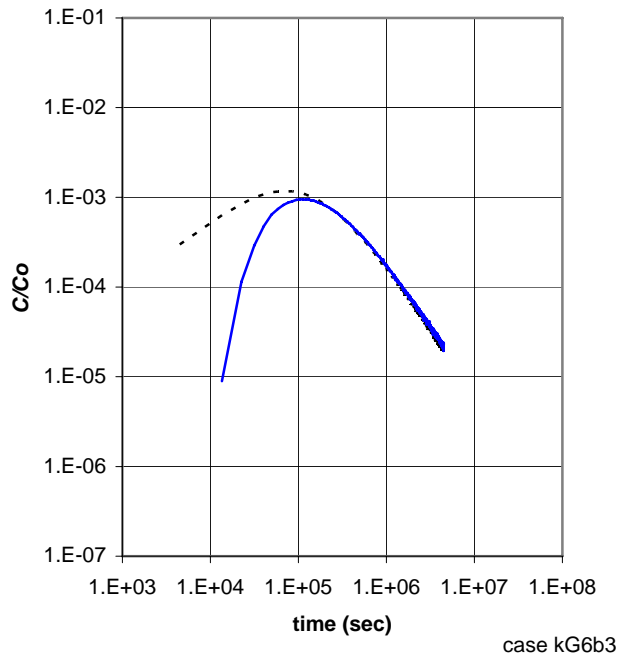


Figure 7c. Relative concentration versus time for a CFTT in two realizations of case kG6b3: mvG with $\sigma_{\ln T}^2 = 0.25$ and $I = 3.5$ m.

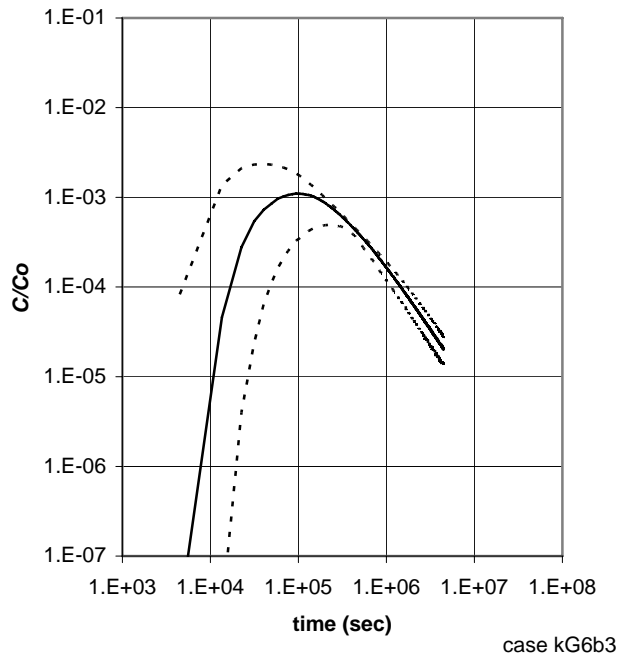


Figure 7d. Relative concentration versus time for 100 realizations of a CFTT, median (solid line) and 95 percent nonparametric CI for the population (dashed lines), case kG6b3: mvG with $\sigma_{\ln T}^2 = 0.25$ and $I = 3.5$ m.

Table 3. Summary of CFTT Results by Model. Note: I is the linear integral scale, $\sigma_{\ln T}^2$ is the variance of the natural logarithm of transmissivity, C/C_{0p} is the peak of the median relative concentration, and t_p is the time to the peak of the median relative concentration.

<i>Stochastic Model (algorithm)</i>	<i>Case</i>	$\sigma_{\ln T}^2$	I (m)	t_p (days)	C/C_{0p}	<i>Late-time slope of log-log median BTC (Comments)</i>
mvG (sgsim)	kG2b3	0.0625	7	1.20	1.10×10^{-3}	-3/2
	kG3b3	0.25	7	1.31	1.03×10^{-3}	-3/2
	kG4b3	1.0	7	0.885	1.28×10^{-3}	-3/2
	kG6b3	0.25	3.5	1.09	1.10×10^{-3}	-3/2
	kG5b3	4.0	7	0.885	8.86×10^{-4}	-5/4
	kG8b3	9.0	7	0.260	2.00×10^{-3}	-5/4
fBm (sgsim)	kB1b3	NA	NA	1.09	1.19×10^{-3}	-3/2
Percolation (gsim)	kPfb3	20.2	$p = 0.61$	0.156	5.74×10^{-3}	-5/4
	kPeb3	45.4	$p = 0.61$	0.156	7.45×10^{-3}	-3/2 < slope < -5/4 (Particles lost)
	kPcb3	NA	$p = 0.61$	0.05^*	1.01×10^{-2}	-3/2
	kPdb3	20.2	$p = 0.61$	0.05^*	7.69×10^{-2}	-2 (No matrix diffusion)
	kPbb3	20.4	$p = 0.60$	0.156	5.27×10^{-3}	> -5/4
Uncorrelated (sgsim)	kN1b3	1.0	< 1 m	0.990	1.12×10^{-3}	-3/2
	kN16b3	16.0	< 1 m	0.260	1.97×10^{-3}	-3/2 < slope < -5/4

* the peak relative concentration occurs on or before the first arrival time of this case

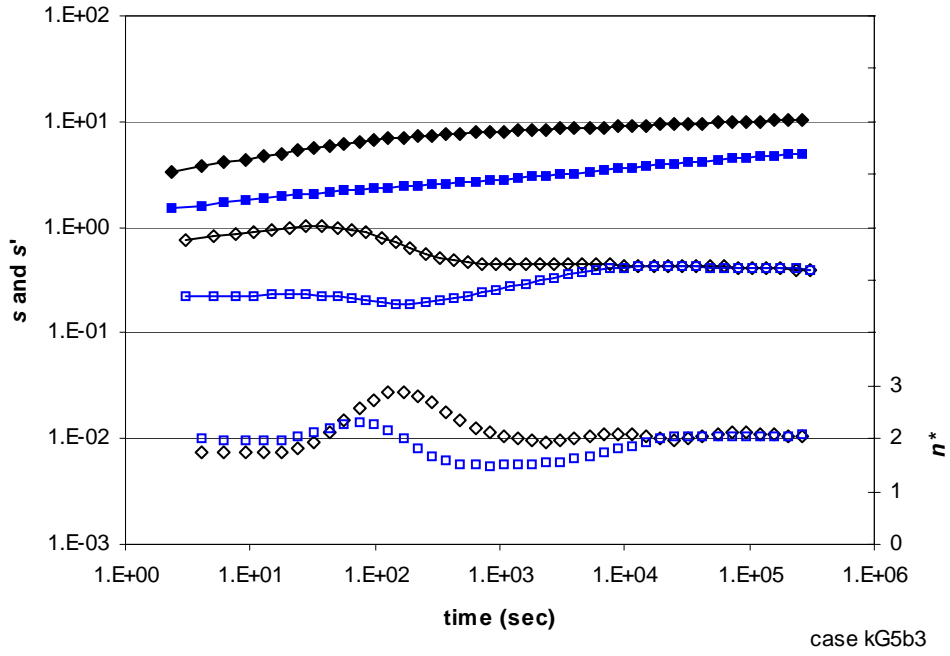


Figure 8a. Drawdown (closed symbols), derivative (open symbols with line), and flow dimension (open symbols without line) for two realizations of case kG5b3: mvG with $\sigma^2_{\ln T} = 4.0$ and $I = 7$ m; symbol shapes denote realizations.

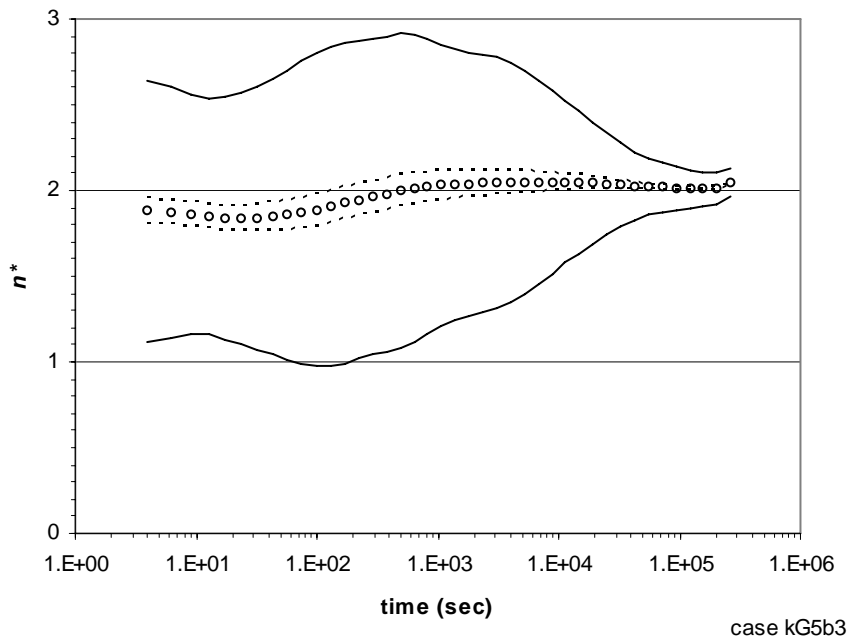


Figure 8b. Average (circle) and 95 percent normal CI for the population (solid lines) and for the mean (dashed lines) for 100 realizations of the flow dimension, case kG5b3: mvG with $\sigma^2_{\ln T} = 4.0$ and $I = 7$ m.

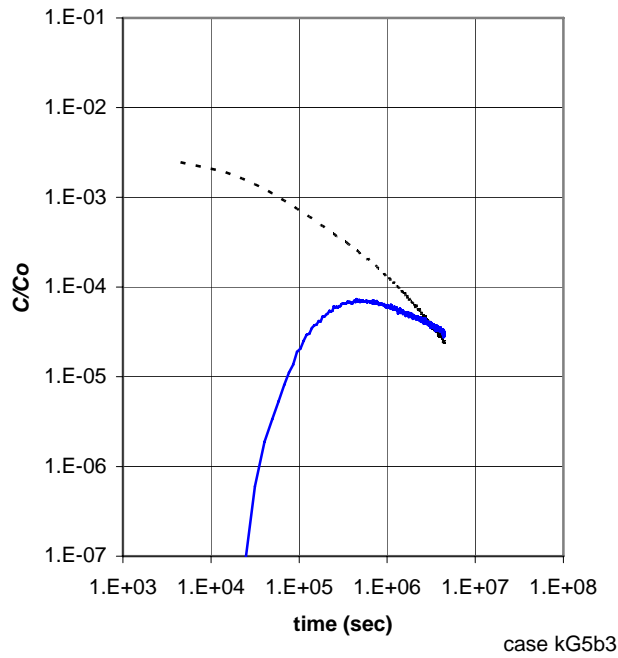


Figure 8c. Relative concentration versus time for a CFTT in two realizations of case kG5b3: mvG with $\sigma_{\ln T}^2 = 4.0$ and $I = 7$ m.

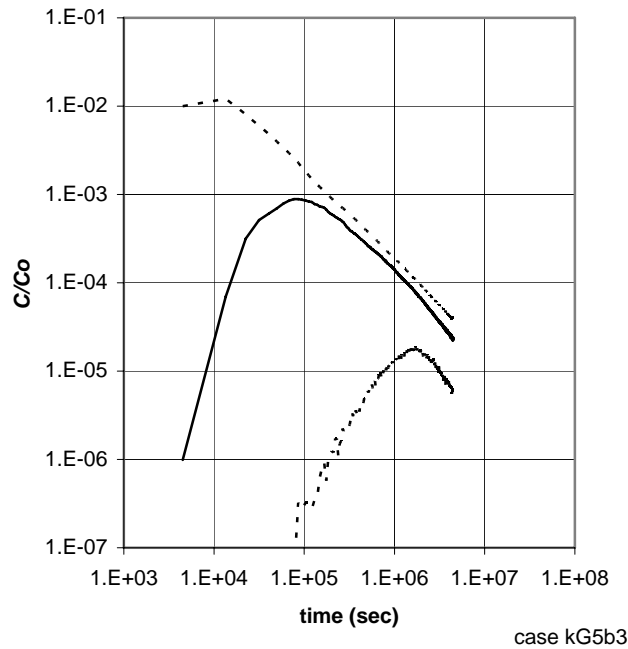


Figure 8d. Relative concentration versus time for 100 realizations of a CFTT, median (solid line) and 95 percent nonparametric CI for the population (dashed lines), case kG5b3: mvG with $\sigma_{\ln T}^2 = 4.0$ and $I = 7$ m.

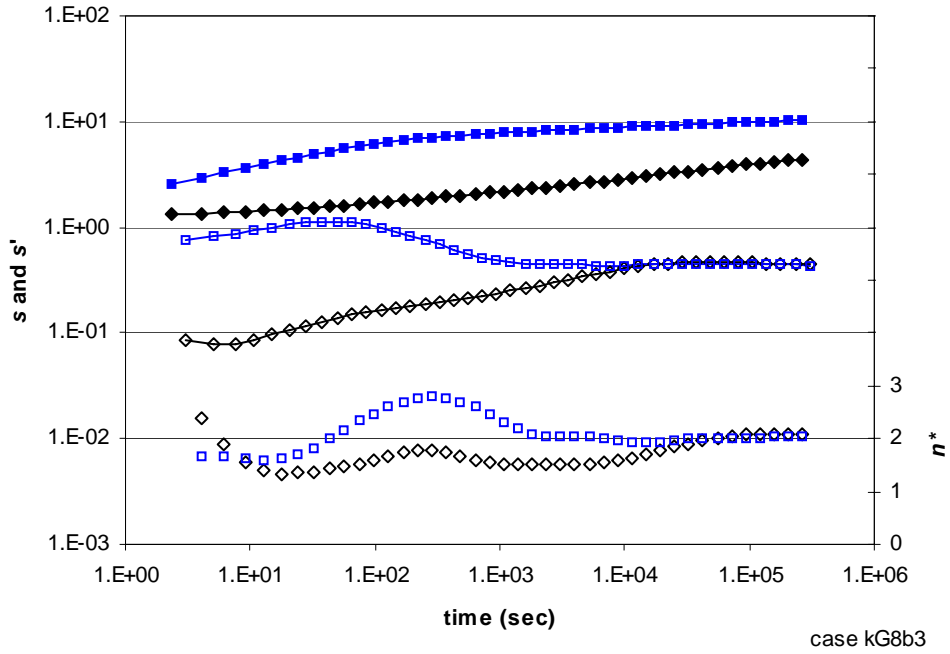


Figure 9a. Drawdown (closed symbols), derivative (open symbols with line), and flow dimension (open symbols without line) for two realizations of case kG8b3: mvG with $\sigma^2_{\ln T} = 8.0$ and $I = 7$ m; symbol shapes denote realizations.

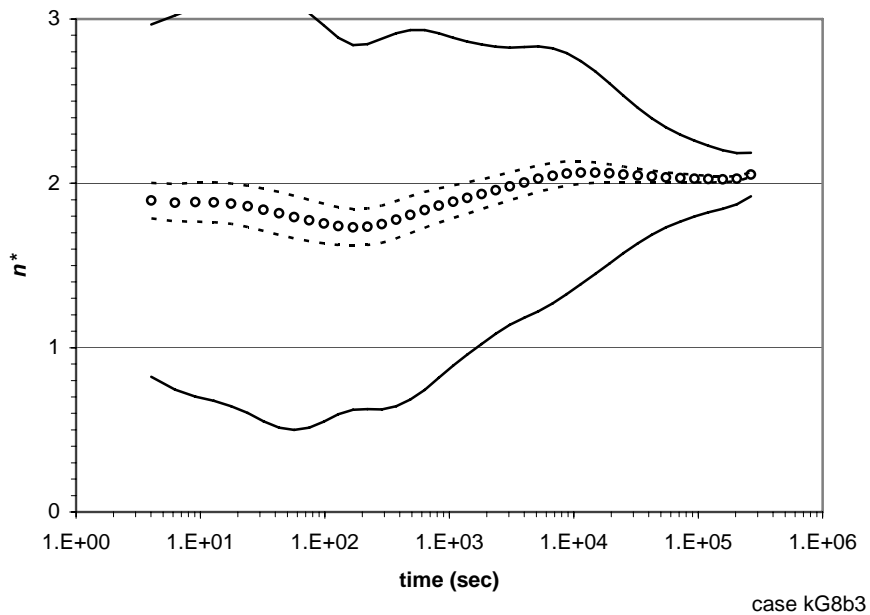


Figure 9b. Average (circle) and 95 percent normal CI for the population (solid lines) and for the mean (dashed lines) for 100 realizations of the flow dimension, case kG8b3: mvG with $\sigma^2_{\ln T} = 9.0$ and $I = 7$ m.

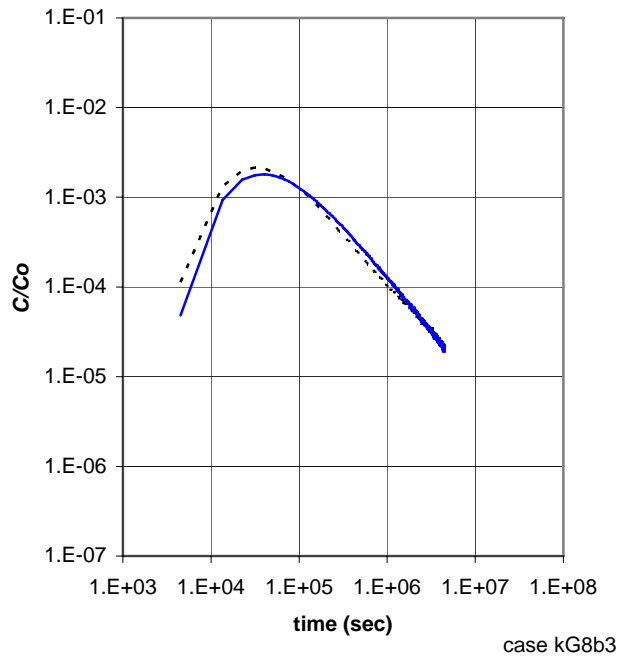


Figure 9c. Relative concentration versus time for a CFTT in two realizations of case kG8b3: mvG with $\sigma_{\ln T}^2 = 9.0$ and $I = 7$ m.

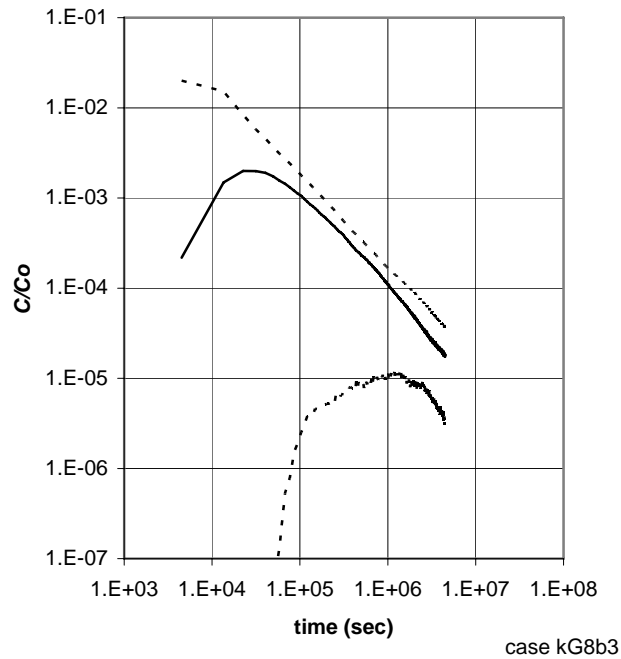


Figure 9d. Relative concentration versus time for 100 realizations of a CFTT, median (solid line) and 95 percent nonparametric CI for the population (dashed lines), case kG8b3: mvG with $\sigma_{\ln T}^2 = 9.0$ and $I = 7$ m.

speculate that the decrease in the apparent flow dimension at early times in the high-variance cases quantifies the development of flow channeling with increasing variance as discussed by Moreno and Tsang (1994). The similarities between the apparent flow dimensions of the high-variance mvG cases and the percolation network are discussed in subsequent sections of this report.

Figures 8c and 9c present two realizations of the BTC for the CFTT of these higher-variance cases of the mvG model. The early arrival times of the realizations show a high degree of variability. Figures 8d and 9d present the median and the upper and lower percentiles of the 95 percent nonparametric CI for 100 realizations of the relative BTC. Although the process of matrix diffusion is included in these simulations, the slope of last log cycle of the median BTC has an approximate slope of $-5/4$, rather than the $-3/2$ slope that is characteristic of matrix diffusion. A comparison of Figures 5d, 4d, 6d, 8d and 9d shows that increasing the variance from $\sigma_{\ln T}^2 = 0.0625$ to $\sigma_{\ln T}^2 = 9.0$ increases the width of the confidence intervals. Table 3 summarizes the peak median relative concentration, C/C_{0p} , and t_p , the time to C/C_{0p} , for these cases. As with the low-variance cases, t_p generally decreases with increasing variance. However, the previously noted inconsistencies with Matheron's relationship suggest that the calculations for the high-variance cases should be refined before further conclusions can be drawn. Additional statistical analysis is also warranted for the significance of the average flow dimension from $n^* = 2$ at early time.

Fractional Brownian Motion (fBm)

This stochastic model represents $\ln T(x)$ as fractional Brownian motion (fBm), and can be viewed as a variant of the mvG model that uses a power model for the semivariogram:

$$\gamma(h) = C_1 h^{2H} \quad (5)$$

where $\gamma(h)$ is the semivariogram of $\ln T(x)$, h is the absolute separation (lag) distance between two points x_1 and x_2 , H is the Hurst coefficient, and C_1 is a scaling constant. The fBm model also can be shown to be a special case of the fractional Levy motion model (Lu et al., 2003). Neuman (1990; 1994) has argued that the observed scale dependence of contaminant transport in the subsurface arises from hydraulic conductivities distributed as a fBm process, and has used observations and theory to argue that $H = 0.25$ and $C_1 = 0.027$. The same model semivariogram with slightly different coefficients also has been proposed for the Culebra Dolomite at the WIPP site (Grindrod and Impey, 1993).

The distinguishing characteristic of fBm is that its variability increases with the size of the field to the power $2H$, creating special challenges for numerical analysis. Strictly speaking, fBm is an infinite fractal process that cannot be represented by a discretized, finite domain. Further, because the sequential simulation algorithm requires a finite variance, the distributed version of *sgsim* does not accept the power model (Equation 5) as a valid semivariogram (Deutsch and Journel, 1998). Similar to Meier et al. (1998), *sgsim* has been modified to accept a power semivariogram model with the maximum variance equal to Equation 5 at h_{\max} for the model domain, i.e., $\sigma_{\ln T}^2 \approx 1.4$.

The numerical challenges in creating this field suggest that at least some checks are necessary to confirm that the variance scales appropriately. Figure 10 is a log-log plot of the resulting experimental semivariogram for one realization of *sgsim* using $H = 0.25$ and $C_1 = 0.027$ in a domain of 3001 m x 3001 m. The departure from the ideal slope of $2H = 0.5$ at the furthest lags may be as much a reflection of the finite field effect as it is the inefficiency of the experimental semivariogram for separations greater than $h_{\max}/3$. Although the field truncates the fBm process at the smallest and largest scales, this method of generating an fBm process is consistent with previous investigations and approximately reproduces the required semivariogram. It would be useful to compare the effective transmissivity and the variance to the solutions of, e.g., di Federico and Neuman (1997), and should rerun the simulation using a more robust simulation algorithm designed for the fBm process, e.g., Lu et al. (2003), but such analyses are beyond the scope of the present study.

As noted in the “Approach” section, one conditioning value is required for the fBm model to have a defined mean, and this value is located at the pumped well (and, for consistency, in all the stochastic models analyzed in this study). This conditioning value and the shape of the semivariogram model force the variability of the fBm process to be small near the well and increase slowly and continuously with distance from the well. This radial change in the variability of the fBm transmissivity field is reflected in the increasing variability of the drawdown and of the apparent flow dimension with time (Figures 11a and b). The increasing variability of the apparent flow dimension is the opposite of the behavior observed for the mvG model of roughly comparable field-wide variance (Figure 6b). For mvG model, the scale of the

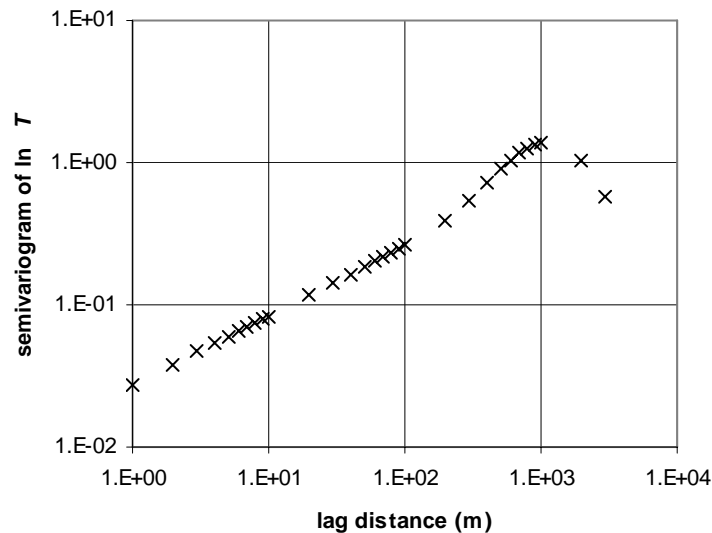


Figure 10. Experimental semivariogram for one realization of $\ln T$ as an fBm process, $H = 0.25$.

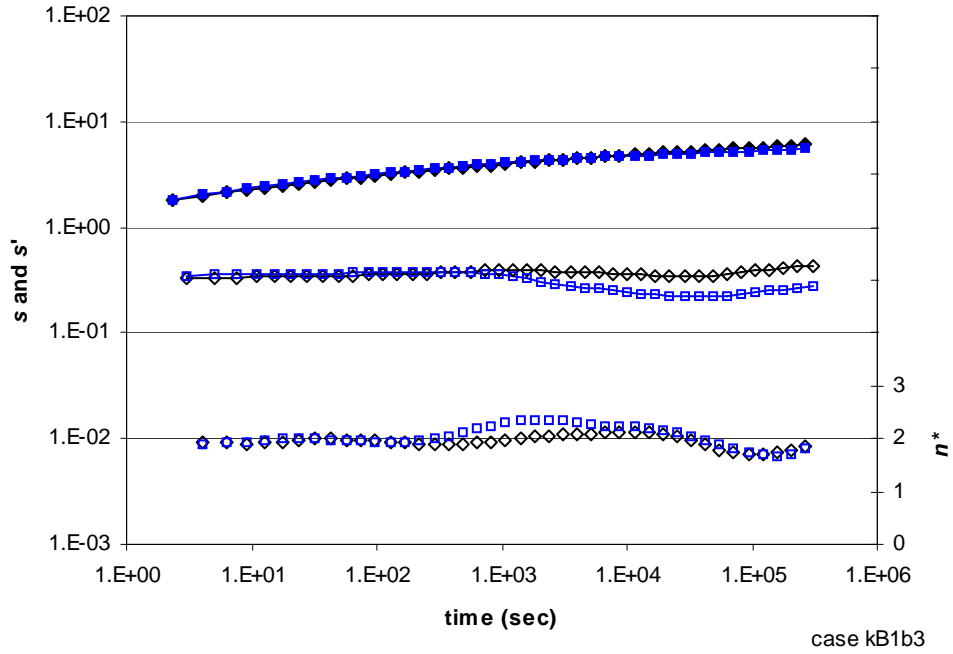


Figure 11a. Drawdown (closed symbols), derivative (open symbol with line), and flow dimension (open symbols without line) for two realizations of case kB1b3: fBm with $H = 0.25$; symbol shapes denote realizations.

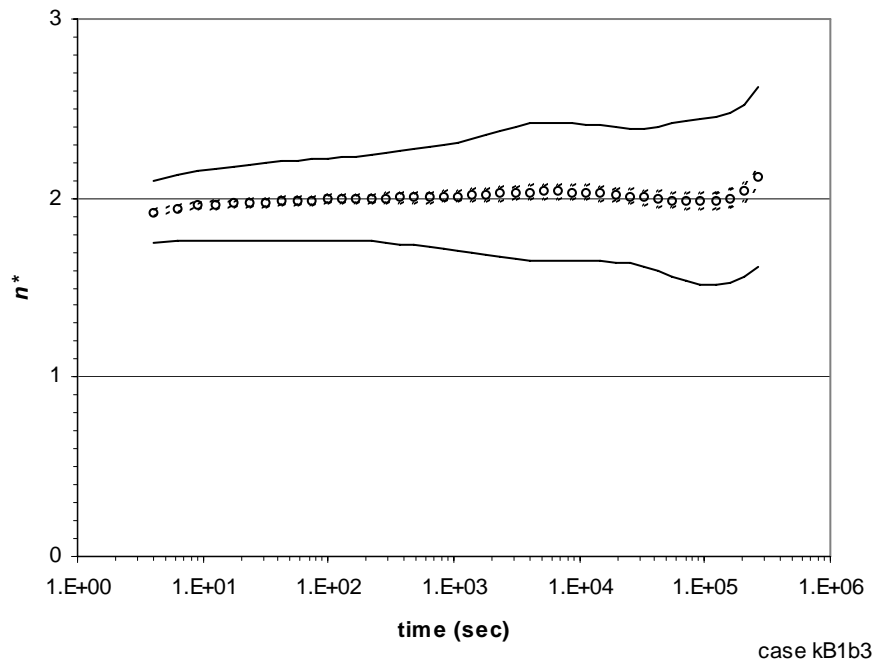


Figure 11b. Average (circle) and 95 percent normal CI for the population (solid lines) and mean (dashed lines) for 100 realizations of the flow dimension, case kB1b3: fBm with $H = 0.25$.

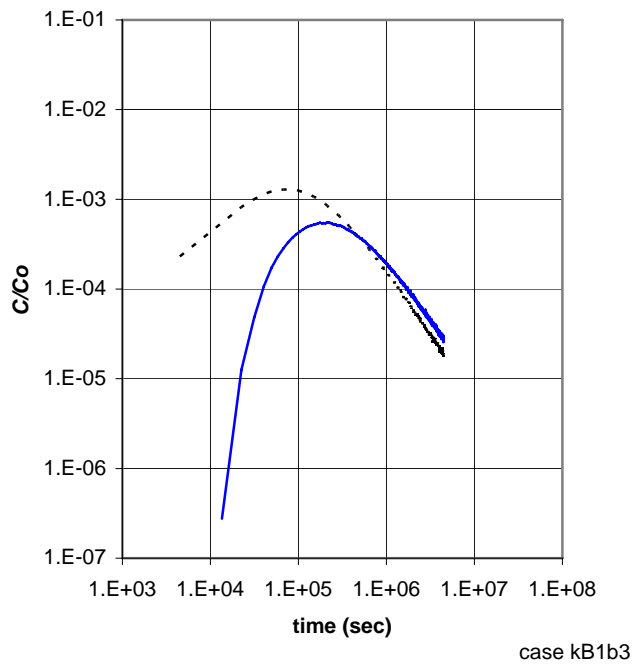


Figure 11c. Relative concentration versus time for a CFTT in two realizations of case kB1b3: fBm with $H = 0.25$.

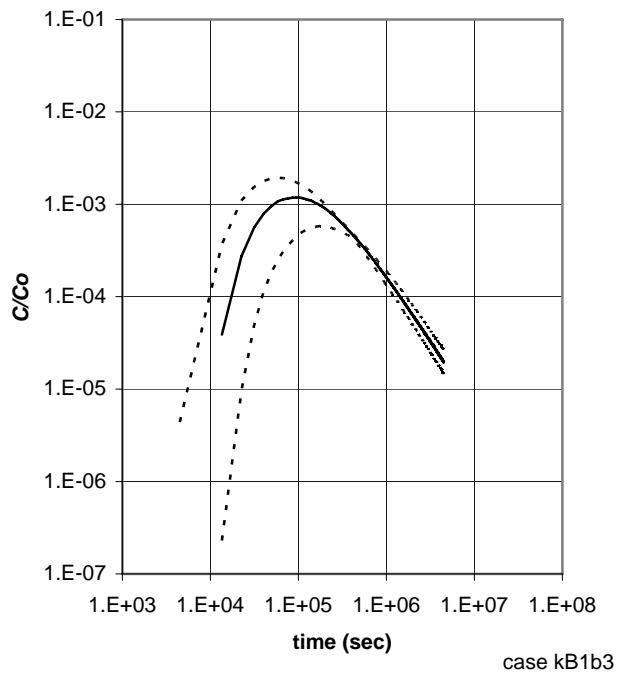


Figure 11d. Relative concentration versus time for 100 realizations of a CFTT, median (solid lines) and 95 percent nonparametric CI for the population (dashed lines), case kB1b3: fBm with $H = 0.25$.

aquifer test is much larger than the integral scale, so that the averaging effects of the aquifer test increase (and the variability of the apparent flow dimension decreases) with time. For the fBm model, the integral scale is infinite, and the aquifer test encounters increasing levels of heterogeneity with time. This difference between the models suggests that the variability of the apparent flow dimension with time might be useful in distinguishing between the fBm and mvG models, given a sufficiently large set of aquifer tests. Further, because the mvG cases show that the variability of the apparent flow dimension depends on the variance of the transmissivity, it may be possible to infer the exponent of the power semivariogram (i.e., infer the Hurst coefficient of the fBm model) from the increasing variability with time of the apparent flow dimension. Table 2 indicates that the average geometric mean of the realizations for the fBm model is a good match to the estimated effective transmissivity (i.e., $T_e^*/T_g^* = 0.997$). The average apparent transmissivity of the Cooper-Jacob solution is a relatively poor estimator of the average geometric mean of the realizations (i.e., $T_{CJ}^*/T_g^* = 1.10$).

The results of the CFTT for the fBm model are characteristic of transport influence by matrix diffusion in a transmissivity field of low variance. Similar to the low-variance cases of the mvG model, the fBm model results in a BTC with a log-log slope at late time of approximately $-3/2$ for individual realizations (Figure 11c) and for the median BTC (Figure 11d). Figure 11d shows that the early arrival times of a CFTT in the fBm model have noticeably less variability than those of the mvG model with a comparable field-wide variance (e.g., Figure 6d). These differences between the CFTT in the mvG and fBm cases can be explained by noting that the conditional variance of the simulated transmissivity fields is, by definition, zero at a conditioning value (in this study, located at the withdrawal well). This variance increases with distance from the single conditioning value at a rate prescribed by their respective semivariogram models (Deutsch and Journel, 1998). At the scale of the CFTT (travel distance of 20.6m), the power semivariogram for the fBm model reaches a maximum of $\gamma(h) = C_1 h^{2H} = 0.027 \cdot 21^{2(0.25)} \approx 0.12$, while the exponential semivariogram for the comparable mvG model (case kG4b3) reaches a maximum of $\gamma(h) = C_1 [1 - \exp(-h/I)] = 1.0 \cdot [1 - \exp(-20.6/7)] \approx 0.95$. That is, the fBm model is less heterogeneous at the CFTT scale than the comparable mvG model, resulting in less flow channeling, later arrival times, and less variability between realizations.

Percolation Network

The third model considered in this study is a percolation network, a model sometimes used by physicists and petroleum engineers as a representation of a porous medium (Feder, 1988). In its purest form, a percolation network has a single parameter, p , the probability that a location in a lattice is able to conduct flow. As the probability of being conductive increases to the critical probability, p_c , the interconnected clusters of the network finally grow large enough to span the domain and flow can percolate across the system. Percolation clusters with $p \approx p_c$ have been shown to have fractal geometries, and are the subject of much study (Isichenko, 1992; Saadatfar and Sahimi, 2002; Stauffer and Aharony, 1994). Polek (1990) numerically simulated hydraulic tests in a percolation network and found that the flow dimension reaches a value slightly less than the mass fractal dimension of the percolation cluster, a result that is consistent with that of Acuna and Yortsos (1995).

MODFLOW-2000 uses a node-centered finite difference grid, which in percolation network terms is a quadratic, site-percolation network with $p_c \approx 0.593$ (Stauffer and Aharony, 1994). A percolation network can be approximated by assigning a random proportion p of the grid to be percolating nodes with transmissivity T_p , and the remaining (nonpercolating) nodes set to the value $T_{1-p} \ll T_p$. This renders the $1-p$ nonpercolating nodes as relatively impermeable, similar to the intact rock within a fractured rock aquifer. For this study, $T_p = T_g = 4.70 \times 10^{-5}$ m²/sec and the nonpercolating nodes are set to $T_{1-p} = T_p / 10^4$, with $p = 0.61$. The resulting fields have a geometric mean $T = 1.294 \times 10^{-6}$ m²/sec and $\sigma_{\ln T}^2 = 20.2$. Because $p = 0.61$ is slightly greater than p_c , the resulting field should have fractal characteristics. The choices of contrast in transmissivity and percolation probability are evaluated further through sensitivity cases. The *gsim* algorithm creates a percolation network as a categorical indicator simulation with a cutoff proportion p and no spatial correlation. The node representing the pumping well is always a percolating node in these simulations, but it is not a conditioning value in the same sense as a spatially correlated model of heterogeneity such as mvG.

Feder (1988) and Stauffer and Aharony (1994) have noted that percolation networks also have a correlation length, ξ_p , defined for a two-dimensional lattice as:

$$\xi_p = \Delta x \cdot |p - p_c|^{-4/3} \quad (6)$$

At length scales between Δx and ξ_p , a percolation network has fractal properties; at scales greater than ξ_p , a percolation network appears to be homogeneous and behaves as a two-dimensional field (Polek, 1990). Substituting the constants used in this percolation network model yields $\xi_p = 230$ m, a distance that is much less than the radial distance from the well to the edge of the domain (1500 m). As noted earlier, the radius of influence of an aquifer test is poorly defined, making it difficult to use Equation 6 in practice. However, the mvG cases indicate that the drawdowns of the aquifer test are approaching the model boundaries, so it is possible that the test scale will be greater than ξ_p . This does not invalidate the percolation network model, but suggests that a transition might be observable in the apparent flow dimensions of the percolation network.

Figure 12a presents the results for the apparent flow dimension of 1000 realizations of a percolation network simulated with the above parameters. The variability of the apparent flow dimension among realizations is quite high, and some realizations show a wide range of values. Figure 12b illustrates two realizations whose apparent flow dimensions range from less than 0.5 to over 6.0. These realizations are of wells pumped in small, finite percolation clusters, whose apparent flow dimensions are overwhelmed by the aquifer test contacting the limits of the cluster. Such finite clusters behave as small reservoirs with slightly permeable boundaries; the reservoir is rapidly drawn down, then registers the flow through the boundaries from the surrounding clusters. The apparent flow dimensions in these finite clusters are consistent with the analytical solutions for idealized impermeable boundaries and leaky systems (Walker and Roberts, 2003), and also are consistent with some aquifer tests in highly heterogeneous formations (R. Roberts, Personal Communication, 2005).

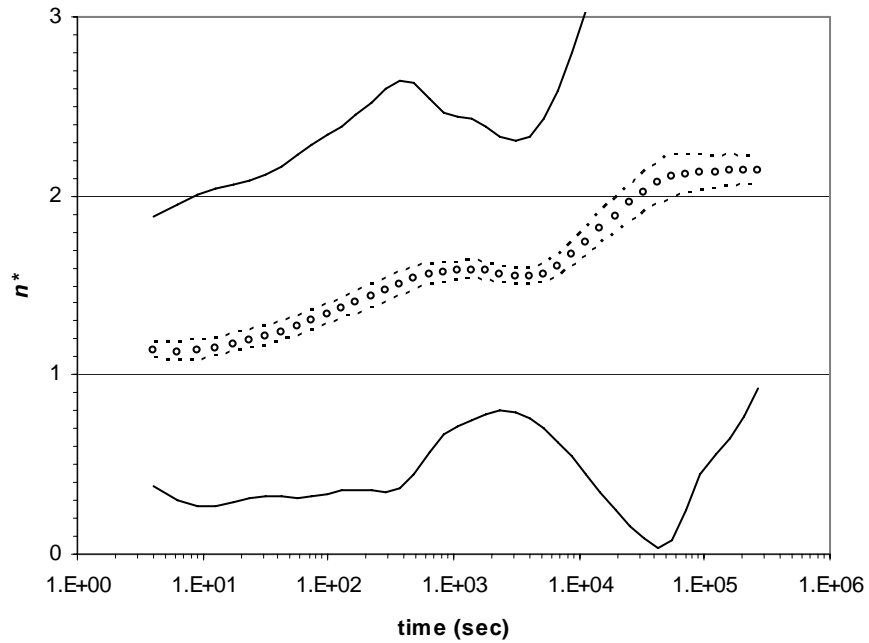


Figure 12a. Average (circle) and 95 percent normal CI for the population (solid lines) and mean (dashed lines) for 1000 realizations of the flow dimension, case kPfb3: percolation with $p = 0.61$, $T_{1-p} = T_p / 10^4$, no trimming; symbol shapes denote realizations.

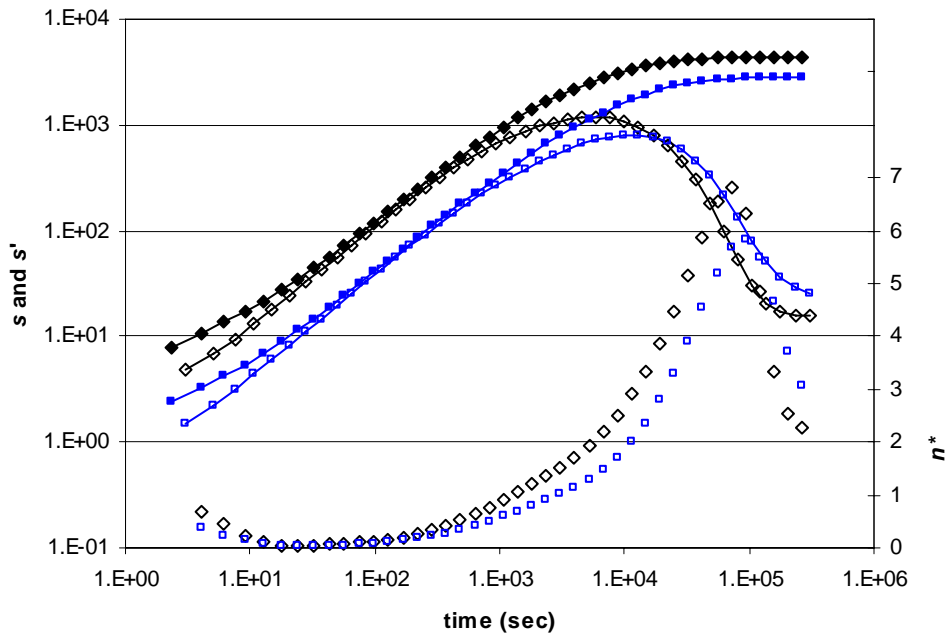


Figure 12b. Drawdown (closed symbols), derivative (open symbols with line), and flow dimension (open symbols without line) for two realizations outside $0.5 < n^* < 2.5$, case kPfb3: percolation with $p = 0.61$, $T_{1-p} = T_p / 10^4$; symbol shapes denote realizations.

The small, finite percolation clusters indicated by near-zero values of the flow dimension (Figure 12b) present several challenges to the application of this stochastic model to a real aquifer. Realizations with the pumping well falling into a small, finite cluster are consistent with field experiments, since tracer tests sometimes fail to recover the injected tracer and observation wells sometimes fail to respond during an aquifer test. However, these isolated regions occur randomly in a percolation network, and the realizations dominated by internal boundaries of the cluster limits reveal little about the structure of a percolation cluster. Doughty et al. (1994) have experimented with adding connections to a fractal network, but this remains an area for further research. Feder (1988) notes that the probability of being in a finite cluster and can be estimated from p and p_c , yet even a finite percolation cluster can yield valid estimates of the flow dimension if the cluster is larger than the radius of investigation of the aquifer test. For the present study, we use extreme values of the apparent flow dimension to identify finite clusters and omit them from the statistical summaries and plots. Inspecting 1000 realizations, the lower and upper bounds of the 95 percent nonparametric confidence interval (CI) for the apparent flow dimension are approximately 0.5 and 2.5, respectively. These values are used as trimming limits to filter out realizations of the well being pumped within finite clusters, i.e. the Monte Carlo analysis for this stochastic model is conducted until a sufficient number of realizations are accumulated with apparent flow dimensions inside the range $0.5 < n^* < 2.5$ for all time steps. As discussed in the “Approach” section and shown in Appendix D, 200 realizations are sufficient for the purposes of this study.

Figure 13a presents the drawdown, the derivative, and the apparent flow dimension for two of the 200 realizations for case kPfb3. The slopes and variability of these simulated tests are similar to those of aquifer tests observed in fractured dolomite aquifers (Figure 1). Figure 13b presents the statistics of the apparent flow dimension for the 200 realizations. The average of the apparent flow dimension is similar to that of the full set of 1000 realizations (Figure 12a), but removes the extremes at early and late times. The average apparent flow dimension appears to slowly increase, oscillates around the value 1.6, then steadily increases to approach the value $n^* = 2.0$. Table 2 indicates that the estimated effective transmissivity of the field is a poor match to the average of the geometric mean of transmissivity (i.e., $T_e^*/T_g^* = 0.880$). This is not necessarily cause to doubt the validity of these simulations, since Matheron’s solution of $T_e = T_g$ for a two-dimensional domain also assumed the mvG model for transmissivity. The average apparent transmissivity of the Cooper-Jacob solution is a comparatively good match (i.e., $T_{CJ}^*/T_g^* = 1.059$).

The CFTT simulation for this case (kPfb3) yields several results of note. Figure 13c presents two realizations of the BTC, which gradually settle into slopes $> -3/2$. These characteristics are also reflected in the statistics of the 200 realizations (Figure 13d), whose confidence intervals have a wide range at early times, and the median BTC reaches a slope of approximately $-5/4$. This slope is greater than the $-3/2$ slope that Tsang (1995) reported for transport influenced by matrix diffusion, indicating that the heterogeneity of this stochastic model is increasing the tailing behavior. Subsequent cases attempt to determine if the $-5/4$ slope is a hallmark of percolation networks in general or a consequence of the chosen parameters (e.g., the contrast in transmissivity). Arrival times tend to be shorter than in the mvG case, with $t_p =$

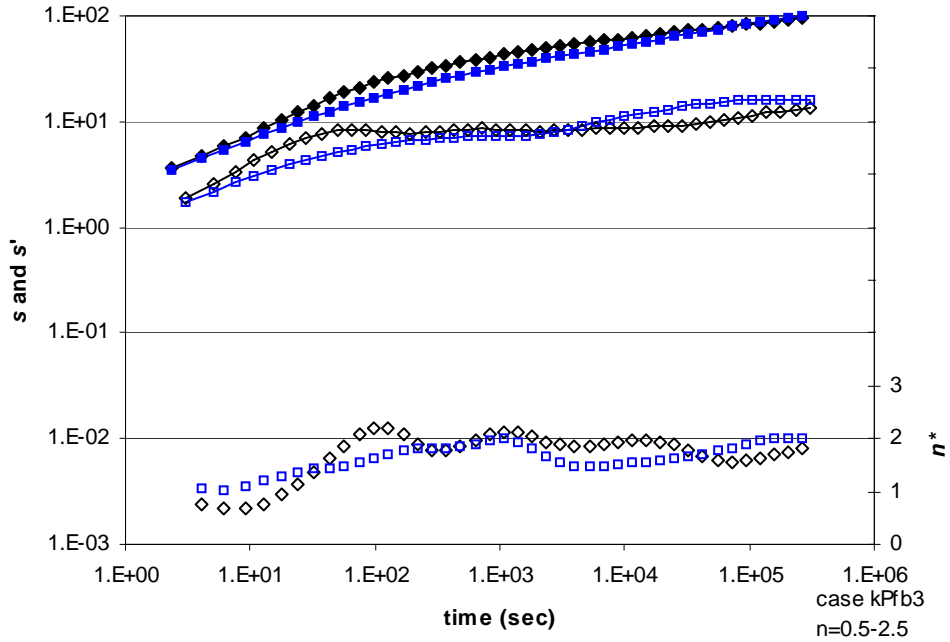


Figure 13a. Drawdown (closed symbols), derivative (open symbols with line), and flow dimension (open symbols without line) for two realizations $0.5 < n^* < 2.5$, case kPfb3: percolation with $p = 0.61$, $T_{l-p} = T_p / 10^4$; symbol shapes denote realizations.

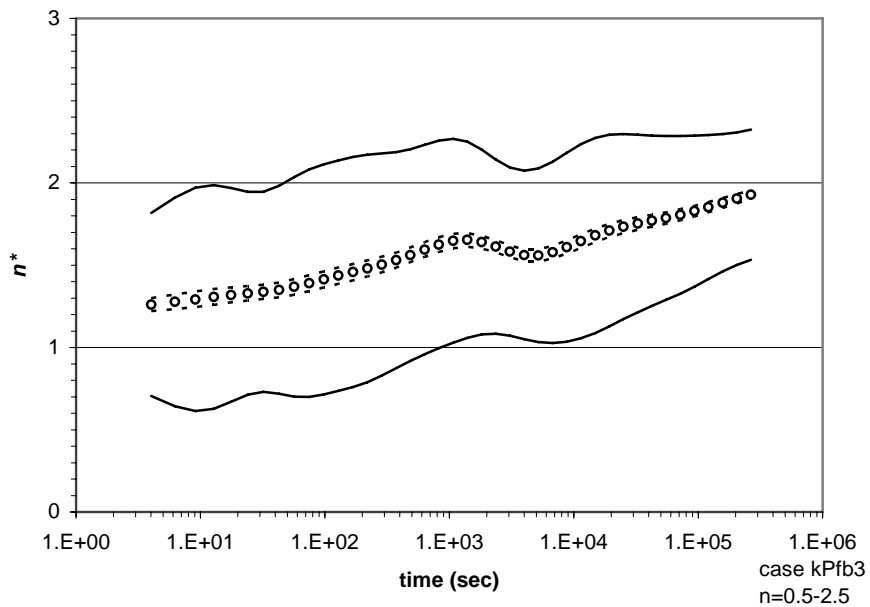


Figure 13b. Average (circle) and 95 percent normal CI for the population (solid lines) and mean (dashed lines) flow dimension for 200 realizations $0.5 < n^* < 2.5$, case kPfb3: percolation with $p = 0.61$, $T_{l-p} = T_p / 10^4$.

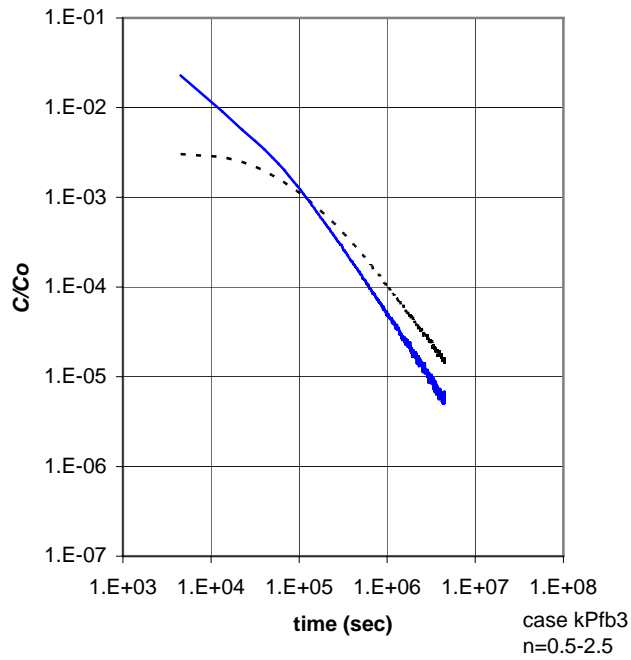


Figure 13c. Relative concentration versus time for a CFTT in two realizations with $0.5 < n^* < 2.5$, case kPfb3: percolation with $p = 0.61$, $T_{1-p} = T_p / 10^4$.

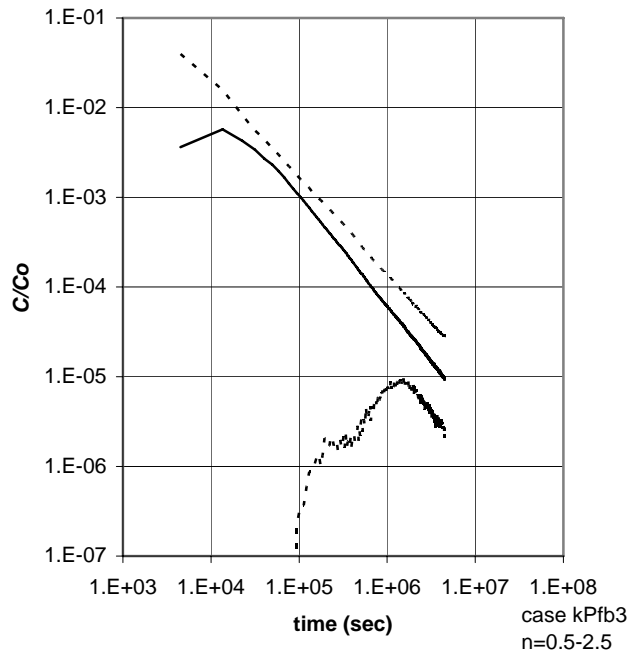


Figure 13d. Relative concentration versus time of a converging flow tracer test for 200 realizations with $0.5 < n^* < 2.5$, median (solid line) and 95 percent nonparametric CI for the population (dashed lines), case kPfb3: percolation with $p = 0.61$, $T_{1-p} = T_p / 10^4$.

0.156 days. At the lower bound of the 95 percent confidence interval, some realizations show extremely slow tracer recoveries; if these were data from a field study, they might be overlooked and an observer would conclude that the tracer had been lost.

The first variant case of the percolation network model, case kPgb3, simply turns off the constant-head boundaries on the exterior of the model to rule out boundary effects. Specifically, this case tests the hypothesis that contact with the constant-head boundaries is the cause of the increasing trend in the apparent flow dimensions (Figure 13b). This variant (case kPgb3, not presented) showed no change in the results, thus the increasing trend in the average of the apparent flow dimension is not caused by the constant-head boundaries.

The next variant of the percolation network model, case kPeb3, increases the transmissivity contrast between the percolating and nonpercolating nodes from $T_{l-p} = T_p / 10^4$ (as in kPfb3) to $T_{l-p} = T_p / 10^6$. The reduced transmissivity for the nonpercolating nodes results in extremely slow simulations, with each realization requiring 25-43 hours of CPU time. As a consequence, only 100 realizations could be completed, with 58 of these within the trimming limits $0.5 < n^* < 2.5$. Figures 14a and 14b show that increasing the contrast reduces the apparent flow dimension in general. The average of the apparent flow dimension at early time oscillates around $n^* = 1.4$, and the width of the confidence intervals is approximately the same as when using a contrast of 10^4 (case kPfb3). The reduced number of realizations make the late-time slope of the median BTC less obvious (Figures 14c and 14d), but the slope with this increased contrast is still noticeably less steep than the characteristic $-3/2$ slope of matrix diffusion alone (Tsang, 1995). The lower bound for the nonparametric CI is below the scale of the plot for this case (Figure 14d) and warning messages are recorded in many realizations because particles have become trapped in cells with inflow but no outflow. In this instance, the advective particle tracking fails due to local mass balance errors (even though the global mass balance error is < 0.05 percent). These nonexiting particles are only a small portion of the injected mass, but might be important at the lowest relative concentrations at late times. It may be possible to refine the particle tracking algorithm to address this problem, but such modifications are beyond the scope of this study.

Variant case kPcb3 uses no-flow cells for the impermeable nodes rather than a contrast in transmissivity, making this case more like an idealized percolation network. This is done using the IBOUND array (part of the input parameters for MODFLOW-2000) to designate a $1-p$ proportion of the nodes as no-flow cells. Unfortunately, multigrid algorithms such as the GMG solver of MODFLOW-2000 are unsuited to discontinuous domains (S. Mehl, Personal Communication, 2004), requiring this case to use the less-efficient PCG2 solver. Despite the change of solvers, the transient solution becomes numerically unstable as radius of influence encounters the uniform constant-head boundaries. The problem is made tractable by reducing the simulated duration of the aquifer test (the pumping period length) by several time steps, and omitting the estimation of the effective transmissivity under uniform flow conditions. The analysis is otherwise unchanged relative to case kPfb3, with $p = 0.61$.

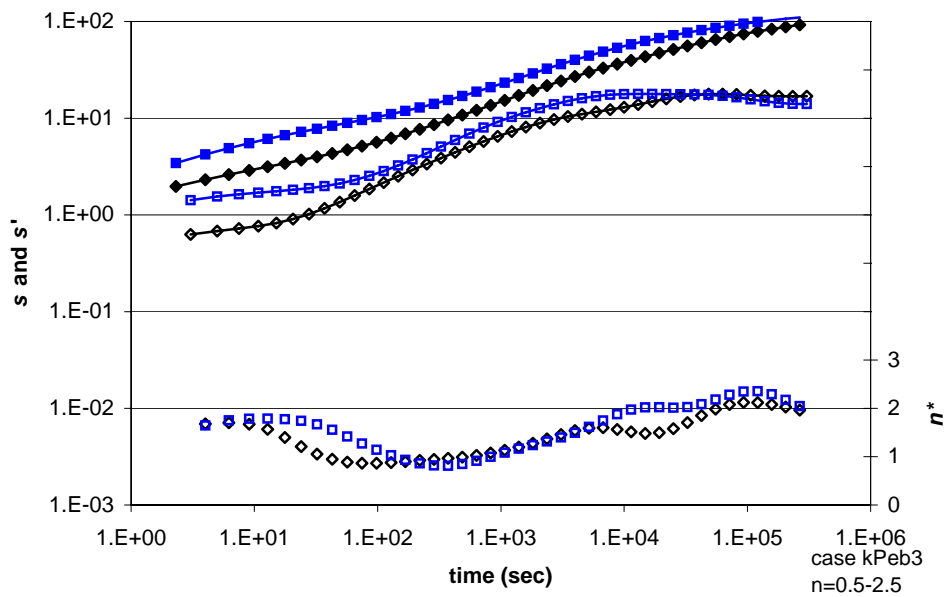


Figure 14a. Drawdown (closed symbols), derivative (open symbols with line), and flow dimension (open symbols without line) for two realizations with $0.5 < n^* < 2.5$, case kPeb3: percolation with $p = 0.61$, $T_{l-p} = T_p / 10^6$; symbol shapes denote realizations.

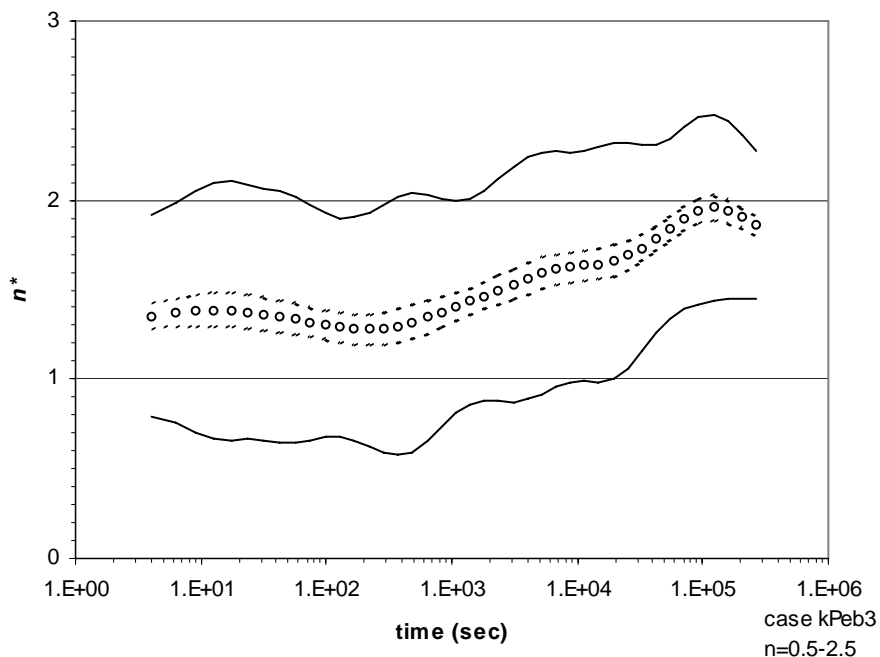


Figure 14b. Average (circle) and 95 percent normal CI for the population (solid lines) and mean (dashed lines) flow dimension for 58 realizations with $0.5 < n^* < 2.5$, case kPeb3: percolation with $p = 0.61$, $T_{l-p} = T_p / 10^6$.

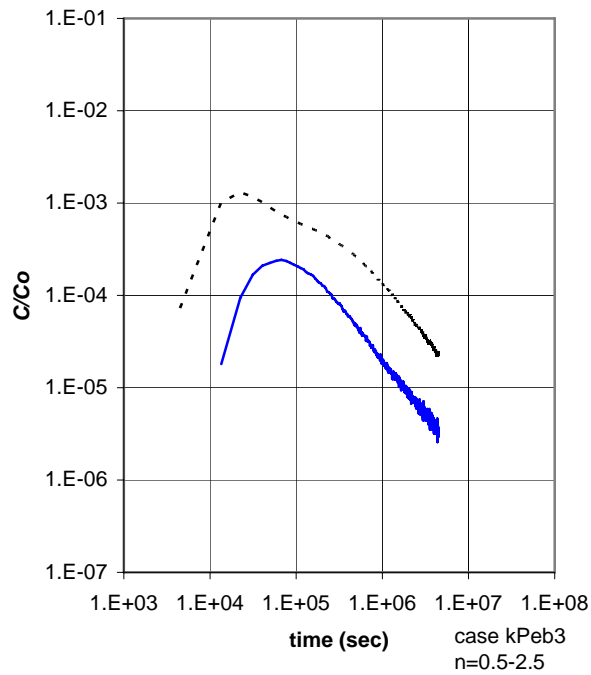


Figure 14c. Relative concentration versus time for a CFTT in two realizations with $0.5 < n^* < 2.5$, case kPeb3: percolation with $p = 0.61$, $T_{1-p} = T_p / 10^6$.

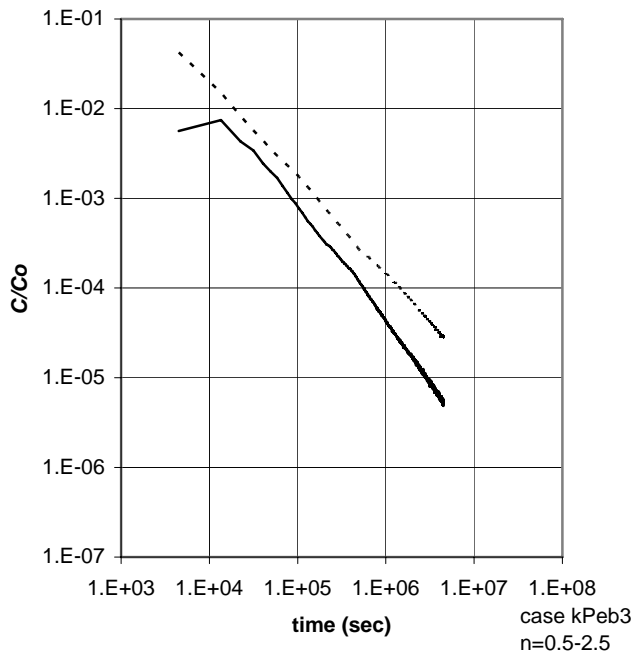


Figure 14d. Relative concentration versus time of a converging flow tracer test for 58 realizations with $0.5 < n^* < 2.5$, median (solid line) and 95 percent nonparametric CI for the population (dashed lines), case kPeb3: percolation with $p = 0.61$, $T_{1-p} = T_p / 10^6$.

Figure 15a presents the log-log diagnostic plot for two realizations of case kPcb3, and Figure 15b presents the apparent flow dimensions for 200 realizations within the trimming limits $0.5 < n^* < 2.5$. Relative to an increased contrast in transmissivity (case kPeb3, shown in Figure 14b), converting impermeable nodes to no-flow cells reduces the average apparent flow dimension and smoothes its trend. In the interval between 100 and 10,000 seconds, the average of the apparent flow dimension is approximately stable at $n^* = 1.5$, then steadily increases. The relative BTCs in this case (Figures 15c and d) are highly variable, and the slope of the median relative BTC is approximately $-3/2$. This slope reflects the process of matrix diffusion that is included in this simulation, and suggests that eliminating slow advection through the nonpercolating nodes has decreased the tailing behavior. This indicates that the increased slope noted earlier for the percolation network is not a consequence of the fractal geometry.

Case kPdb3 is a variant of the percolation network model that examines the affect of heterogeneity apart from the influence of matrix diffusion. This variant repeats the base case of the percolation network model (kPfb3, with $p = 0.61$, $T_{1-p} = T_p / 10^4$) but excludes matrix diffusion. The aquifer test is simulated for this case to permit trimming the realizations to those $0.5 < n^* < 2.5$, but because flow is unaffected by matrix diffusion, the apparent flow dimensions are identical to those of kPfb3 (Figures 13a and 13b) and are not discussed further. Figures 16a and 16b present the relative BTC for this case, which show a high degree of variability between realizations. The median BTC forms an erratic line in this case, but appears to have an overall slope of -2 . This slope agrees with the analytical solution of Becker and Shapiro (2003), who found that a late-time slope of -2 for the log-log BTC of a CFTT in a highly heterogeneous medium.

The final variant of the percolation network model, case kPbb3, examines the sensitivity of the results to a decrease in the percolation probability from $p = 0.61$ to $p = 0.60$. Because this reduces the percolation probability closer to the threshold value of $p_c \approx 0.593$, this is expected to decrease the connectedness of the percolation network (i.e., decrease the probability of any node being connected to the domain-spanning cluster) (Feder, 1988). Substituting $p = 0.60$ into Equation 6 yields a percolation correlation length of $\xi_p = 746$ m, a distance that is less than the radial distance from the well to the limits of the model domain. This suggests that the flow dimension might reflect a transition from fractal to homogenous (two-dimensional) behavior, and the transition might occur later than in the base case (case kPfb3) where $\xi_p = 230$ m. This case is otherwise unchanged relative to case kPfb3, and 200 realizations within the trimming limits $0.5 < n^* < 2.5$ are simulated. Figures 17a and 17b show that the apparent flow dimension oscillates around $n^* = 1.5$, which is slightly lower than the base case. Although this decrease would be consistent with the conclusion of Polek (1990) that flow dimension decreases with the percolation probability, a comparison of the confidence intervals (Figures 13b and 17b) indicates that the change is not significant. It is not clear if the transition to the late-time increasing trend in the apparent flow dimension has been shifted as a consequence of the increase in ξ_p . Figures 17b and 17c present log-log plots of the relative BTC for this case; the slope of the median BTC has been increased ($> -5/4$). This increased tailing reflects the decreased connectivity of the network that results from decreasing the percolation probability, and confirms the conclusion of Zinn and Harvey (2003), who found that both connectivity and slow advection could affect the late-time slope of the BTC.

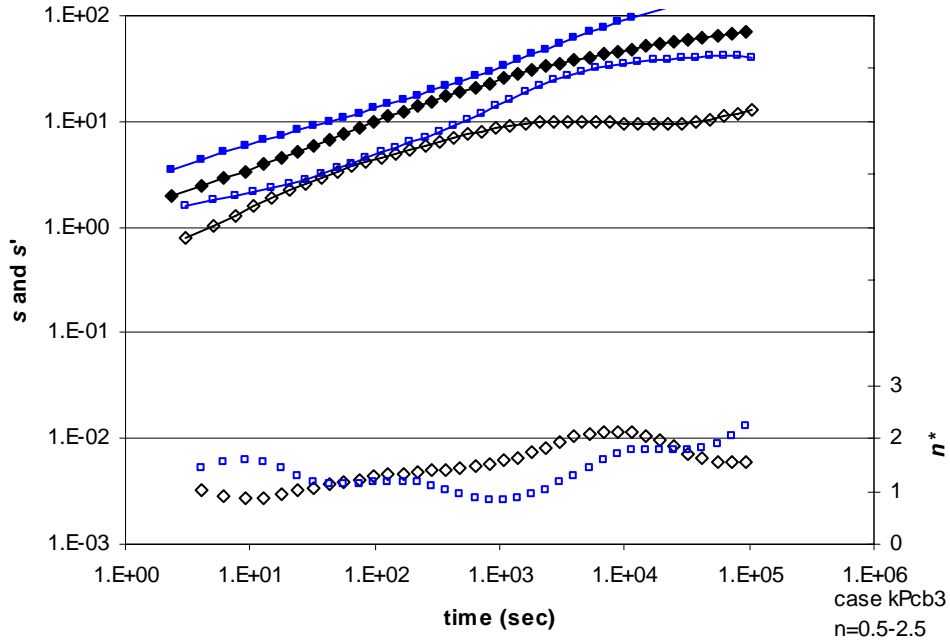


Figure 15a. Drawdown (closed symbols), derivative (open symbols with line), and flow dimension (open symbols without line) for two realizations with $0.5 < n^* < 2.5$, case kPcb3: percolation with $p = 0.61$, no-flow cells; symbol shapes denote realizations.

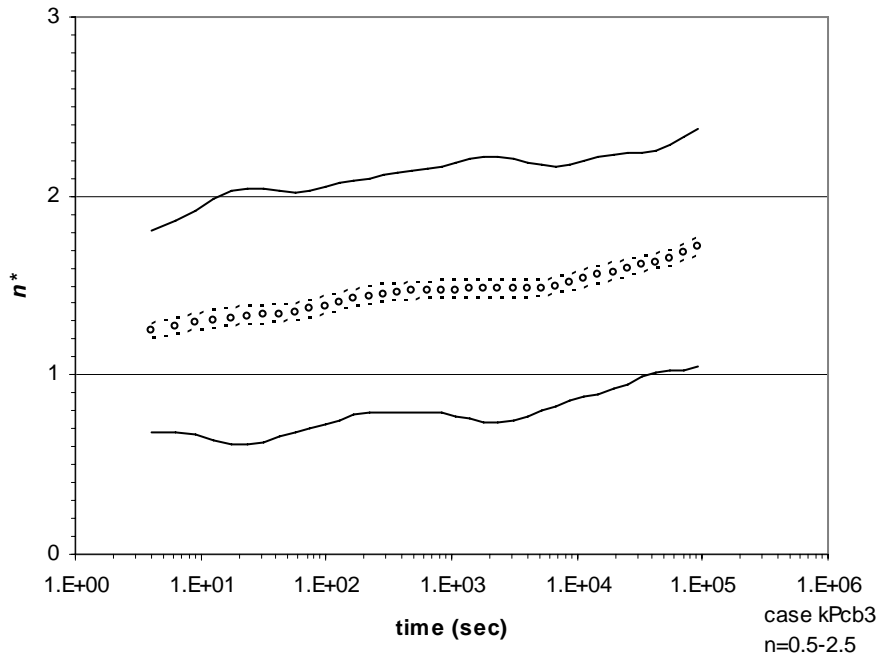


Figure 15b. Average (circle) and 95 percent normal CI for the population (solid lines) and mean (dashed lines) flow dimension for 200 realizations $0.5 < n^* < 2.5$, case kPcb3: percolation with $p = 0.61$, no-flow cells.

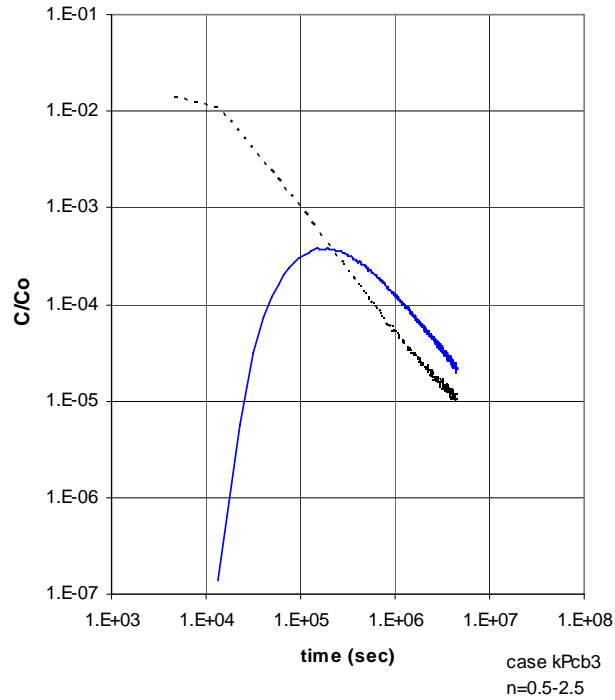


Figure 15c. Relative concentration versus time for a CFTT in two realizations $0.5 < n^* < 2.5$, case kPcb3: percolation with $p = 0.61$ and no-flow cells.

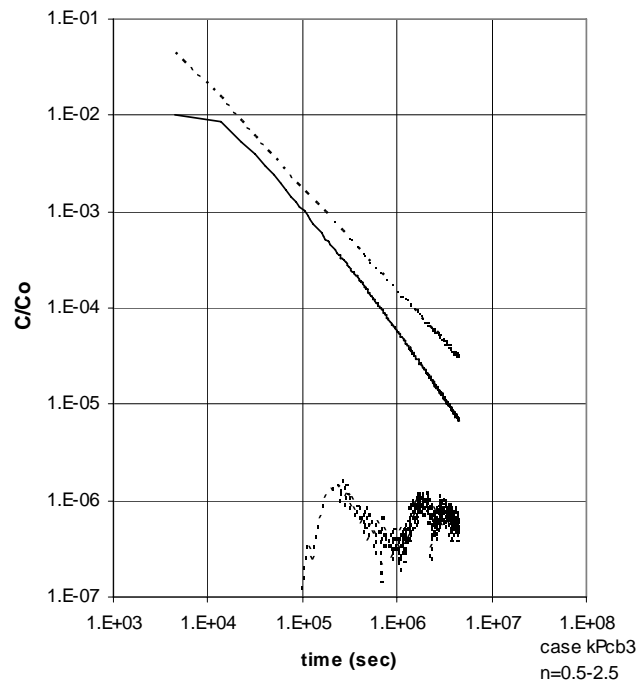


Figure 15d. Relative concentration versus time of a converging flow tracer test for 200 realizations $0.5 < n^* < 2.5$, median (solid line) and 95 percent nonparametric CI for the population (dashed lines), case kPcb3: percolation with $p = 0.61$ and no-flow cells.

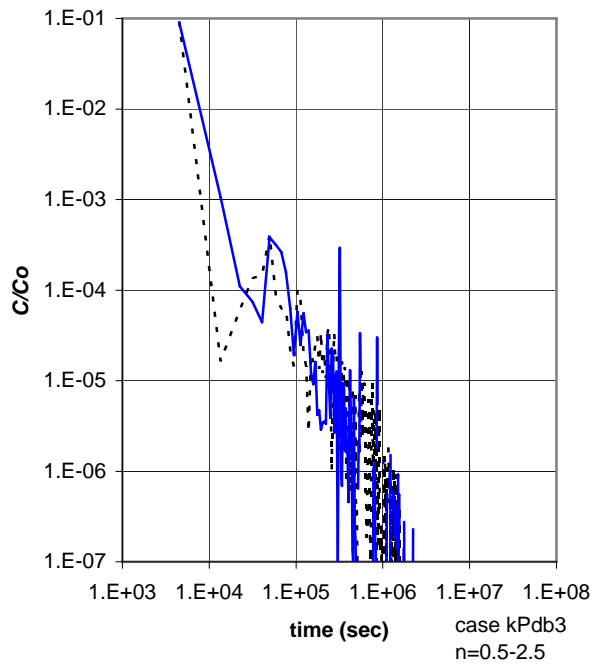


Figure 16a. Relative concentration versus time for a CFTT in two realizations with $0.5 < n^* < 2.5$ from case kPdb3: percolation with $p = 0.61$, no matrix diffusion; symbol shapes denote realizations.

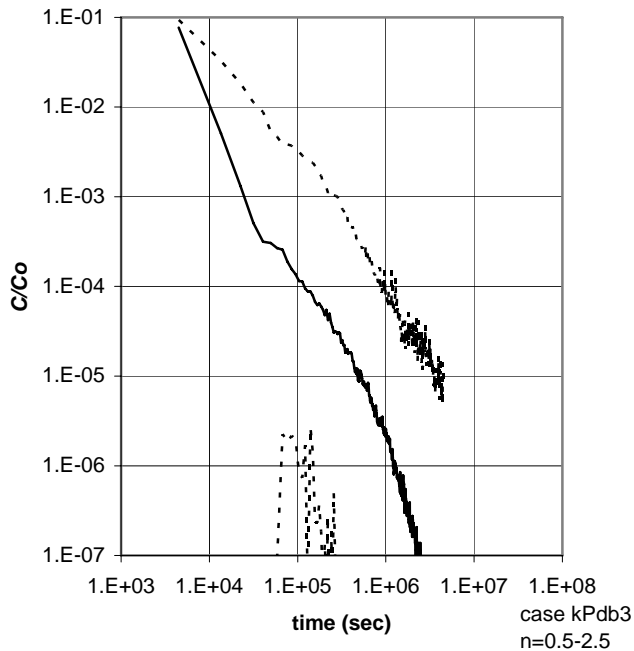


Figure 16b. Relative concentration versus time for 200 realizations of a converging flow tracer test with $0.5 < n^* < 2.5$, median (solid line) and 95 percent nonparametric CI for the population (dashed lines), case kPdb3: percolation with $p = 0.61$, no matrix diffusion.

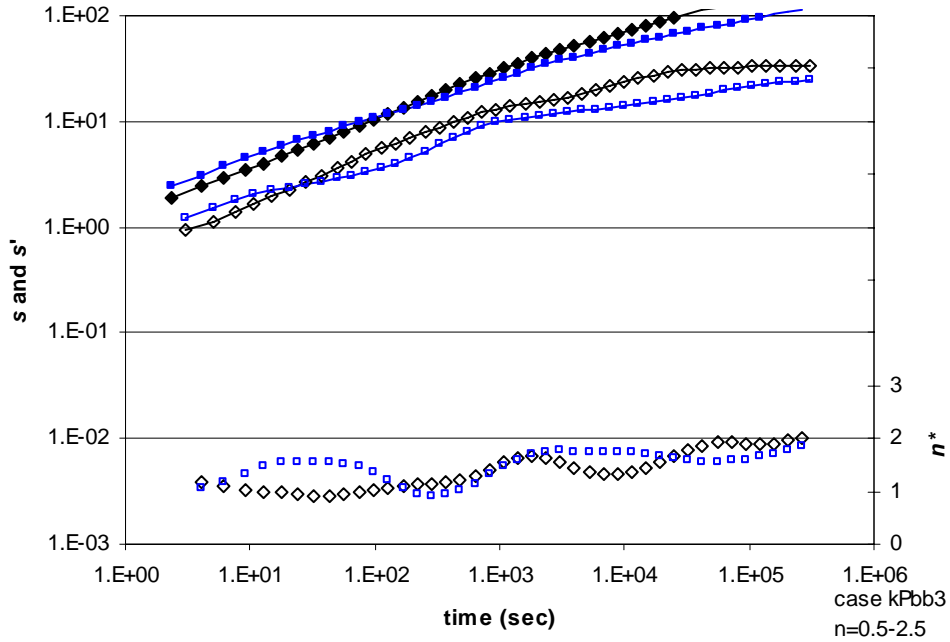


Figure 17a. Drawdown (closed symbols), derivative (open symbols with line), and flow dimension (open symbols without line) for two realizations with $0.5 < n^* < 2.5$, case kPbb3: percolation with $p = 0.60$, $T_{l-p} = T_p / 10^4$; symbol shapes denote realizations.

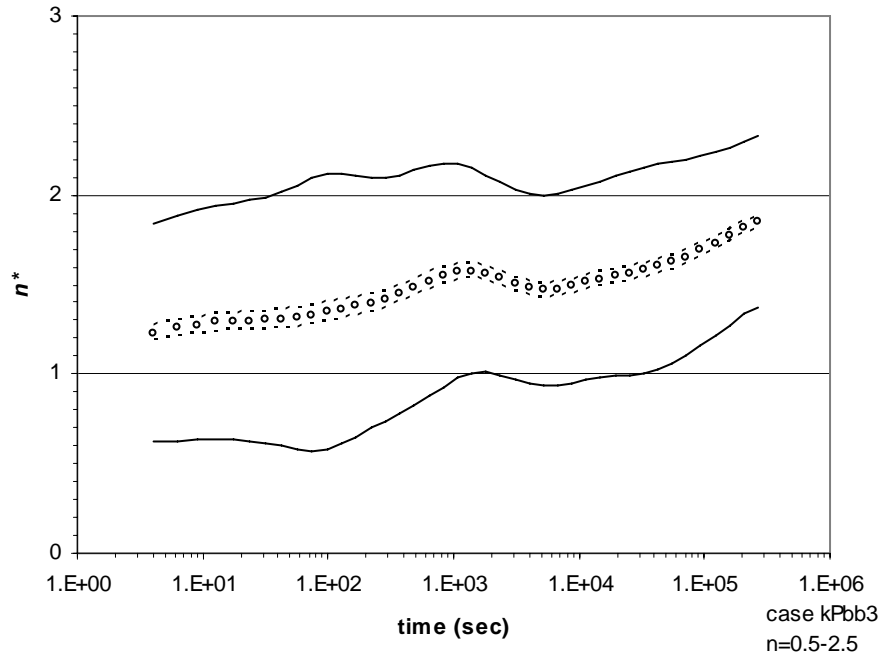


Figure 17b. Average (circle) and 95 percent normal CI for the population (solid lines) and mean (dashed lines) flow dimension for 200 realizations $0.5 < n^* < 2.5$, case kPbb3: percolation with $p = 0.60$, $T_{l-p} = T_p / 10^4$.

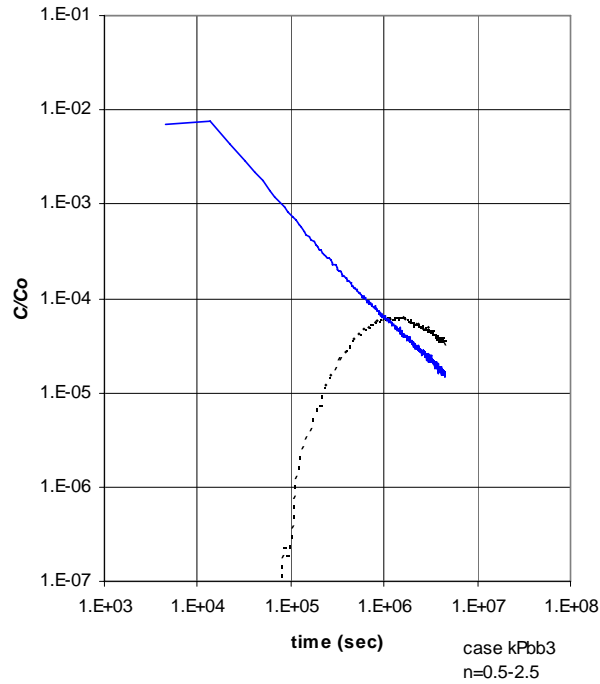


Figure 17c. Relative concentration versus time for a CFTT in two realizations $0.5 < n^* < 2.5$, case kPbb3: percolation with $p = 0.60$, $T_{1-p} = T_p / 10^4$.

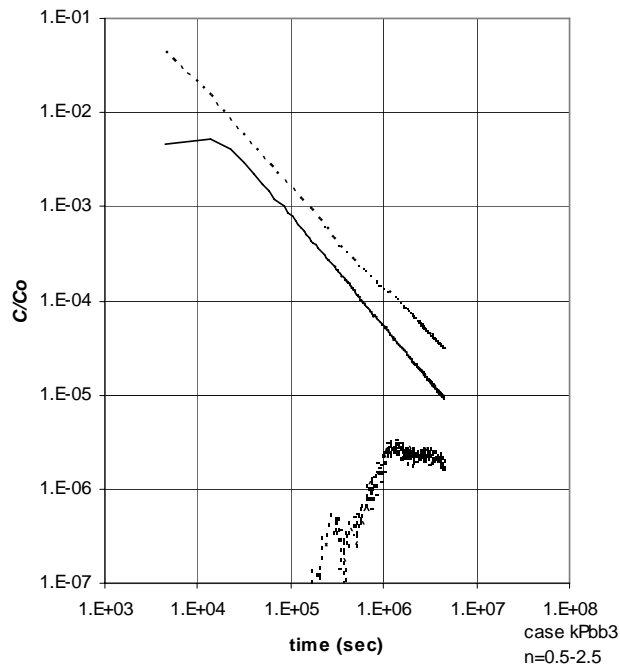


Figure 17d. Relative concentration versus time of a converging flow tracer test for 200 realizations $0.5 < n^* < 2.5$, median (solid line) and 95 percent nonparametric CI for the population (dashed lines), case kPbb3: percolation with $p = 0.60$, $T_{1-p} = T_p / 10^4$.

Log Gaussian (Uncorrelated)

The fourth model is a simple log Gaussian model, i.e., transmissivities are assigned to the finite difference blocks using values of $\ln T(x)$ randomly taken from the normal (Gaussian) distribution. This model is in a sense the limiting ‘uncorrelated’ case of the mvG model. Realizations of the log Gaussian model are created using *sgsim* with $I \ll 1$ m, i.e., no correlation between finite-difference blocks. As with the mvG model, the input geometric mean of the transmissivity is $T_g = 4.70 \times 10^{-5}$ m²/sec. Dagan (1981) found that random transmissivities assigned to homogeneous blocks of uniform size have an integral scale that is less than the block dimension. Since representing the spatial correlation of heterogeneity generally requires several nodes per integral scale, the weak correlation function of this stochastic model is poorly represented and the flow simulations will not necessarily satisfy Matheron’s relationship of $T_e/T_g = 1$. However, this stochastic model does provide at least a heuristic check on variability of the apparent flow dimension when the spatial scale of the test is much larger than that of the heterogeneity.

Two cases are simulated for the uncorrelated log Gaussian model, examining $\sigma_{\ln T}^2 = 1.0$ (case kN1b3) and $\sigma_{\ln T}^2 = 16.0$ (case kN16b3). The apparent flow dimensions of aquifer tests in these cases rapidly stabilize to a value of $n = 2$ (Figures 18a and 19a). The variability between realizations decreases with time (Figures 18b and 19b) and does so more rapidly than in the comparable mvG stochastic model with $\sigma_{\ln T}^2 = 1.0$ and $I = 7$ m (case kG4b3, in Figure 6b). Increasing the variance to $\sigma_{\ln T}^2 = 16.0$ apparently has little effect on the stabilization of the apparent flow dimension to $n = 2$. Table 2 indicates that the average geometric mean of the realizations is a poor match to the estimated effective transmissivity for both variances (i.e., $T_e^*/T_g^* = 0.875$ and 0.445). Likewise, the average apparent transmissivity of the Cooper-Jacob solution is a poor estimator of the average geometric mean of the realizations (i.e., $T_{CJ}^*/T_g^* = 0.875$ and 0.445). This is attributed to the poor representation of the small correlation inherent to this stochastic model. Several attempts were made to improve the agreement with Matheron’s relationship of $T_e/T_g = 1$, including switching convergence tolerances, solvers, grids, stochastic simulation algorithms, and flow models; all attempts led to nearly identical numerical results. On the other hand, the average apparent transmissivities of the Cooper-Jacob solution are good estimators of the estimated effective transmissivities (i.e., $T_{CJ}^*/T_e^* \approx 1.000$, calculated from Table 2).

Figures 18c and 19c present two realizations of the breakthrough curve (BTC) for the CFTT of these models. Both realizations eventually approach the characteristic -3/2 slope of matrix diffusion (Tsang, 1995), although their early arrival times differ substantially. Figures 12d and 13d present the median and the upper and lower percentiles of the 95 percent nonparametric confidence interval for the BTC of 100 realizations. The confidence intervals are widest for the early arrival times, and the median of the BTC also approach the characteristic -3/2 slope of matrix diffusion (although the slope of kN16 is arguably between -3/2 and -5/4). Comparing Figures 16d and 17d indicates that increasing the variance tends to increase the width of the confidence intervals in general. Table 3 shows that t_p , the time to the peak of the median of the relative BTC, is somewhat longer (0.990 seconds) for the uncorrelated log Gaussian case (kN1b3) relative to the mvG case with a comparable variance (kG4b3).

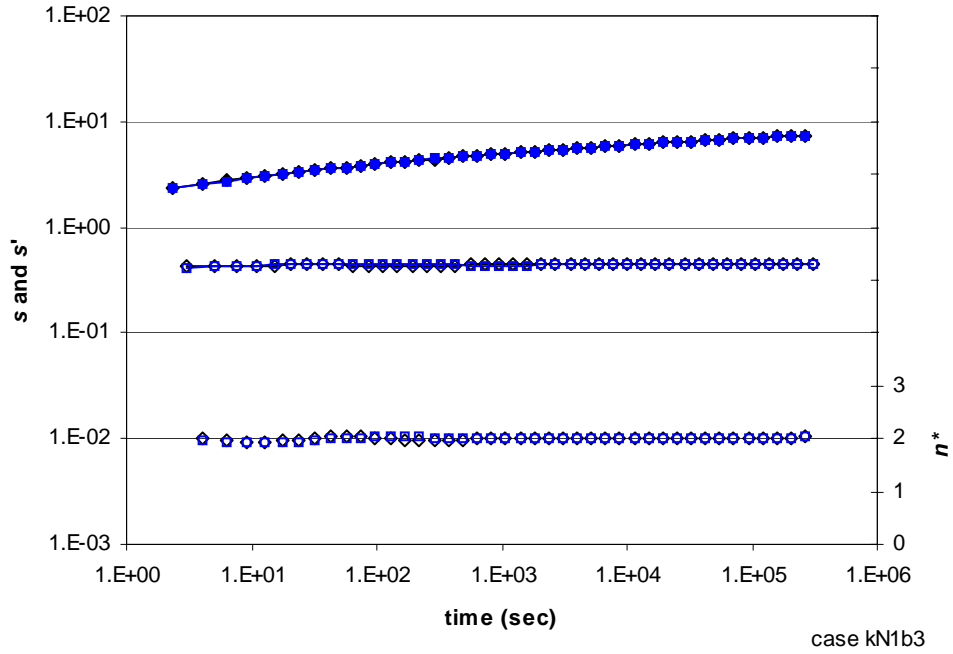


Figure 18a. Drawdown (closed symbols), derivative (open symbols with line), and flow dimension (open symbols without line) for two realizations of case kN1b3: log Gaussian with $\sigma^2_{\ln T} = 1.0$; symbol shapes denote realizations.

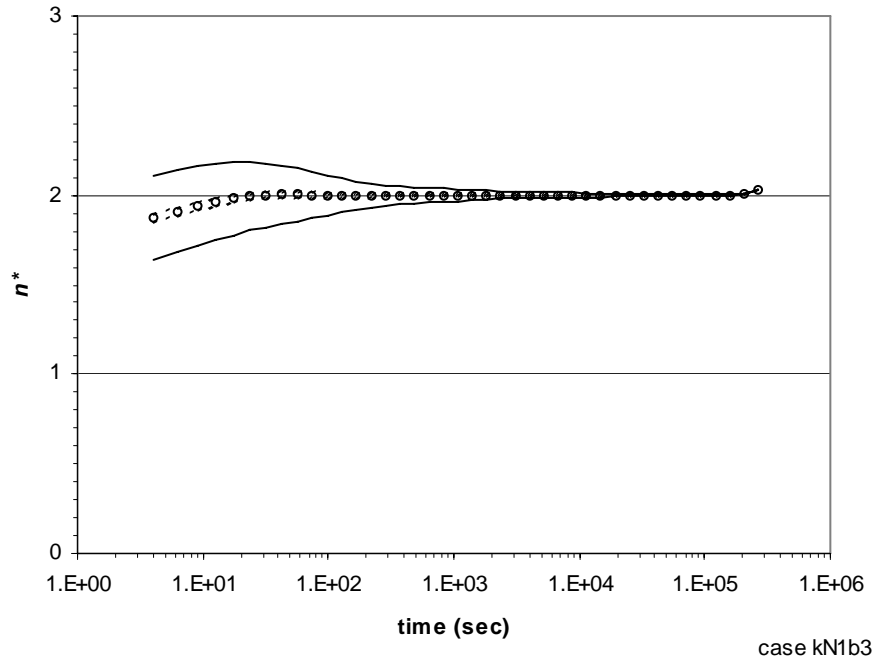


Figure 18b. Average (circle) and 95 percent normal CI for the population (solid lines) and for the mean (dashed lines) for 100 realizations of the flow dimension, case kN1b3: log Gaussian with $\sigma^2_{\ln T} = 1.0$.

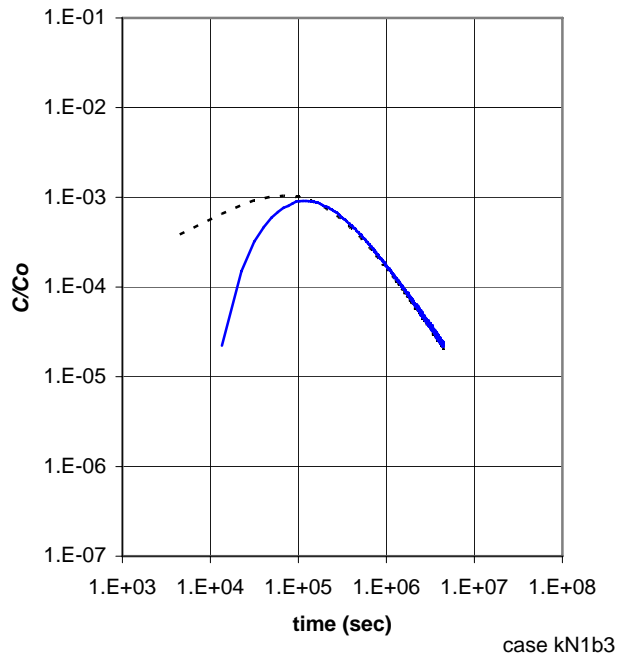


Figure 18c. Relative concentration versus time for a CFTT in two realizations of case kN1b3: log Gaussian with $\sigma^2_{\ln T} = 1.0$.

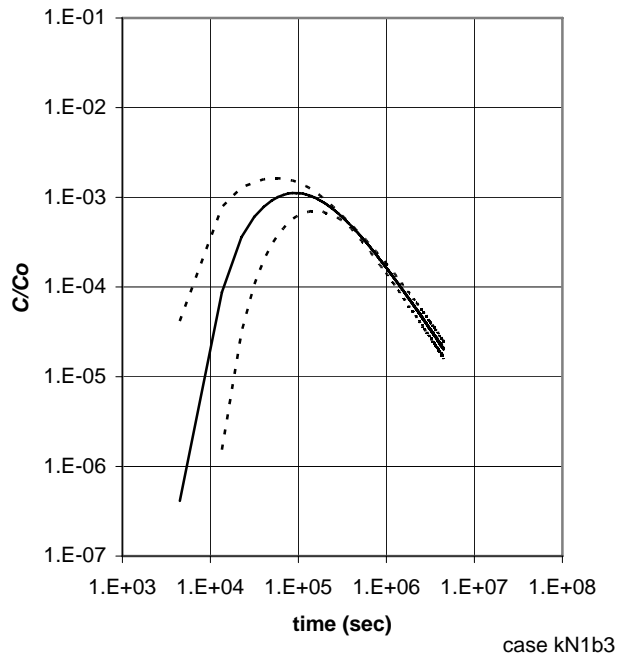


Figure 18d. Relative concentration versus time for 100 realizations of a CFTT, median (solid line) and 95 percent nonparametric CI for the population (dashed lines), case kN1b3: log Gaussian with $\sigma^2_{\ln T} = 1.0$.

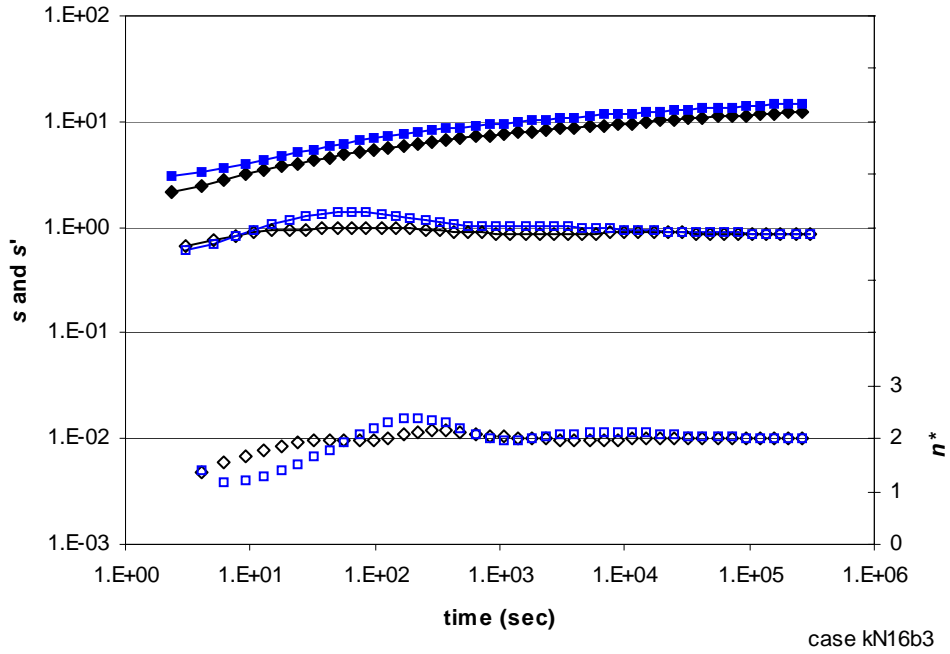


Figure 19a. Drawdown (closed symbols), derivative (open symbols with line), and flow dimension (open symbols without line) for two realizations of case kN16b3: log Gaussian with $\sigma^2_{\ln T} = 16.0$; symbol shapes denote realizations.

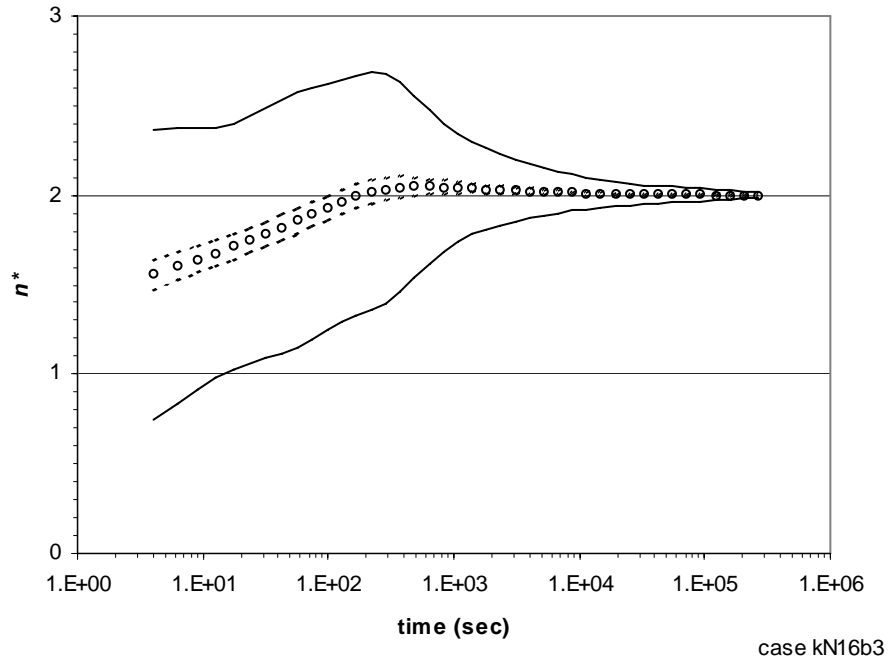


Figure 19b. Average (circle) and 95 percent normal CI for the population (solid lines) and for the mean (dashed lines) for 100 realizations of the flow dimension, case kN16b3: log Gaussian with $\sigma^2_{\ln T} = 16.0$.

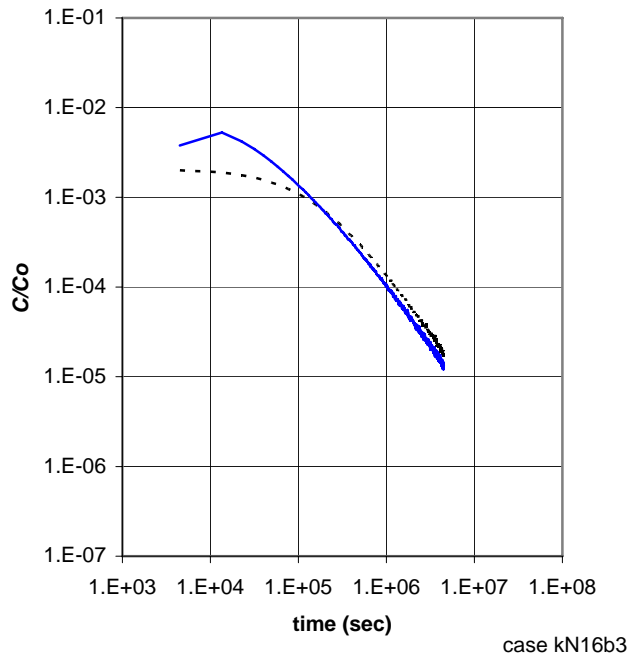


Figure 19c. Relative concentration versus time for a CFTT in two realizations of case kN16b3: log Gaussian with $\sigma^2_{\ln T} = 16.0$.

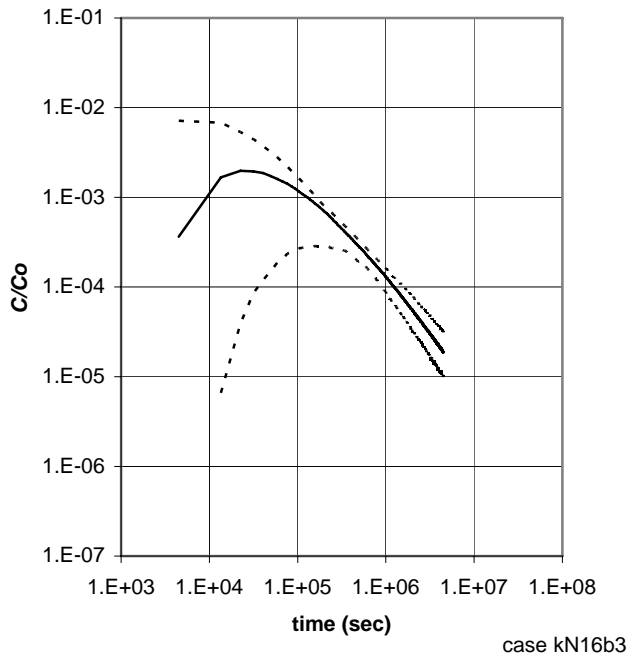


Figure 19d. Relative concentration versus time for 100 realizations of a CFTT, median (solid line) and 95 percent nonparametric CI for the population (dashed lines), case kN16b3: log Gaussian with $\sigma^2_{\ln T} = 16.0$.

Summary

This study has examined the behavior of aquifer tests and tracer tests in fractured rock aquifers from the perspective of the Generalized Radial Flow (GRF) approach to hydraulic test interpretation. The GRF approach infers the flow dimension, n , a parameter which describes the geometry of the flow paths in the tested aquifer. The study incorporated an algorithm for transport influenced by matrix diffusion into an existing series of programs, then executed the series in Monte Carlo fashion to determine the flow dimension, effective transmissivities, and break-through curves in realizations of heterogeneous transmissivity. Four widely used stochastic models were considered for the logarithm of transmissivity, $\ln T(x)$: the lognormal, or spatially correlated (multivariate) Gaussian distribution (mvG); fractional Brownian motion (fBm); uncorrelated lognormal (simple random); and an approximation of a percolation network. Although the parameter ranges considered in this study are taken from hydraulic and tracer tests performed at the Waste Isolation Pilot Plant site near Carlsbad, New Mexico, USA, the results of the study are broadly relevant to the characterization and modeling of flow and transport in fractured rocks in Illinois and world-wide.

For the mvG model, the apparent flow dimension of an aquifer test converges to $n^* = 2$ if the scale of the test is large relative to the scale of correlation. The variability of the apparent flow dimension around $n^* = 2$ diminishes as the radius of investigation increases. Simulations with variances ranging from $\sigma^2_{\ln T} = 0.0625$ to 9.0 demonstrate that the variability of the apparent flow dimension increases with the variance of the field. Decreasing the integral scale decreases the time required to reach the maximum variability of the apparent flow dimension. These dependencies suggest that it may be possible to identify the variance and integral scale of a stationary mvG field from a set of aquifer tests, similar to the approach of Copty and Findikakis (2004). For a mvG model of low variance ($\sigma^2_{\ln T} < 1.0$), the average (arithmetic mean of realizations) of the apparent flow dimension is $n^* = 2$. The breakthrough curves (BTC) of a converging-flow tracer test (CFTT) influenced by matrix diffusion in the low-variance mvG model yielded a log-log plot with a late-time slope of $-3/2$. Although the variability of early arrival times increases as the variance increases from $\sigma^2_{\ln T} = 0.0625$ to 1.0, the late-time slopes of median of the BTC retained a late-time slope of $-3/2$, consistent with published studies of CFTT influenced by matrix diffusion.

Numerical inconsistencies limit the conclusiveness of the results for an mvG model of moderate variance ($\sigma^2_{\ln T} = 4.0$ and 9.0), but the results are still noteworthy. For either variance, the average of the apparent flow dimension converges to $n^* = 2$ at late-time. The average of the apparent flow dimension is significantly less than 2.0 at early time and has short periods when it is not significantly different from $n^* = 1.75$ and 1.6 (for $\sigma^2_{\ln T} = 4.0$ and 9.0, respectively). These results suggest that a mvG model of moderate variance has short periods where it is not inconsistent with the observed flow dimensions of fractured dolomite aquifers. The BTC of a CFTT in the moderate-variance mvG model do not appear to be consistent with published studies for CFTT influenced by matrix diffusion, yielding a log-log plot with a late-time slope of $-5/4$ or greater. This suggests that the effect of heterogeneity on a CFTT is additive and predictable, rather than simply incorporating variability into the BTC. Inconsistencies with Matheron's solution for the effective transmissivity of a two-dimensional mvG field (i.e., $T_e^*/T_g^* = 0.936$ for $\sigma^2_{\ln T} = 4.0$ and 0.880 for $\sigma^2_{\ln T} = 9.0$) suggest that the calculations be refined for the mvG model at moderate variances.

The second stochastic model of heterogeneous transmissivity studied was that of $\ln T(x)$ distributed as a fractional Brownian motion (fBm), a fractal variant of the mvG model that uses a power model for the semivariogram with an exponent of 0.5. The average of the apparent flow dimension of this model had a value of $n^* = 2$ and the variability of the apparent flow dimension increases with time. This increase in variability is consistent with the power semivariogram that characterizes the fractal nature of this model and is the opposite of the behavior found for the mvG model. This difference suggests that the variability of the apparent flow dimension with time might be useful in distinguishing between the fBm and mvG models, given a sufficiently large set of aquifer tests. This effect may be exaggerated by the necessity of providing a conditioning value for transmissivity at the well. Because the variability of the apparent flow dimension appears to depend on the variance of the field, it may be possible to infer H , the Hurst coefficient, from the increasing variability of the apparent flow dimension. The BTC of a CFTT in this model yielded a log-log plot with a late-time slope of $-3/2$, which is consistent with transport in a transmissivity field of low variance influenced by matrix diffusion. Relative to the cases of the mvG model with comparable field-wide variances, the early arrival times of the fBm model have lower variability.

This study also examined an approximate percolation network as a stochastic model of heterogeneous transmissivity, setting the percolating nodes to T_g , the geometric mean of transmissivity, and the nonpercolating nodes to $T_g/10^4$. The chosen value of the percolation probability, $p = 0.61$, is near the critical value of p_c for this system so that the network has fractal characteristics. The apparent flow dimensions indicate that some realizations are of wells pumped in small percolation clusters that behave as small, closed reservoirs with slightly permeable barriers. Although such flow dimensions are consistent with percolation networks and with highly heterogeneous formations, they limit inferences that can be drawn regarding the apparent flow dimension and are trimmed from the set of realizations. The remaining realizations have log-log diagnostic plots and a range of apparent flow dimensions that are similar to those observed for aquifer tests in fractured dolomites. The average of the apparent flow dimension oscillates around $n = 1.6$, then steadily increases to $n^* = 2$ over time. The relative BTC of the CFTT are highly variable but the median BTC eventually settles down to a log-log slope of $-5/4$. Reducing the transmissivity of the nonpercolating nodes reduces the flow dimension and reduces the slope of the BTC. Converting the nonpercolating nodes to no-flow nodes reduces the flow dimension and creates a stable period of $n^* = 1.5$ and reduces the slope of the BTC to $-3/2$. Reducing the percolation probability decreases the flow dimension and increases the slope of the BTC. These variations on the percolation model indicate that slow advection through the nonpercolating nodes systematically adds to the tailing behavior of matrix diffusion. None of these parameter variations or changes to the boundary conditions changed the tendency of the flow dimension to converge to $n^* = 2.0$ at late times. We conclude that this tendency toward $n^* = 2.0$ is the consequence of the radius of influence growing larger than the correlation length of the network ($r_e > \xi_p$) and the network becoming effectively two dimensional at large scales. Removing matrix diffusion results in a log-log BTC with a late-time slope of -2 , confirming the solution of Becker and Shapiro (2003) for a CFTT in highly heterogeneous media.

The fourth stochastic model was intended to be the zero-correlation limiting case of the mvG model, here referred to as an uncorrelated log Gaussian transmissivity field. The inability of these cases to reproduce Matheron's relationship of $T_e = T_g$ for the effective transmissivity of a lognormal field indicates that this simulation is confounded by the effect of the poorly modeled

correlation within a finite difference block. However, the simulations suggest that the decreasing variability of the apparent flow dimension with time is not a boundary effect. The BTC associated with this case show late-time slopes similar to those of the mvG model, i.e., $-3/2$ for low variances, and the slope increases with increasing variance of $\ln T$.

Discussion

As noted in the “Introduction”, the GRF approach to hydraulic test interpretation was developed because traditional methods of test interpretation do not address the complex geometry of flow in highly heterogeneous aquifers. The GRF approach does this by introducing another fitting parameter, the flow dimension, to describe how the flow geometry changes over the course of the test. This study has attempted to interpret the flow dimension in the context of stochastic modeling, examining several stochastic models of aquifer heterogeneity to sketch out the relationships between the flow dimension, model parameters, and transport behavior.

Relatively few investigations have reported the flow dimension for their study site, leaving a gap in the current knowledge. With the notable exceptions of several studies of fractured crystalline rocks (Borgne et al., 2004; Doe and Geier, 1991; Geier et al., 1996; Kuusela-Lahtinen et al., 2003), studies that have inferred the flow dimension have small sets of hydraulic tests, limiting confidence in the conclusions regarding the general behavior of the flow dimension (Bangoy et al., 1992). Preliminary analyses of fractured dolomites in Illinois (e.g., Figure 1) and in New Mexico show flow dimensions between 1.4 and 2.0 (R. Roberts, Personal Communication, 2005), suggesting that flow does not fill the available volume of the aquifer. These few studies do not clearly define the distribution of the flow dimension associated with a particular site or for this rock type, yet these are necessary if a calibration exercise is to be successful. This indicates a need to reanalyze existing data and infer the distributions of flow dimensions in a variety of settings. Such an exercise is the objective of an ongoing study of aquifer tests in the fractured dolomite aquifers of in northeastern Illinois, jointly conducted by the ISWS, UIUC, and NCSA.

Figure 20 summarizes the flow dimension results for the stochastic models, plotting the arithmetic average of the apparent flow dimension at the pumped well versus time since the start of the test. The apparent flow dimensions of the mvG and fBm cases appear to stabilize to approximately $n^* = 2$, while that of the percolation network oscillates around $n^* = 1.6$. The variability of the apparent flow dimension decreases over time for the mvG model, is roughly constant for the percolation network, and steadily increases for the fBm model. These differences suggest that it may be possible to use the variability and average of the flow dimension of a set of aquifer tests to differentiate between alternative models of heterogeneity and estimate their parameters. The confidence intervals for the apparent flow dimensions indicate that, while short intervals of individual aquifer tests might have $n^* < 2$, the low-variance mvG and fBm models do not consistently produce flow dimensions less than the Euclidean dimension of the aquifer. Among the models examined in this study, only the percolation model consistently produces flow dimensions less than two, thus it is the best choice among these models for representing fractured dolomite aquifers. However, flow dimensions observed in the field can be stable for many log cycles of an aquifer test, while those simulated by the percolation model in this study are not. The duration of the stable interval of the mean flow dimension has been attributed to the correlation length of the percolation network, thus we speculate that models with variable lattice lengths might overcome this limitation. Such models include Boolean models for discrete features with length distributions following a power law, and might possibly be combined with the above models.

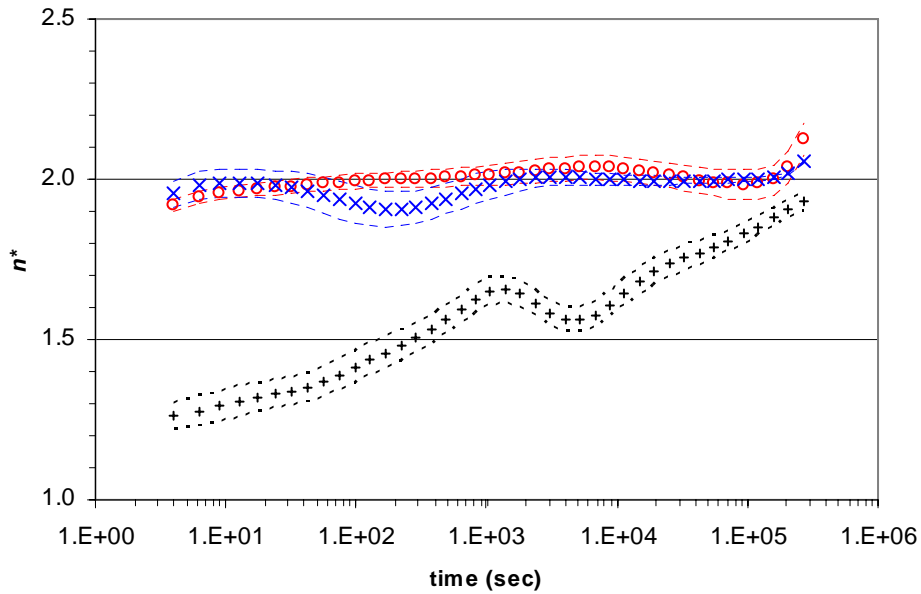


Figure 20. Apparent flow dimensions for a constant-rate aquifer test in a two-dimensional domain. The average and 95 percent normal confidence interval for the mean for three cases: \times = 100 realizations of mvG with $\sigma^2_{\ln T} = 1.0$ and $I = 7$ m (case kG4b3); o = 100 realizations of fBm with $H = 0.25$ (case kB1b3); and $+$ = 200 realizations of a percolation network with $p = 0.61$ (case kPfb3).

Much of the analysis has focused on the multivariate Gaussian (mvG) model and the percolation network model. At low variances of the mvG model ($\sigma^2_{\ln T} < 1.0$), these models are quite different: the mvG model has an average apparent flow dimension of $n^* = 2$, and the variability around this value is related to the variance and integral scale of the mvG model. The percolation network model shows apparent flow dimensions with an arithmetic average $n^* < 2$ at early times, then slowly increasing toward $n^* = 2$ (e.g., Figure 13b). As the variance increases to $\sigma^2_{\ln T} = 4.0$ and 9.0 , the mvG model develops apparent flow dimensions with an arithmetic average $n^* < 2$ at early times, then slowly increases toward $n^* = 2$ (Figures 8b and 9b). This tendency of the mvG model at higher variances to behave like a percolation network also is reflected in the tracer test results: at low variances, the mvG model shows extended tailing due to matrix diffusion (log-log BTC with late-time slope of $-3/2$, see e.g., Figure 6d); at variances of $\sigma^2_{\ln T} = 4.0$ and 9.0 , slow advection pathways add to the tailing behavior until it resembles that of a percolation network with matrix diffusion (a late-time slope of $-5/4$ or greater; see Figures 8d and 9d). While these results for the high-variance mvG cases require confirmation with refined grids, other investigators have noted the tendency of porous media to develop behavior similar to a percolation network. Katz and Thompson (1986) found that steady flow in sandstones could be modeled by a percolation network, and Acuna et al. (1995) speculated that transient flow in porous media also behaves like a percolation network. On the other hand, the present study shows that many realizations of the mvG model have flow dimensions greater than 2 (Figure 9b),

and very few of the percolation network realizations produce flow dimensions greater than two (even if no realizations are trimmed).

We speculate that a fractured dolomite aquifer might be represented well by some combination of stochastic models in a single domain, creating a hybrid stochastic model of heterogeneity. This hybrid approach to stochastic models of aquifer heterogeneity has an intuitive appeal: use a discrete model to represent the observed jointing, and a continuous model to represent the unfractured rocks (NRC, 1996). Although this approach has seen successful applications (McKenna et al., 2003), it increases the number of parameters that must be inferred and thus increases difficulty in applying the model. Unlike mvG models of low variance (Indelman and Dagan, 1993) and idealized percolation networks (Feder, 1988), there are no analytical solutions for upscaling arbitrary combinations of models. We speculate that each application of the hybrid modeling approach will require an analysis of upscaling for creating coarse-grid models that can address a domain of any useful size for evaluating management alternatives.

A key to understanding the transport results for the percolation model is that, except for one case (kPcb3), this study does not examine an idealized percolation network. In this study, the nonpercolating nodes are assigned a very small transmissivity value to simulate the unfractured rocks in the aquifer. Decreasing the transmissivity (case kPeb3) or using no-flow cells to represent the nonpercolating nodes (case kPcb3) showed that eliminating the small amount of flow in the nonpercolating nodes stabilizes the apparent flow dimension at somewhat lower values than the base case model (kPfb3). Eliminating this slow advection also decreases the late-time slope of the log-log BTC to $-3/2$, the characteristic behavior of matrix diffusion in the absence of strong heterogeneity. These results agree with Zinn and Harvey (2003), who concluded that both the connectivity and slow advection contributed to tailing behavior. It should be noted that all the percolation cases had flow dimensions in similar range (1.4 to 1.6), thus flow dimensions less than the Euclidean dimension are not necessarily correlated with tailing behavior. On the other hand, Doughty and Karasaki (2002) found that flow dimensions less than the Euclidean dimension are associated with earlier arrival times and other anomalous transport behaviors. The investigation of transport behavior under other flow conditions is left to future studies.

Except for a single variant case of the percolation network model (case kPdb3), all simulations of the CFTT in this study included the effects of matrix diffusion. The results generally confirm the conclusions of Tsang (1995) that transport influenced by matrix diffusion tends to have a log-log BTC with a late-time slope of $-3/2$, even for heterogeneous models. Tsang (1995) also noted that high heterogeneity tended to obscure the differences in late-time slopes of BTC with and without matrix diffusion. This effect of heterogeneity may be why the observed BTC for the CFTT for WIPP wells H-11 and H-19 show a range of log-log slopes from approximately -1 to less than -2 (see Figures 2 and 3 of McKenna et al. (2001)). However, rather than simply adding randomness to the BTC, this study has found that slow advection through areas of low transmissivity adds to the tailing systematically, increasing the late-time slope (Figure 21). This confirms the conclusion of Haggerty et al. (2000) that advective velocities with a high degree of variability would invalidate the direct relationship between matrix diffusion and the late-time slope of the BTC. Tsang (1995) also found that heterogeneity had varying effects depending on the type of tracer test, which suggests that follow-up studies should examine other

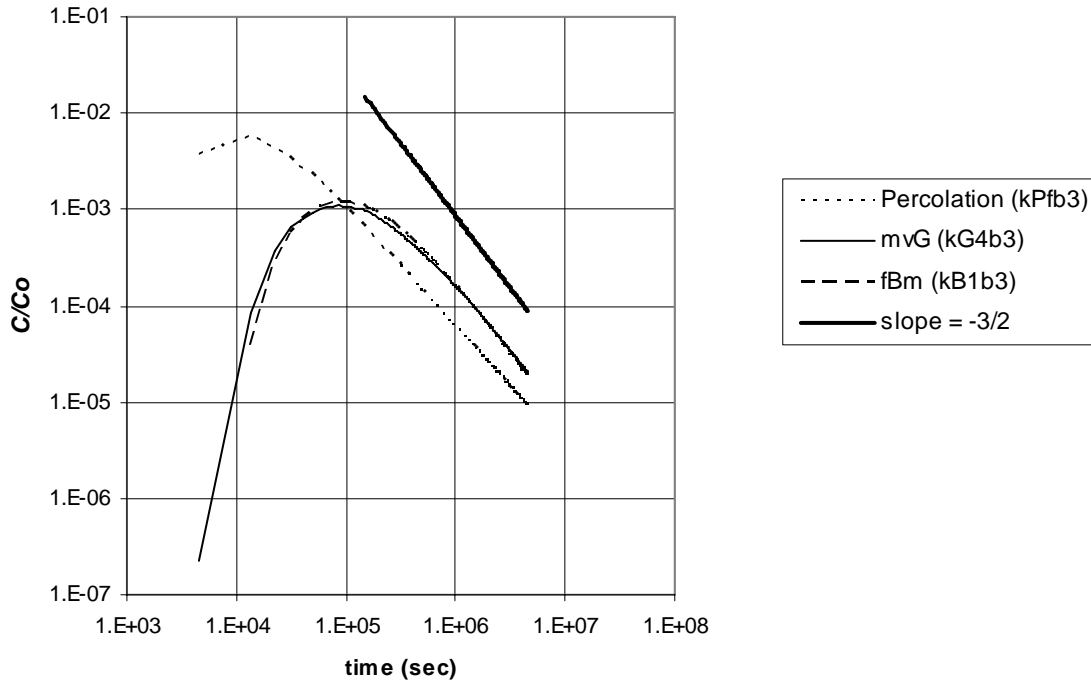


Figure 21. Relative concentration versus time for a CFTT influenced by matrix diffusion. The median BTCs for: mvG with $\sigma_{\ln T}^2 = 1.0$ and $I = 7$ m (case kG4b3); fBm with $H = 0.25$ (case kB1b3); and a percolation network with $p = 0.61$ (case kPfb3). The heavy line with $-3/2$ slope is for reference only.

test types, e.g., single-well injection-withdrawal tracer tests. It should be noted that all slopes discussed in this study were determined ‘by inspection’, in a manner similar to previous investigators. The comparison of slopes would be greatly clarified by statistical analysis and hypothesis testing. This is an area for further analysis, and is not included in the present report.

This study has used Monte Carlo simulation to infer the flow dimension and tracer test behavior of stochastic models, but it is important to place these Monte Carlo results in a practical context. The individual realizations for a particular stochastic model (e.g., Figure 6a) are analogous to non-overlapping aquifer tests scattered throughout a large aquifer, and the averages taken over the set of realizations are analogous to the inferred properties of that large aquifer (e.g., Figure 6b). Looking at the confidence intervals for the population (Figure 6b), we can see that individual aquifer tests at early times might have apparent flow dimensions ranging from 1.3 to 2.5. The narrow confidence intervals for the average of the apparent flow dimension indicate that, on average, the flow dimension observed for tests in this mvG aquifer would be $n^* = 2$. If the average flow dimension inferred from all aquifer tests in a field is, for example, $n^* = 1.6$, then the mvG model with $\sigma_{\ln T}^2 = 1.0$ is a poor choice for representing the heterogeneity

of transmissivity of that aquifer. As aquifer test durations increase (and the radius of investigation grows much larger than the integral scale) the confidence intervals for the population (Figure 6b) indicate that flow dimension of individual aquifer tests approaches $n^* = 2$. That is, even *individual* aquifer tests of sufficient duration will have an apparent flow dimension close to $n^* = 2$ for an mvG aquifer with $\sigma^2_{\ln T} = 1.0$. An apparent flow dimension of, e.g., $n^* = 1.6$ for an individual aquifer test of long duration indicates that the mvG model of low variance is a poor choice for representing the heterogeneous transmissivity of that aquifer.

The results for the effective transmissivity of the mvG model have an important implication for numerical modeling of spatially correlated transmissivities. Although the low-variance mvG cases showed good agreement with Matheron's solution for the effective transmissivity (i.e., $T_e = T_g$), they also showed that the ability to reproduce the effective transmissivity decreases with increasing variance and decreasing number of nodes per integral scale (Table 2). This result is consistent with that of previous investigators (Ababou et al., 1988; Meier et al., 1998) and suggests that numerical models may not be able to reproduce the effective transmissivities of highly heterogeneous, spatially correlated fields with currently available computers. Results reported by studies based on high-variance models with coarsely discretized grids may not be representative because they incorrectly model the mean transport velocity.

As noted in the report, there are several opportunities to improve the statistical analysis and to refine the calculations. These include:

- Reevaluate the high-variance cases of the mvG model using greater resolution to confirm the tendency of the flow dimension to $n^* < 2$ at early time;
- Address the impact of skewness on the confidence intervals for the apparent flow dimension, using nonparametric approaches to confirm the results;
- Similar to Desbarats (1992), plot the specific flux as a visual analysis of the emergence of flow channeling;
- Similar to the present results for the Cooper-Jacob solution, evaluate the n -dimensional (GRF) interpretation for the transmissivity and compare this to other parameters, e.g., the effective transmissivity;
- Normalize each realization of the BTC to the mean velocity, and develop statistical analyses for the significance of the slope estimates; and
- Further evaluate the relationship between the flow dimension and tracer transport, e.g., examining the spatial moments of tracer plumes.

Recommendations for future study include simply expanding the range of the parameter values and stochastic models examined, such as:

- Cases for the low-variance mvG model with $I = 14$ m and 28 m, to help establish the relationship between the time to the maximum variability of the apparent flow dimension and the integral scale of the field;
- Use an alternative simulation algorithm for the fBm stochastic model to verify the creation of the fBm process and evaluate a range of parameters for this and the related fractional Levy motion model;

- Evaluate the Sequential Indicator model after creating a more memory-efficient simulation algorithm; and
- Evaluate additional models of aquifer heterogeneity, including Transition Probability simulation of facies changes, and Boolean models of discrete linear features.

Conclusions

The objectives of this study were to establish the behavior of the flow dimension for widely used stochastic models of aquifer heterogeneity, and to perform a preliminary assessment of the relationship between the flow dimension and the BTCs of CFFT. With regard to those objectives, the conclusions of this study are as follows:

- For $\ln T(x)$ distributed as an mvG variable with $\sigma_{\ln T}^2 < 1.0$, the apparent flow dimension of an aquifer test converges to $n^* = 2$ if the scale (duration) of the test is large relative to the scale of correlation. The variability of the apparent flow dimension depends on the variance and integral scale of the transmissivity, suggesting that it may be possible to identify the variance and integral scale of a heterogeneous aquifer given a set of aquifer tests.
- The study results for $\sigma_{\ln T}^2 > 1.0$ suggest that the average of the apparent flow dimension is less than two initially, then converges to $n^* = 2$, similar in some respects to a percolation network. This result requires confirmation with a refined grid.
- Although problematic, the simulation of an uncorrelated log-Gaussian model suggests that the flow dimension of an aquifer test converges to $n^* = 2$ for variances of $\ln T(x)$ up to 16.0.
- For $\ln T(x)$ distributed as fractional Brownian motion (fBm), the apparent flow dimension averages to $n^* = 2$ and its variability increases with time.
- An approximation of a percolation network model showed an average apparent flow dimension stabilizing between $n^* = 1.4$ to 1.6, and is followed by an increasing trend. These characteristics apparently are functions of the transmissivity contrast between the percolating and nonpercolating fractions.
- In the low-variance mvG, uncorrelated log-Gaussian, and fBm models, simulations of CFFT influenced by matrix diffusion showed BTC with late-time log-log slopes of $-3/2$, the characteristic behavior of matrix diffusion.
- In the percolation network model, a simulated CFFT influenced by matrix diffusion had late-time BTC with log-log slopes of $-5/4$, attributed to slow advection through low transmissivity regions. This indicates that some heterogeneity models can systematically affect the late-time behavior of a BTC for a CFFT.

Taken as a whole, these results suggest that the flow dimension is a useful diagnostic for selecting models of heterogeneity, and that flow dimensions $n \neq 2$ may be associated with unique tracer behavior. Additional research is advocated to infer the general behavior of the flow dimension at various field sites, to assess a broader range of parameters, to examine other stochastic models, and to conduct a more detailed examination of transport behavior versus the flow dimension.

References

- Ababou, R., L. Gelhar and D. McLaughlin. 1988. *Three-Dimensional Flow in Random Porous Media*. Massachusetts Institute of Technology, Department of Civil Engineering, Ralph M. Parsons Laboratory Report 318, Cambridge, MA.
- Acuna, J.A., I. Ershaghi and Y.C. Yortsos. 1995. Practical Application of Fractal Pressure-Transient Analysis in Naturally Fractured Reservoirs. Paper SPE 24705. *Society of Petroleum Engineering Journal Formation Evaluation*:73-179.
- Acuna, J.A. and Y.C. Yortsos. 1995. Application of fractal geometry to the study of networks of fractures and their pressure transient. *Water Resources Research* 31(3):527-540.
- Altman, S.J., L.C. Meigs, T.L. Jones and S.A. McKenna. 2002. Controls of mass recovery rates in single-well injection-withdrawal tracer tests with a single-porosity, heterogeneous conceptualization. *Water Resources Research* 38(7):1125. doi:10.1029/2000WR000182.
- Anderson, P.F. 1993. *A Manual of Instructional Problems for the U.S.G.S. MODFLOW Model*. U.S. Environmental Protection Agency Report EPA/600/R-93/010, Ada, OK.
- Bangoy, L.M., P. Bidaux, C. Drouge, R. Plégat and S. Pistre. 1992. A new method of characterizing fissured media by pumping tests with observation wells. *Journal of Hydrology* 138(1-2):77-88.
- Barker, J.A. 1988. A generalized radial-flow model for pumping tests in fractured rock. *Water Resources Research* 24(10):1796-1804.
- Beauheim, R.L. and G.J. Ruskauff. 1998. *Analysis of Hydraulic Tests of the Culebra and Magenta Dolomites and Dewey Lake Redbeds Conducted at the Waste Isolation Pilot Plant Site*. Sandia National Laboratories Report SAND98-0049, Albuquerque, NM.
- Becker, M.W. and A.M. Shapiro. 2000. Tracer transport in fractured crystalline rock: Evidence of nondiffusive breakthrough tailing. *Water Resources Research* 36(7):1677-1686.
- Becker, M.W. and A.M. Shapiro. 2003. Interpreting tracer breakthrough tailing from different forced-gradient tracer experiment configurations in fractured bedrock. *Water Resources Research* 39(1):1024. doi:10.1029/2001WR001190.
- Benson, D.A., C. Tadjeran, M.M. Meerschaert, I. Farnham and G. Pohl. 2004. Radial fractional-order dispersion through fractured rock. *Water Resources Research* 40(12):W12416. doi:10.1029/2004WR003314.
- Berkowitz, B., J. Klafter, R. Metzler and H. Scher. 2002. Physical pictures of transport in heterogeneous media: Advection-dispersion, random-walk, and fractional derivative formulations. *Water Resources Research* 38(10):1191. doi:10.1029/2001WR001030.

- Borgne, T.L., O. Bour, J.R. de Dreuzy, P. Davy and F. Touchard. 2004. Equivalent mean flow models for fractured aquifers: Insights from a pumping tests scaling interpretation. *Water Resources Research* 40(3):W03512. doi:10.1029/2003WR002436.
- Butler, J.J., Jr. 1991. A stochastic analysis of pumping tests in laterally nonuniform media. *Water Resources Research* 27(9):2401-2414.
- Chen, C.-S. 1986. Solutions for Radionuclide Transport from an Injection Well into a Single Fracture in a Porous Formation. *Water Resources Research* 22(4):508-518.
- Cooper, H.H. and C.E. Jacob. 1946. A generalized graphical method for evaluating formation constants and summarizing well field history. *Transactions of the American Geophysical Union* 27:526-534.
- Coptly, N.K. and A. Findikakis. 2004. Bayesian identification of the local transmissivity using time-drawdown data from pumping tests. *Water Resources Research* 40(12):W12408. doi:10.1029/2004WR003354.
- Cravens, S.J., S.D. Wilson and R.C. Barry. 1990. *Regional Assessment of the Ground-Water Resources in Eastern Kankakee and Northern Iroquois Counties*. Illinois State Water Survey Report of Investigation 111, Champaign, IL.
- Dagan, G. 1981. Analysis of flow through heterogeneous random aquifers by the method of embedding matrix; 1, Steady flow. *Water Resources Research* 17(1):107-121.
- Dagan, G. 1989. *Flow and Transport in Porous Formations*. Springer-Verlag, New York, NY.
- Desbarats, A.J. 1992. Spatial Averaging of Transmissivity in Heterogeneous Fields with Flow Toward a Well. *Water Resources Research* 28(3):757-767.
- Deutsch, C.V. and A.G. Journel. 1998. *GSLIB: Geostatistical software library and user's guide*. Oxford University Press, New York, NY.
- Di Federico, V. and S.P. Neuman. 1997. Scaling of random fields by means of truncated power variograms and associated spectra. *Water Resources Research* 33(5):1075-1085.
- Doe, T.W. 1991. Fractional dimension analysis of constant-pressure well tests. Paper SPE 22702. *Society of Petroleum Engineering Journal Formation Evaluation*:461-467.
- Doe, T.W. and J.E. Geier. 1991. *Interpretation of fracture system geometry using well test data*. Swedish Nuclear Fuel and Waste Management (SKB) Stripa Project Technical Report TR 91-03, Stockholm.
- Doughty, C. and K. Karasaki. 2002. Flow and transport in hierarchically fractured rock. *Journal of Hydrology* 263(1-4):1-22.

- Doughty, C., J.C.S. Long, K. Hestir and S. Benson. 1994. Hydrologic characterization of heterogeneous geologic media with an inverse method based on iterated function systems. *Water Resources Research* 30(6):1721-1745.
- Feder, J. 1988. *Fractals*. Plenum, New York, NY.
- Geier, J.E., T.W. Doe and H.L. Benabderrahman. 1996. *SITE-94: Generalized radial flow interpretation of well tests for the SITE-94 Project*. Swedish Nuclear Power Inspectorate (SKI) Report 96:4, Stockholm.
- Grindrod, P. and M.D. Impey. 1993. Channeling and Fickian Dispersion in Fractal Simulated Porous Media. *Water Resources Research* 29(12):4077-4089.
- Haggerty, R., S. McKenna and L.C. Meigs. 2000. On the late-time behavior of tracer test breakthrough curves. *Water Resources Research* 36(12):3467-3480.
- Hale, F.V. and Y.W. Tsang. 1996. *THEMM User Guide*. Lawrence Berkeley Laboratories, Berkeley, CA.
- Hantush, M.S. and C.E. Jacob. 1955. Non-Steady Radial Flow in an Infinite Leaky Aquifer. *Transactions of the American Geophysical Union* 36:95-100.
- Harbaugh, A.W., E.R. Banta, M.C. Hill and M.G. McDonald. 2000. *MODFLOW-2000, the U.S. Geological Survey modular ground-water models; user guide to modularization concepts and the ground-water flow process*. U.S. Geological Survey Open-File Report 00-0092, Reston, VA.
- Horne, R.N. 1995. *Modern Well Test Analysis: A Computer-Aided Approach*. Petroway, Palo Alto, CA.
- Indelman, P. and G. Dagan. 1993. Upscaling of Permeability of Anisotropic Heterogeneous Formations: 1. The General Framework. *Water Resources Research* 29(4):917-923.
- Isichenko, M.B. 1992. Percolation, statistical topography, and transport in random media. *Reviews of Modern Physics* 64(4):961-1043.
- Katz, A.J. and A.H. Thompson. 1986. Quantitative prediction of permeability in porous rocks. *Physical Review B* 34(11):8179-8181.
- Kuusela-Lahtinen, A., A. Niemi and A. Luukkonen. 2003. Flow Dimension as an Indicator of Hydraulic Behavior in Site Characterization of Fractured Rock. *Ground Water* 41(3):333-341.
- Lu, S., F.J. Molz and H.H. Liu. 2003. An efficient, three-dimensional, anisotropic, fractional Brownian motion and truncated fractional Levy motion simulation algorithm based on successive random additions. *Computers & Geosciences* 29(1):15-25.
- Matheron, G. 1967. *Elements pour une theorie des milieux poreux*. Masson et Cie, Paris.

McKenna, S., D. Walker and B. Arnold. 2003. Modeling sub gridblock scale dispersion in three-dimensional heterogeneous fractured media. *Journal of Contaminant Hydrology* 62-63:577-594.

McKenna, S.A. 2000. Controls on Multiwell Convergent-Flow Tracer-Breakthrough-Curve Tailing for a Single-Porosity, Heterogeneous Conceptualization. In *Interpretations of Tracer Tests Performed in the Culebra Dolomite at the Waste Isolation Pilot Plant Site, Report SAND 97-3109*, 69-83. Edited by L.C. Meigs, R.L. Beauheim and T.L. Jones. Sandia National Laboratory, Albuquerque, NM.

McKenna, S.A., L.C. Meigs and R. Haggerty. 2001. Tracer Tests in a Fractured Dolomite: 3. Double-Porosity, Multiple-Rate Mass Transfer Processes in Convergent Flow Tracer Tests. *Water Resources Research* 37(5):1143-1154.

Meier, P.M., J. Carrera and X. Sánchez-Vila. 1998. An evaluation of Jacob's method for the interpretation of pumping tests in heterogeneous formations. *Water Resources Research* 34(5):1011-1025.

Meigs, L.C. and R.L. Beauheim. 2001. Tracer Tests in a Fractured Dolomite: 1. Experimental Design and Observed Tracer Recoveries. *Water Resources Research* 37(5):1113-1128.

Mishra, S. 1991. Part II. Methods for analyzing single- and multi-well hydraulic test data. In *Grimsel Test Site: Interpretation of Crosshole Hydraulic tests and a Pilot Fluid Logging Test for Selected Boreholes Within the BK Site*, 13pp. Edited by S. Vomvoris and B. Frieg. NAGRA, Wettingen, Switzerland.

Mishra, S., W.E. Brigham and F.M. Orr. 1991. Tracer- and Pressure-Test Analysis for Characterization of Areally Heterogeneous Reservoirs. Paper SPE17385. *Society of Petroleum Engineering Journal Formation Evaluation*:45-54.

Moreno, L. and C.-F. Tsang. 1994. Flow Channeling in Strongly Heterogeneous Porous Media: A Numerical Study. *Water Resources Research* 37(3):831-835.

Neuman, S.P. 1990. Universal Scaling of Hydraulic Conductivities and Dispersivities in Geologic Media. *Water Resources Research* 26(8):1749-1758.

Neuman, S.P. 1994. Generalized scaling of permeabilities: Validation and effect of support scale. *Geophysical Research Letters* 21(5):349-352.

Neuman, S.P. 1995. On advective transport in fractal permeability and velocity fields. *Water Resources Research* 31(6):1455-1460.

Neuman, S.P. and V. di Federico. 2003. Multifaceted nature of hydrogeologic scaling and its interpretation. *Reviews of Geophysics* 41(3):1014. doi:10.1029/2003RG000130.

- NIPC. 2001. *Strategic plan for water resource management*. Northeastern Illinois Planning Commission Public Hearing Draft, Chicago, IL.
- NRC. 1996. *Rock Fractures and Fluid Flow: Contemporary Understanding and Applications*. National Research Council, Washington, DC.
- O'Shaughnessy, B. and I. Procaccia. 1985. Analytical Solutions for Diffusion on Fractal Objects. *Physical Review Letters* 54(5):455-458.
- Oliver, O.S. 1990. The averaging process in permeability estimation from well-test data. Paper SPE 19845. *Society of Petroleum Engineering Journal Formation Evaluation*:319-324.
- Peaceman, D.W. 1978. Interpretation of Well Block Pressure in Numerical Reservoir Simulation. Paper SPE 6893. *Society of Petroleum Engineering Journal Formation Evaluation*:183-194.
- Polek, J.M. 1990. *Studies of the Hydraulic Behavior of Hierarchically Fractured Rock Geometries*. MS Thesis. Engineering Materials Science, University of California at Berkeley, Berkeley, CA.
- Press, W., S. Teukolsky, W. Vetterling and B. Flannery. 1992. *Numerical Recipes in FORTRAN The Art of Scientific Computing*. Cambridge, New York, NY.
- Raghavan, R. 2004. A review of applications to constrain pumping test responses to improve on geological description and uncertainty. *Reviews of Geophysics* 42(4):RG4001. doi:10.1029/2003RG000142.
- Rasmuson, A. and I. Neretnieks. 1981. Migration of radionuclides in fissured rock: the influence of micropore diffusion and longitudinal dispersion. *Journal of Geophysical Research B* 86(B5):3749-3758.
- Riemann, K., G.v. Tonder and P. Dzanga. 2002. Interpretation of single-well tracer tests using fractional flow dimensions. Part 2: A case study. *Hydrogeology Journal* 10(3):357-367. doi:10.1007/s10040-002-0197-5.
- Saadatfar, M. and M. Sahimi. 2002. Diffusion in disordered media with long-range correlations: Anomalous, Fickian, and superdiffusive transport and log-periodic oscillations. *Physical Review E* 65(036116):1-8.
- Sahimi, M. and S. Mukhopadhyay. 1996. Scaling properties of a percolation model with long-range correlations. *Physical Review E* 54(4):3870-3880.
- Sánchez-Vila, X., P.M. Meier and J. Carrera. 1999. Pumping tests in heterogeneous aquifers: An analytical study of what can be obtained from their interpretation using Jacob's method. *Water Resources Research* 35(4):943-952.

- Stauffer, D. and A. Aharony. 1994. *Introduction to Percolation Theory*. Taylor & Francis, Philadelphia, PA.
- Strack, O. 1989. *Groundwater Mechanics*. Prentice-Hall, Englewood Cliffs, NJ.
- Theis, C. 1935. The relation between the lowering of the piezometric surface and the rate and duration of discharge of a well using groundwater storage. *Transactions of the American Geophysical Union* 16:519-524.
- Tsang, Y.W. 1995. Study of alternative tracer tests in characterizing transport in fractured rocks. *Geophysical Research Letters* 22(11):1421-1424.
- Tsang, Y.W. and C.F. Tsang. 2001. A Particle-Tracking Method for Advective Transport in Fractures with Diffusion into Finite Matrix Blocks. *Water Resources Research* 37(3):831-835.
- Walker, D.D. and R.M. Roberts. 2003. Flow Dimensions Corresponding to Hydrogeologic Conditions. *Water Resources Research* 39(12):1349. doi:10.1029/2002WR001511.
- Wilson, J.D. and R.L. Naff. 2004. *MODFLOW-2000, the U.S. Geological Survey Modular Ground-Water Model -- GMG Linear Equation Solver Package Documentation*. U.S. Geological Survey Open-File Report 1261, Reston, VA.
- Zinn, B. and C.F. Harvey. 2003. When good statistical models of aquifer heterogeneity go bad: A comparison of flow, dispersion, and mass transfer in connected and multivariate Gaussian hydraulic conductivity fields. *Water Resources Research* 39(3):1051. doi:10.1029/2001WR001146.

Appendix A. Code Description and Performance Requirements

The Monte Carlo simulations performed in this study use a sequence of programs to simulate a field of heterogeneous transmissivity, simulate an aquifer test, simulate steady regional flow, simulate a tracer test, and analyze the results of these simulations (Figure 2). With the exceptions MODFLOW-2000, the programs are written in FORTRAN 77 and thus may require redimensioning arrays and recompilation depending on the size of the particular problem. The sequence is controlled by scripts in DOS, Bash, or Perl, depending on the operating system of the computing platform. Each program has an associated file with a name of the form *program_name.par* which provides the input parameters and brief definitions. The input parameters are fully discussed and documented in the user manuals of the individual programs. With the exceptions noted below, the programs were taken from the public domain and were modified for the purposes of this study by adapting the input/output:

sgsim v3.100: This algorithm is developed from the GSLIB suite of geostatistical programs (Deutsch and Journel, 1998). *sgsim* simulates a spatially correlated normal variable (multivariate Gaussian, or mvG). For the purposes of this project, *sgsim* v3.100 was modified from the distributed version of *sgsim* (v2.000) to reduce memory requirements, accept a random seed from standard input, and to accommodate the power semivariogram model used when simulating fractional Brownian motion (fBm).

gsim v1.004: This program was written for this project to simulate a site percolation network. It was developed from programs by Press et al. (1992).

con2mod v2.008: This program rescales, transforms, and reformats the variables created by *sgsim* or *gsim*, and outputs files of transmissivity values for use in the groundwater flow and transport models. It was developed by one of the principal investigators and was enhanced for this project to permit exporting a subregion of the simulated field and surrounding it with a uniform region as required by THEM2.

MODFLOW-2000 v1.12gmg: This widely used finite-difference model of groundwater flow (Harbaugh et al., 2000) reads the transmissivity field written by *con2mod*, simulates a transient hydraulic test in two dimensions and also simulates steady, uniform flow over the domain using parallel boundary conditions. MODFLOW-2000 does not use a *.*par* file, but rather an elaborate series of files organized by a control file named *modflow.bf*. MODFLOW-2000 uses FORTRAN 90 extensions for dynamic memory allocation. This particular version of MODFLOW-2000 includes the GMG package, an efficient multi-grid solver (Wilson and Naff, 2004) written in C.

postmod v1.201: This program scans the output drawdown file of MODFLOW-2000 and estimates the derivative and flow dimension using a finite difference approximation. For this project, it was enhanced to include the Cooper-Jacob interpretation approach to infer the corresponding apparent transmissivity.

effmod v1.201: This program scans the cell-by-cell output file of MODFLOW-2000 for the regional, uniform-flow simulation and determines the effective transmissivity.

THEMM2 v2.007: This program reads steady-state flow fields corresponding to pumping stresses and simulates advective transport of solutes influenced by single-rate, matrix diffusion. During the present project, THEMM2 was developed from the *themmb*, the transport algorithm used by THEMM v1.0 (Transport in Heterogeneous Medium with Matrix diffusion) (Hale and Tsang, 1996; Tsang and Tsang, 2001). The modifications included changing the input stream to read the output *.hds file of heads from MODFLOW-2000 and to match the THEMM2 representation of constant-head boundaries to that of MODFLOW-2000. Prior to running THEMM2, *con2mod* must be run to pick out a subregion of the transmissivity field, and surround it with a telescoping grid of homogeneous transmissivity. This subregion is picked up by MODFLOW-2000, which solves for the steady-state head distribution, one for each flow regime (injection, chase, recovery). Unlike THEMM v1.0 which used the flow model *themma* to solve for the distribution of steady-state heads, THEMM2 reads the steady-state heads created by MODFLOW-2000. THEMM2 uses particle tracking to model advective transport (no microdispersion) and simulates matrix diffusion using a random wait time to delay the transit of particles. The output of THEMM2 includes maps of particle distributions at specific times and particle arrival data.

THEMMBTC v2.007: This program reads the THEMM2 output of particle arrivals versus time and computes the BTC. THEMMBTC was adapted from *themmc*, part of the original THEMM v1.0, by modifying the input formats to support THEMM2.

To accomplish the study goals stated in the introduction of this report, the sequence of programs must accomplish certain functions. For each of the functions listed below, one or more requirements must be met and these are the performance criteria for verifying this software. These criteria are listed after each function below:

1. Simulate an infinite-acting aquifer test and analyze the results.
 - a) Match the transient drawdowns for infinite-acting radial flow without wellbore storage, as simulated by nSIGHTS (or similar well-test analysis software).
 - b) Yield flow dimension $n = 2$ for infinite-acting radial flow.
 - c) Satisfy $T_{CJ} / T_g \approx 1$ for homogeneous transmissivity and for $\ln T$ distributed as a mvG variable of modest variance (after (Sánchez-Vila et al., 1999))
2. Simulate steady, regional flow across the full domain to estimate the effective transmissivity.
 - a) $T_e / T_g \approx 1$ for mvG of zero and modest variance.
3. Simulate a simple injection test influenced by matrix diffusion.
 - a) Match (within ergodic fluctuations) the analytical solution of Chen (1986)
 - b) Match (within ergodic fluctuations) the THEMM v1.0 solution for finite blocks (Rasmuson and Neretnieks, 1981)
4. Simulate a converging flow tracer test influenced by matrix diffusion
 - a) Match (within ergodic fluctuations) the THEMM v1.0 solution for infinite blocks / early time.
 - b) Produce BTC with late-time log-log slope of -3/2.
5. Flow balance error less than 0.1 percent (all simulations).

6. Simulate transmissivity fields with particular stochastic models of heterogeneity.
 - a) Match (within ergodic fluctuations) the input parameters (model semivariogram and T_g).
 - b) Satisfy $T_e/T_g \approx 1$ for mvG of modest variance.

These criteria are addressed by the two verification problems provided in appendices B and C. The source codes, driver scripts, and all input and output are available on request from the authors, but are not included with this report.

Appendix B. Code Verification Problem mip_V2

This verification problem examines the performance of the program sequence described in Appendix A for the case of a homogeneous realization of transmissivity. The purpose is to demonstrate the general functionality of the codes and verify the ability of the code to simulate a simple aquifer test and radial transport using the finite-block solution (Rasmuson and Neretnieks, 1981). It also verifies that THEMM2 works no worse than THEMM v1.0 (Hale and Tsang, 1996) for this transport problem. Because the flow problem is deterministic and the transport problem is deterministic (except for the random effects of matrix diffusion), this verification problem is run using a single realization.

The problem configuration and parameters are given in the bulleted lists below. Note that, because the transmissivity field is homogeneous and *sgsim* generates a standard normal variable, $N(0,1)$, the mean of the input field is transformed for each run of *con2mod*. This allows us to use different values of T_g and grid spacing for the aquifer test simulation than for the transport simulation.

The aquifer test simulation imitates MODFLOW Instructional Problem #1 (Anderson, 1993): transient drawdown to a point sink in a confined, infinite-acting homogeneous aquifer (i.e., the Theis problem). The following grid and parameters are used:

- Finite difference grid of 1001 x 1001 nodes, uniform 10 m spacing.
- Withdrawal well at row 501, column 501, pumping at $Q = -4.0 \times 10^{-3} \text{ m}^3/\text{sec}$.
- 40 time steps, time step multiplier of 1.3, maximum time of 2.07×10^6 seconds, starting head of 0.0 m, uniform constant-head boundaries of 0.0 m.
- Uniform transmissivity of $2.3 \times 10^{-3} \text{ m}^2/\text{sec}$, thickness of 1 m, and storage coefficient of 7.5×10^{-4} .
- Wellbore storage is controlled by multiplying by a factor of $\frac{1}{4}$ the storage coefficient in the node representing the well.
- For estimating the effective transmissivity, constant-head boundaries are used to impose a gradient of 9.99×10^{-4} (such that the *effmod.par* parameter '*afactor*' is 0.10 m).

The tracer test imitates Verification Problem 2 of Hale and Tsang (1996): a constant rate of tracer injection in an infinite aquifer influenced by matrix diffusion (i.e., the Chen (1986) problem). It uses the following grid and parameters:

- Uniform 1 m fine grid of 251 x 251 nodes, surrounded by a telescoping region 10 nodes wide (plus 2 more in the MODFLOW-2000 grid for the exterior constant-head boundary cells).
- Tracer injection at $x = 126 \text{ m}$, $y = 126 \text{ m}$ on the fine grid (MODFLOW-2000 row 137, column 137), at a rate of $Q = 1.157 \times 10^{-7} \text{ m}^3/\text{sec}$, and concentration of 0.273881 kg/m^3 .

- Uniform transmissivity of $1.0 \times 10^{-4} \text{ m}^2/\text{sec}$, thickness 1 m, aqueous diffusivity of $1.6 \times 10^{-9} \text{ m}^2/\text{sec}$, fracture porosity of 1.0×10^{-4} , matrix porosity of 0.01, and tortuosity of 0.01.
- Matrix diffusion into spherical blocks with $\lambda = 2r_b = 3.0 \text{ m}$.
- One steady-state flow regime, starting head of 0.0 m, uniform constant-head boundaries of 0.0m, observed at time = $3.15576 \times 10^7 \text{ sec}$.

Problem mip_V2 was run on a P4 2.2 Ghz desktop PC with 512 Mb of RAM, and required approximately 25 min. Two MODFLOW-2000 solvers are used to provide testing coverage: LMG for the transient aquifer test and PCG for the steady-state tracer test are used. An example DOS script to drive the program sequence is given below; note that programs *sgsim*, *con2mod*, *postmod*, *effmod*, THEM2, and THEM2BTC wait for the user to provide a large integer as a random seed (used for stochastic simulation in *sgsim* and THEM2, but only as an identifier in the other programs).

Script 'mcsim.bat':

```

echo "here we go"
sgsim.exe
copy con2mod.parF con2mod.par
con2mod.exe
copy modflow.bfF modflow.bf
mf2k.exe
postmod.exe
effmod.exe
echo "****DONE WITH FLOW****"
copy con2mod.parT con2mod.par
con2mod.exe
copy modflow.bfT modflow.bf
mf2k.exe
themm2.exe
themmbtc.exe
torus.exe
echo "all done"

```

The results of the simulation clearly demonstrate that the sequence of programs is sufficiently accurate for the purposes of this study. Specifically:

- In MODFLOW-2000, output file *mip1.lst*, the flow balance error for all time steps was 0.00 percent (satisfies criterion 5).
- In comparison to a solution using comparable conditions from nSIGHTS, the Sandia well-test analysis program, the solutions are nearly exact (Figure B.1). Note that the inverse parameter match is nearly exact (satisfies criterion 1a).
- In *postmod* output files *mip1_OW1.dpp* (pumped well, effective radius of 1.982 m) and *mip1_OW2.dpp* (60 m radius), the flow dimension vs. time is $n = 2$ for the entire latter half of the simulation (satisfies criterion 1b).
- In *postmod* output file *tcj.out*, the Cooper-Jacob solution yields an apparent transmissivity of $2.3 \times 10^{-3} \text{ m}^2/\text{sec}$, storage coefficient of 8.0×10^{-4} for the pumped well, and nearly identical for the observation well at a radius of 60 m (satisfies criterion 1c).
- In *effmod* output file *teff.out*, the estimated effective transmissivity is $2.3 \times 10^{-3} \text{ m}^2/\text{sec}$ (partially satisfies criterion 2a).
- In MODFLOW-2000 output file *mf_V2.lst* (head solution for the transport problem), the flow balance error for all time steps was 0.00 percent (satisfies criterion 5).
- In THEMM2 output file *themm2.dbg* the maximum head of the field is at the well and the value is 13.77420 m; comparable calculations using THEMM v1.0 yield 13.77137 m (partially satisfies criterion 3b).
- THEMM2 output file *V2_100.pmp* provides the distribution of particles surrounding the injection well at time = 3.15576×10^7 sec. A separate program written by the authors, *torus.f*, reads the *.pmp file and computes the average concentration in a cylinder surrounding the well (Figure B.2). Note that *torus.f* is not part of the program sequence, but rather is only a statistical summary of the output for the purposes of this verification problem. MSEXcel is used to solve the analytical solution and plot the results. (satisfies criterion 3b).
- Figure B.2 also plots the analytical solution of *Chen* [1986] and THEMM v1.0 for comparison, which shows very good agreement. Variations near the injection well are in part due to the coarseness of the finite difference grid and the use of random wait times to simulate matrix diffusion (satisfies criterion 3a).

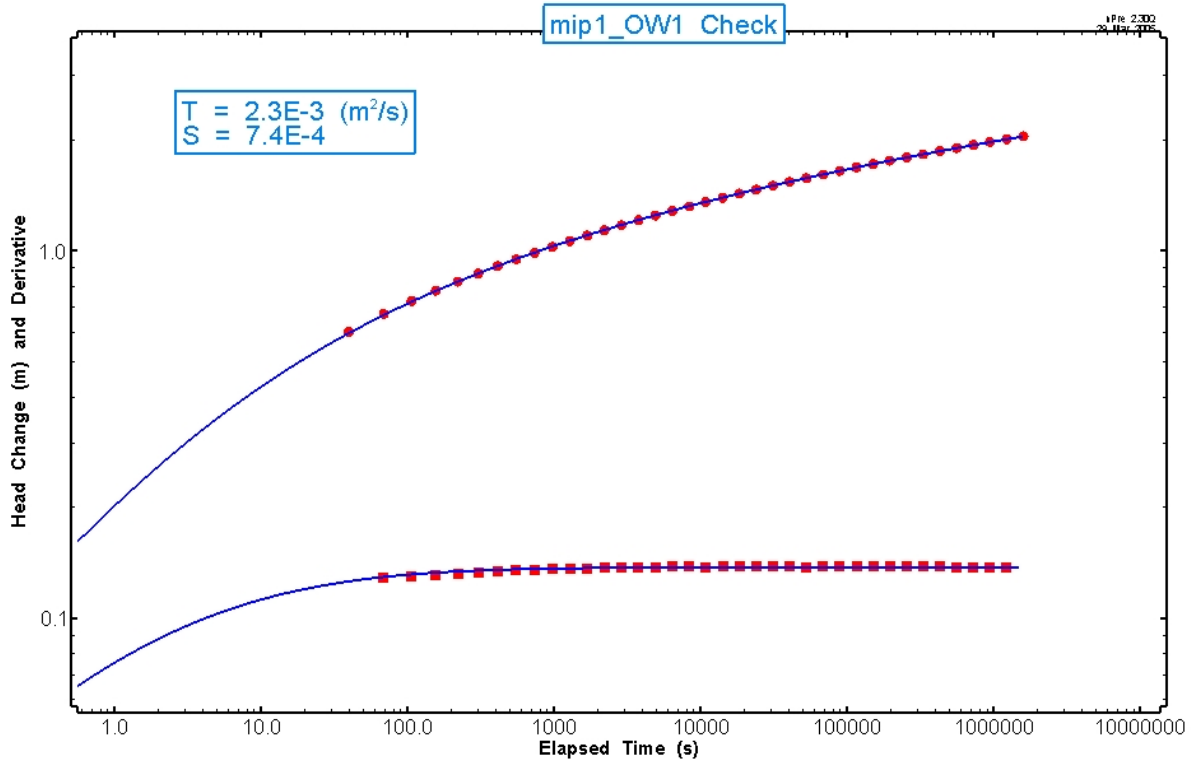


Figure B.1. Drawdowns at the pumped well for verification problem mip_V2. nSIGHTS solution for drawdown (lines) versus drawdowns simulated by MODFLOW-2000 (points) in the sequence of programs used in this study. The nSIGHTS inverse solution for the aquifer test parameters is given in the box.

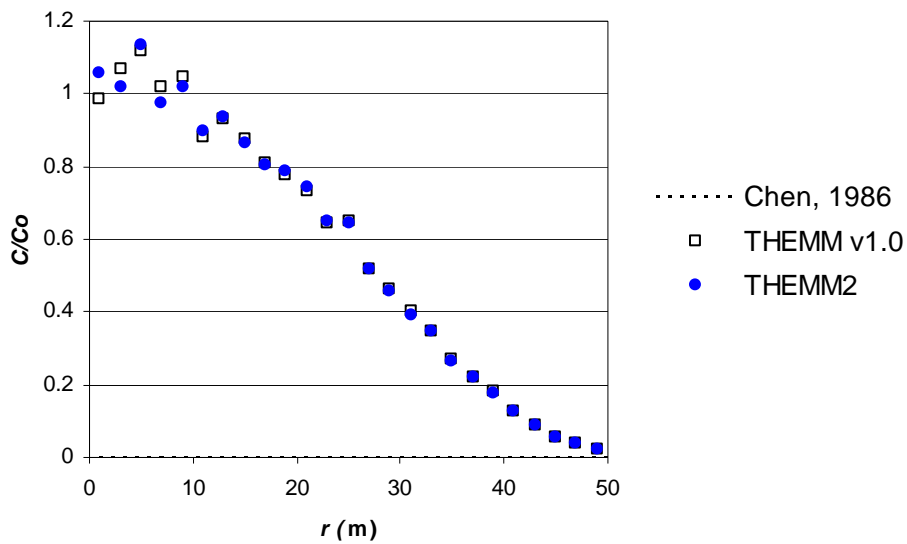


Figure B.2. Comparison of solutions for tracer injection influenced by matrix diffusion: verification problem mip_V2.

Appendix C. Code Verification Problem h11_S1

This verification problem examines the performance of the program sequence described in Appendix A for the case of $\ln T$ distributed as an mvG process of low variance, and a converging flow tracer test in a homogeneous medium. The purpose is to verify the ability of the code to simulate an aquifer test and CFTT in a stochastic simulation to infer ensemble results. It also verifies that THEMM2 is no less accurate than THEMM v1.0 (Hale and Tsang, 1996) using the early-time, infinite-block solution for this transport problem. Because both problems are stochastic, this verification problem is run using 100 realizations.

The problem configuration and parameters are given in the bulleted lists below. As in verification problem mip_V2, the sequence takes advantage of the fact that *sgsim* generates a standard normal variable, $N(0,1)$, to transform the mean of the simulated transmissivity field for each realization using *con2mod*. This allows us to use a homogeneous field, a different value of T_g , and a different grid spacing for the transport simulation.

The aquifer test simulation imitates the H-11 hydropad aquifer test (Beauheim and Ruskauff, 1998). Because skin effects and dual porosity are not included, it cannot be directly compared to the field data. However, we can verify that the ensemble averages yield the results of Matheron (1967) and Sánchez-Vila et al. (1999). The following grid and parameters are used:

- Finite difference grid of 2001 x 2001 nodes, uniform 2 m spacing.
- Withdrawal well at row 1001, column 1001, pumping at $Q = -0.228$ L/sec.
- 44 time steps, time step multiplier of 1.3, maximum time of 5.08×10^5 seconds, starting head of 0.0 m, uniform constant-head boundaries of 0.0 m.
- Transmissivity simulated as an mvG process, with $T_g = 4.70 \times 10^{-5}$ m²/sec, $\sigma_{\ln T}^2 = 0.25$, exponential model semivariogram with integral scale of 20m, thickness 4.4 m, storage coefficient of 4.7×10^{-5} .
- Wellbore storage is controlled by multiplying by a factor of $\frac{1}{4}$ the storage coefficient in the node representing the well.
- For estimating the effective transmissivity, constant-head boundaries are used to impose a gradient of 9.99×10^{-4} (such that the parameter *afactor* in file *effmod.par* is 0.10 m).

The tracer test imitates Sample Problem 2 of Hale and Tsang (1996): a preliminary interpretation of the CFTT conducted at the WIPP H-11b hydropad, using the path from H-11b3 to H-11b1 and a homogeneous transmissivity field. It uses the following grid and parameters:

- Uniform 1 m fine grid of 250 x 250 nodes, surrounded by a telescoping region 10 nodes wide (plus 2 more in the MODFLOW-2000 grid for the exterior constant-head boundary cells).
- Recovery well at $x = 125$ m, $y = 125$ m on the fine grid (MODFLOW-2000 row 137, column 136), pumping at $Q = -0.38 \times 10^{-3}$ m³/sec.

- Tracer injection at $x = 154$ m, $y = 118$ m on the fine grid (MODFLOW-2000 row 144, column 165), injecting tracer at $Q = 9.84 \times 10^{-5}$ m³/sec and 10.55 kg/m³ concentration, followed by chaser injection at $Q = 10.3 \times 10^{-5}$ m³/sec.
- Uniform transmissivity of 4.5×10^{-6} m²/sec, thickness 7.62 m, aqueous diffusivity of 7.4×10^{-10} m²/sec, fracture porosity of 5.0×10^{-4} , matrix porosity of 0.16, tortuosity of 0.11.
- Three steady-state flow regimes, starting head of 0.0 m, uniform constant-head boundaries of 0.0 m.

Problem h11_S1 was run on a P4 3.3 Ghz desktop PC with 2Gb of RAM, and required approximately 72 hours for 100 realizations. This was a Linux platform, and the program sequence was controlled using a Bash shell script (similar to the DOS script shown in Appendix B). The script, *mcsim5.sh*, is available on request. The MODFLOW-2000 GMG solver is used for both the transient aquifer test and for the steady-state tracer test. The results of the simulation clearly demonstrate that the sequence of programs is sufficiently accurate for the purposes of this study. Specifically:

- In MODFLOW-2000, output file *h11_s1.lst*, the flow balance error for all time steps was 0.00 percent (satisfies criterion 5)
- As an average over all realizations, $T_g^*/T_g = 0.998$, $T_e^*/T_g = 0.9965$, $T_{CJ}^*/T_g = 0.9953$. The related calculations for the power model semivariogram (Figure 8) show that the model semivariogram is reproduced by the experimental semivariogram (satisfies criteria 1c, 6a, and 6b).
- In MODFLOW-2000 output file *mf_V2.lst* (head solution for the transport problem), the flow balance error for all flow regimes was 0.00 percent (satisfies criterion 5)
- THEMMBTC output file *S1_3.btc* provides one realization of the relative concentrations that are plotted in Figure C.1, along with one realization of THEMM v1.0 for comparison. The late-time slope of the log-log plot has a slope of -3/2 (satisfies criteria 4a and 4b).

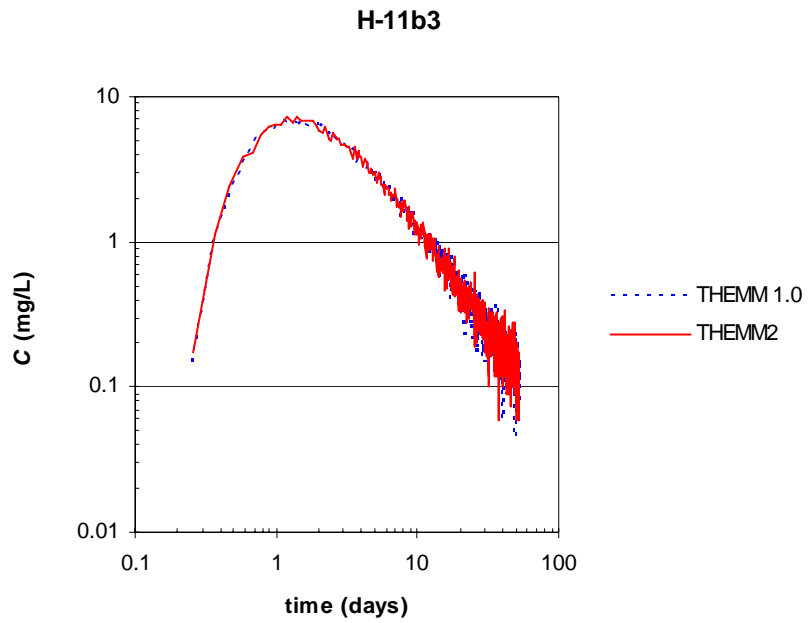


Figure C.1. Breakthrough curves for the H-11 CFTT (verification problem h11_S1).

Appendix D. Monte Carlo Stability Analyses

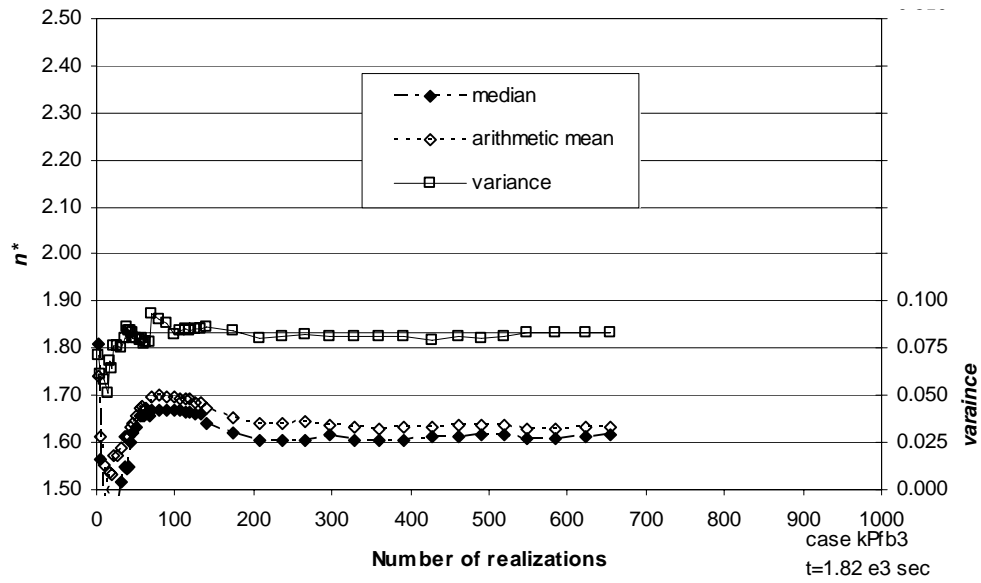


Figure D.1. Apparent flow dimension versus number of realizations at time 1.82×10^3 sec, case kG4b3: mvG with $\sigma_{\ln T}^2 = 1.0$ and $I = 7$ m.

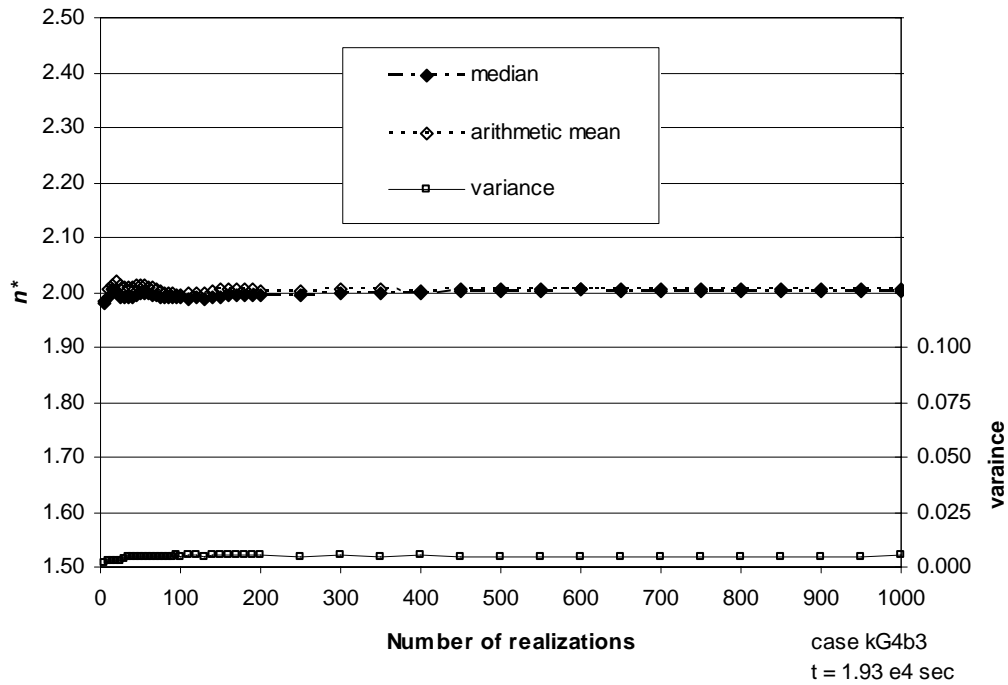


Figure D.2. Apparent flow dimension versus number of realizations at time 1.93×10^4 sec, case kG4b3: mvG with $\sigma_{\ln T}^2 = 1.0$ and $I = 7$ m.

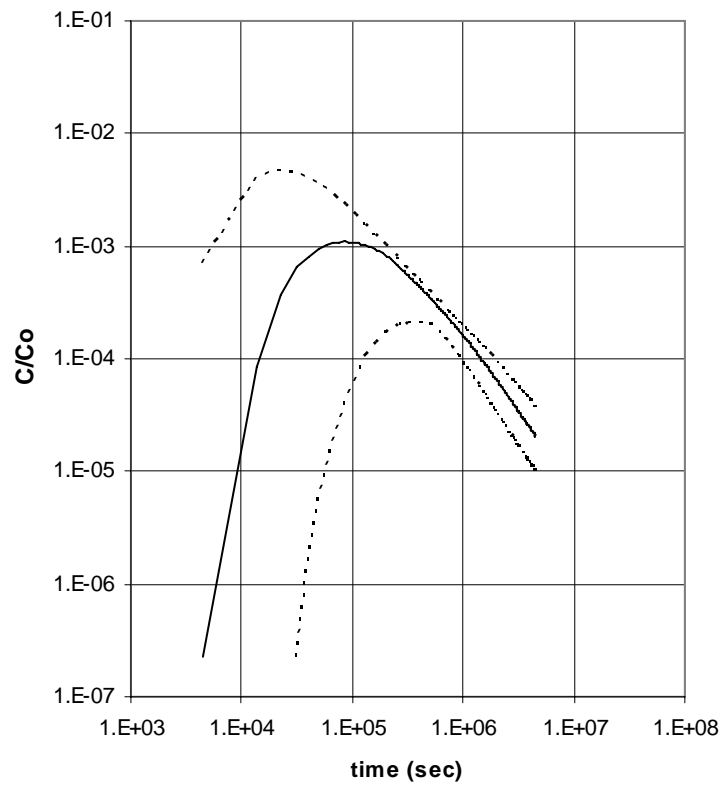


Figure D.3. Relative concentration versus time of a converging flow tracer test for 1000 realizations, median (solid line) and 95 percent nonparametric CI for the population (dashed lines), case kG4b3: mvG with $\sigma_{\ln T}^2 = 1.0$ and $I = 7$ m.

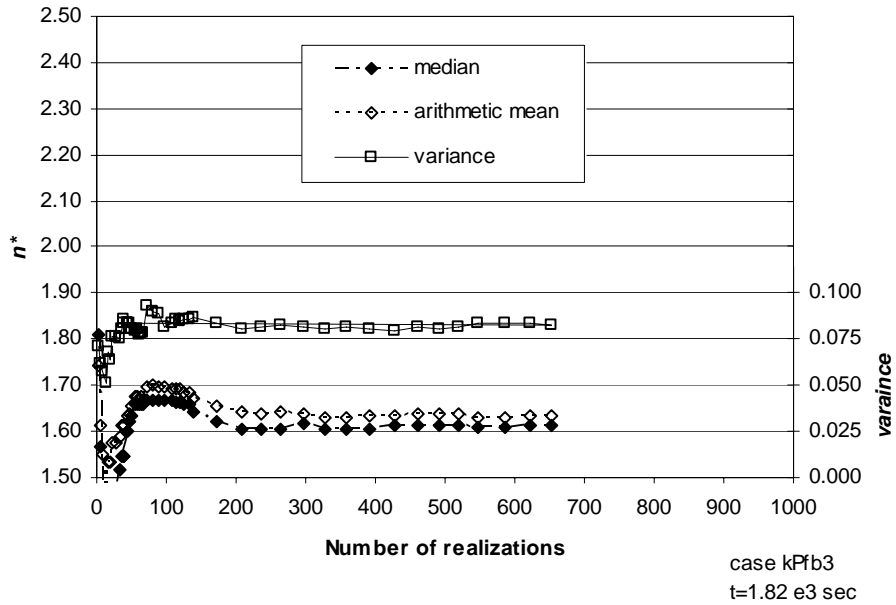


Figure D.4. Apparent flow dimension versus number of realizations at time 1.82×10^3 sec, case kPfb3: percolation with $p = 0.61$, $T_{1-p} = T_p / 10^4$.

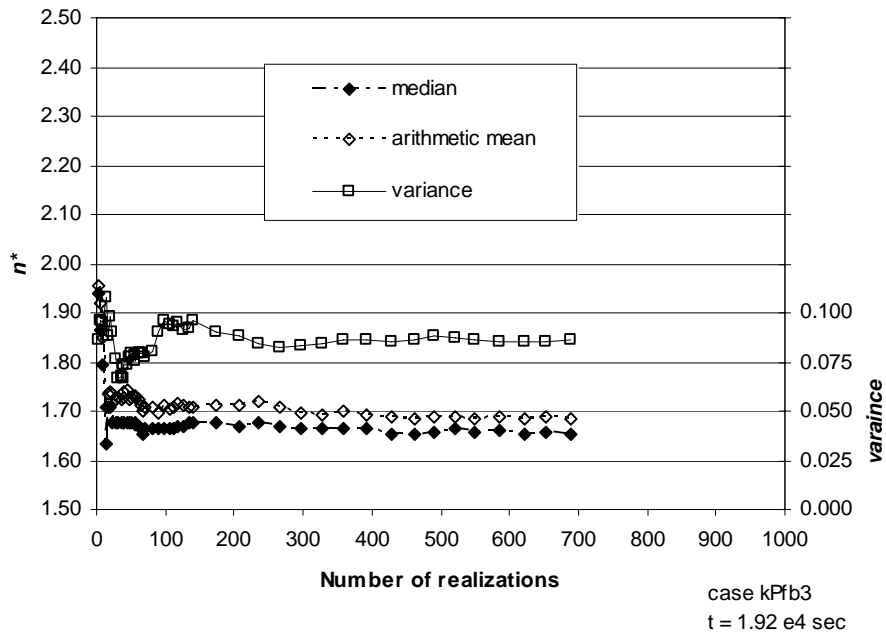


Figure D.5. Apparent flow dimension versus number of realizations at time 1.93×10^4 sec, case kPfb3: percolation with $p = 0.61$, $T_{1-p} = T_p / 10^4$.

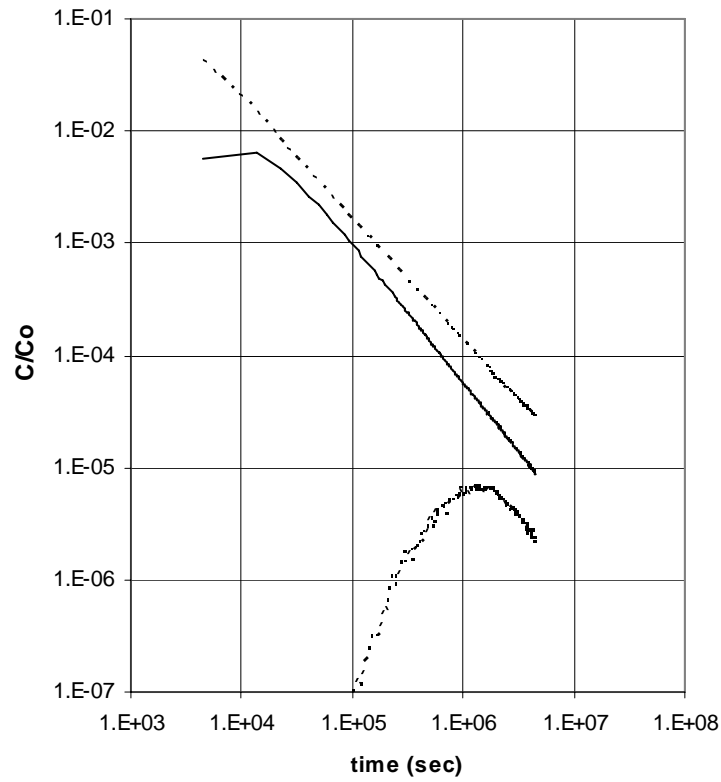


Figure D.6. Relative concentration versus time of a converging flow tracer test for 654 realizations with $0.5 < n^* < 2.5$, median (solid line) and 95 percent nonparametric CI for the population (dashed lines), case kPfb3: percolation with $p = 0.61$, $T_{1-p} = T_p / 10^4$.

Illinois State **WATER** Survey (1895)



Equal opportunity to participate in programs of the Illinois Department of Natural Resources (IDNR) and those funded by the U.S. Fish and Wildlife Service and other agencies is available to all individuals regardless of race, sex, national origin, disability, age, religion, or other non-merit factors. If you believe you have been discriminated against, contact the funding source's civil rights office and/or the Equal Employment Opportunity Officer, IDNR, One Natural Resources Way, Springfield, IL 62702-1271; 217/785-0067; TTY 217/782-9175.

